ABSTRACT

Title of dissertation: PHASE MIXING IN TURBULENT MAGNETIZED PLASMAS

Anjor Vishwas Kanekar,
Doctor of Philosophy, 2015

Dissertation directed by: Professor William Dorland
Department of Physics

Landau damping (phase mixing) is perhaps the most salient feature of weakly collisional plasmas. Phase mixing plays a crucial role in kinetic plasma turbulence—it transfers energy to small velocity space scales, and provides a route to dissipation to the turbulent cascade. Phase mixing has been well understood in the linear limit for nearly seventy years, however, we do not yet fully understand the behavior of phase mixing in presence of a fluid-like turbulent cascade—a common scenario in weakly collisional systems.

In this thesis, we consider simple models for kinetic passive scalar turbulence that simultaneously incorporate phase mixing and turbulent cascade, in order to study the effects of turbulence on phase mixing. We show that the nonlinear cascade scatters energy in the phase space so as to generate a turbulent version of the plasma echo. We find that this *stochastic plasma echo* suppresses phase mixing by reducing the net flux to small velocity space scales.

Further, we study the problem of compressive fluctuations in the solar wind at

scales larger than the ion Larmor radius (the so-called inertial range). The compressive perturbations at these scales are passively mixed by the Alfvénic turbulence. Hence, the general results regarding kinetic passive scalar turbulence are directly applicable to this problem. We find that the suppression of phase mixing by the stochastic plasma echo is key to the persistence of the turbulent cascade of compressive fluctuations at scales where these fluctuations are expected to be strongly damped.

A new code, *Gandalf* was developed for the GPU architecture using the CUDA platform in order to study these systems, in particular to study solar wind turbulence in the inertial range.

Phase mixing in Turbulent Magnetized Plasmas

by

Anjor Vishwas Kanekar

Dissertation submitted to the Faculty of the Graduate School of the
University of Maryland, College Park in partial fulfillment
of the requirements for the degree of
Doctor of Philosophy
2015

Advisory Committee:
Professor William Dorland, Chair
Professor Thomas Antonsen
Professor Ramani Duraiswami
Professor Adil Hassam
Professor Edward Ott

Dedication

To my loving wife, Jui

Acknowledgments

I am deeply grateful to my advisor, Prof. William Dorland. Bill has been a tremendous support, as a physicist, and more importantly, as a friend. None of this work could have been possible without his help. I am indebted to Prof. Alexander Schekochihin who played a vital role in the completion of this thesis. I have learned a lot from Alex, and hope to continue doing so in coming years. I am thankful to the extended research-family I have been fortunate enough to be a part of. This includes Dr. Nuno Loureiro, Prof. Greg Hammett, Prof. Steven Cowley, Dr. Ian Abel, Dr. Edmund Highcock, George Wilkie, Wrick Sengupta, Dr. Jason TenBarge, Prof. Greg Howes, Dr. Matthew Kunz, Prof. Michael Barnes, Dr. Gabe Plunk, Prof. Felix Parra, Prof. Tomo Tatsuno, Prof. Ryusuke Numata, among others. I would like to specially mention "the tome" [1], a paper which started me off on the path of plasma physics.

I have benefited considerably from the support of my friends and colleagues in Maryland—Jonathan Hoffman, Matthew Reed, Kristen Voigt, Evan Berkowitz, Eric Kuo, David Green, Shane Squires to name a few. Rufus Reed deserves a special mention in this category for being the most affectionate Vizsla, who often cheered me up when it was required.

Finally, I am eternally thankful to my loving and supportive wife, Jui. This dissertation would not have been possible without her support.

Table of Contents

List of Figures

Chapter 1

Introduction

1.1 Phase mixing

Weakly collisional plasmas are quite common in nature—the solar wind, the interstellar medium, the core of fusion devices like tokamaks being a few examples of such plasmas. Since collisions are rare, the particle velocity distribution functions $f(v)$ of these plasmas are not necessarily Maxwellian. Hence, a kinetic description that evolves $f(v)$ may be required to describe some phenomena accurately.

One of the most important features of these systems is Landau damping, a property of weakly collisional plasmas whereby waves in the plasma get damped as non-Maxwellian structure in the distribution function is generated. In his original paper, Landau [4] considered the longitudinal electron oscillations [5] in the collisionless limit as an initial value problem, and solved it using a Laplace transform technique. A different approach was used by Van Kampen [6], in which he solved the same problem by means of a normal mode expansion, and found a larger set of solutions (beyond the ones that satisfy the dispersion relation). Case [7] demonstrated the equivalence of these two approaches*, and showed that Landau damping is fundamentally a phase mixing process, where a plane wave perturbation, written as a linear combination of the eigenmodes, is damped due to the systematic

*He modified the Landau approach slightly, in order to derive the full set of Van Kampen's solutions.

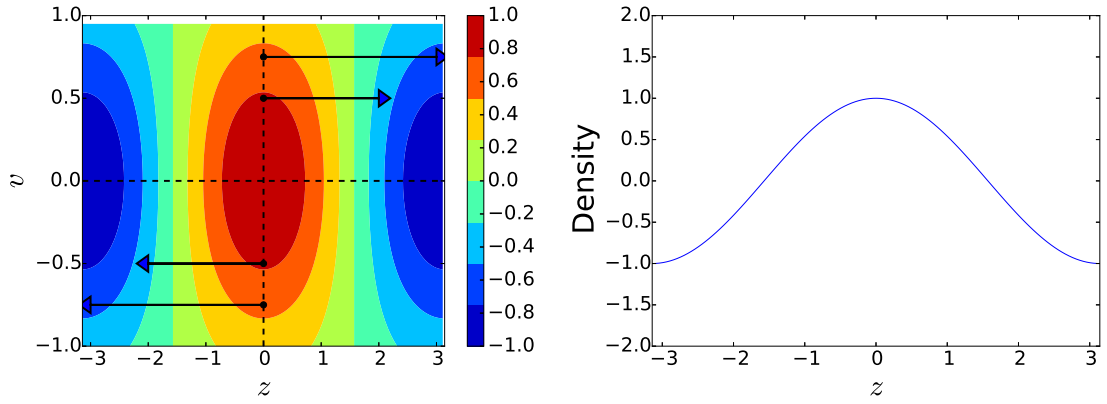

Figure 1.1: The initial perturbed distribution function (left), and the corresponding density perturbation (right).

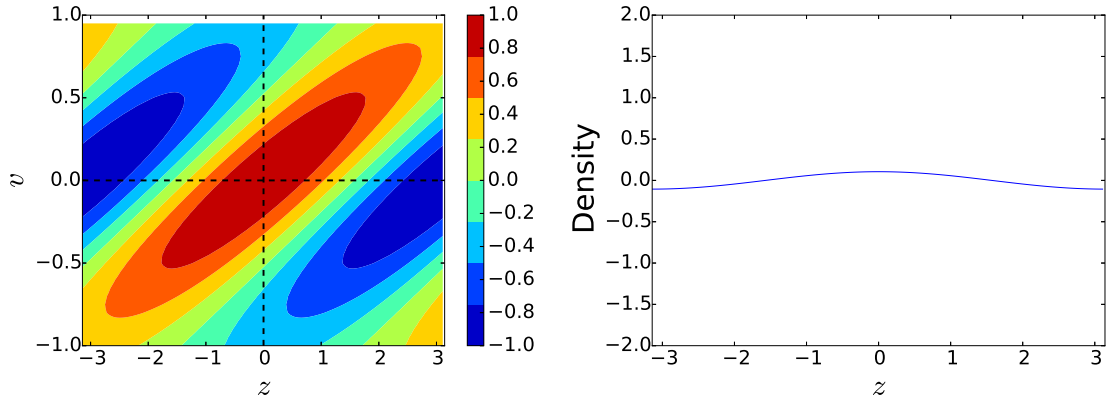

Figure 1.2: The perturbed distribution function (left), and the corresponding density perturbation (right) at time t.

smearing of the normal modes.

For a simple illustration of phase mixing, consider a homogeneous 1D plasma in equilibrium, with a perturbed ion distribution function δf:

$$\delta f(z, v, t = 0) = \cos(kz) F_0(v). \tag{1.1}$$

Here, the perturbation is assumed to be a cosine in the spatial direction z, and

Maxwellian in velocity space, $F_0(v) = \exp\left(-v^2/v_{\rm th}^2\right)/\sqrt{\pi}v_{\rm th}$, where $v_{\rm th} = \sqrt{2T/m}$ is the thermal velocity of the ions, T is the ion temperature, and m is the ion mass. This perturbed distribution function corresponds to a density perturbation δn:

$$\delta n(z, t = 0) = \cos(kz), \tag{1.2}$$

where $\delta n = \int dv\, \delta f$. The initial condition given by Eqs. (1.1–1.2) is plotted in Fig. 1.1. Ignoring electromagnetic effects, as time evolves, ions with different velocities move to different locations in space, generating structure in the perturbed distribution function with respect to v at a constant z:

$$\delta f(z, v, t) = \cos(kz - kvt)F_0(v). \tag{1.3}$$

Since density is the integral of the distribution function over velocity ($\delta n = \int dv\, \delta f$), as the distribution function becomes more and more striated, the density diminishes:

$$\delta n(z, t) = \cos(kz) \exp\left(-k^2 v_{\rm th}^2 t^2/4\right). \tag{1.4}$$

The perturbed distribution function and the perturbed density at time t are plotted in Fig. 1.2. This transfer of structure from real to velocity space, resulting in damping of low order velocity moments is known as phase mixing[†].

[†]There is another, nonlinear, phase mixing process [8] which plays an important role in the turbulence of weakly collisionless plasmas at scales comparable to the ion Larmor radius. However, in this thesis we only consider turbulence at scales larger than the ion Larmor radius, and ignore this process. As a result, the linear phase mixing discussed here is the only phase mixing process in our models.

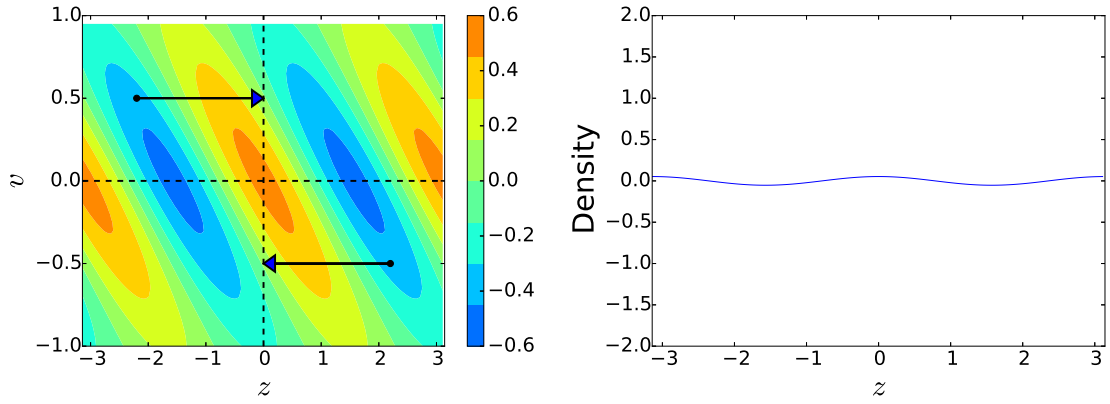

Figure 1.3: The perturbed distribution function (left), and the density perturbation (right), for a mode that is nonlinearly generated by the mode in Fig. 1.2. It is assumed that this new mode has a wavenumber p, such that $\mathrm{sgn}\,(p) = -\mathrm{sgn}\,(k)$.

In the collisionless limit, phase mixing is a reversible process. The distribution function does not "forget" the original perturbation that gets damped, and in theory, can return the system to its original state. The most famous example of such reversibility is the plasma echo [9–12]. In these experiments, a perturbation of the electric potential is excited, which Landau damps away; later, another perturbation of the electric potential is excited, which also damps away; subsequently, a non-zero electric potential perturbation (the echo) is observed to appear in the plasma. The two original electric pulses couple nonlinearly to generate this echo.

The cartoon for phase mixing discussed above (see Figs. 1.1 and 1.2) can be extended to include the echo as follows. Imagine that the perturbation shown in Fig. 1.2 nonlinearly couples with another perturbation to generate a mode which has an oppositely signed wavenumber p:

$$\delta f_{\mathrm{echo}}(z, v, t) = A \cos(pz - kvt) F_0(v), \tag{1.5}$$

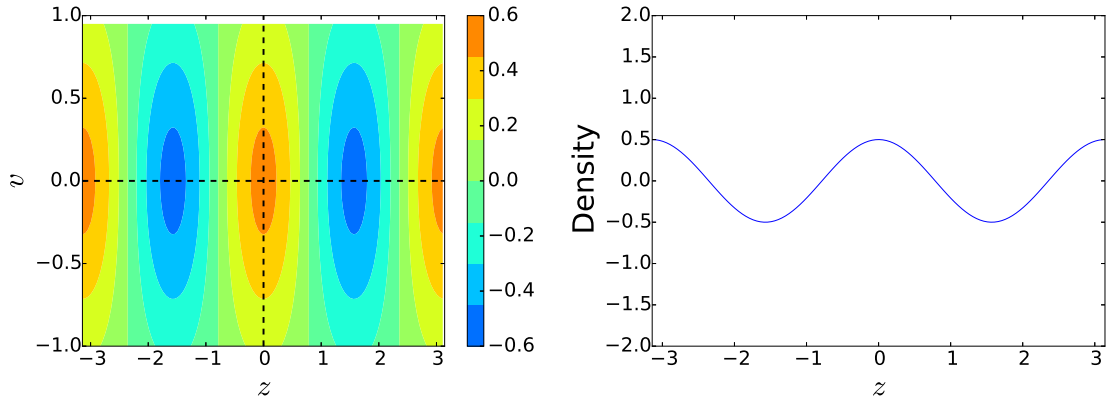

Figure 1.4: The perturbed distribution function (left), and the density perturbation (right), for the mode shown in Fig. 1.3, at a later time $t\,(1 - k/p)$.

where A is the amplitude of this new perturbation. This mode corresponds to a density perturbation given by

$$\delta n_{\rm echo}(z, v, t) = A\cos(pz)\exp\left(-k^2t^2/4\right). \tag{1.6}$$

The perturbed distribution function, and the density perturbation for this mode are plotted in Fig. 1.3. Observe that due to the change in sign of the wavenumber, the phase space contours of the perturbed distribution function are now tilted in the opposite way. At a later time $t+t'$, this perturbed distribution function evolves into

$$\delta f_{\rm echo}(z, v, t + t') = A\cos(pz - pvt' - kvt)F_0(v). \tag{1.7}$$

Since p and k are oppositely signed, the corresponding density perturbation at this

later time is larger than the one in Eq. (1.6):

$$\delta n_{\text{echo}}(z, v, t + t') = A \cos(pz) \exp\left(-(kt + pt')^2/4\right). \tag{1.8}$$

This perturbation is plotted in Fig. 1.4 for time $t + t' = t\,(1 - k/p)$.

It is shown in Chapter 3 that the echo is inherently a nonlinear phenomenon, and is not observed for an isolated Fourier mode. In Chapters 4 and 5 nonlinear models are considered, where different Fourier modes are coupled to each other. Nonlinearly, the plasma echo may be observed. The necessary conditions required for an echo are discussed in detail within these chapters.

1.2 Turbulence

Turbulence is ubiquitous, yet a precise definition of turbulence does not exist. A simple picture of a turbulent system is depicted in Fig. 1.5: energy is injected into the system at some large scale, which then cascades down to smaller and smaller scales. Eventually a dissipative process like viscosity takes over and dissipates the injected energy[‡]. The driving scale and the dissipative scale need to be far removed from each other for the system to exhibit turbulence. For this to be true the ratio of the driving length scale to the dissipation length scale, also known as the Reynolds number, is required to be large—a basic requirement for turbulence.

For our purposes we broadly classify models of turbulence into two categories—

[‡] *Big whorls have little whorls that feed on their velocity, and little whorls have lesser whorls and so on to viscosity.*—Lewis F. Richardson

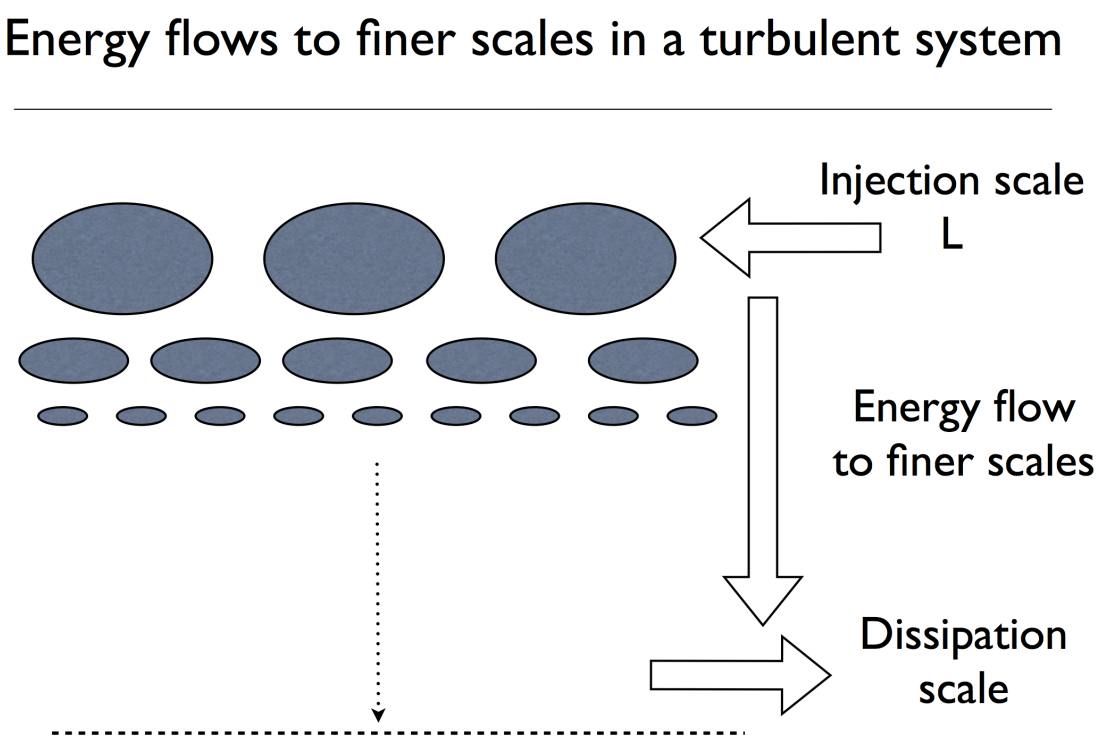

Figure 1.5: A cartoon picture of turbulence.

fluid models and kinetic models. Fluid models describe systems where the mean free path for collisions is smaller than any length scale of interest, *i.e.*, collisions are frequent. Whereas, kinetic models are applicable to systems where the mean free path is comparable to, or larger than the system size, *i.e.*, collisions are rare. Henceforth, we use the terms "fluid/kinetic model of turbulence", and "fluid/kinetic turbulence" interchangeably.

1.2.1 Fluid turbulence

One of the first theories describing turbulence in neutral fluids was by Kolmogorov [13], in which he predicts the famous $k^{-5/3}$ power law spectrum for homogeneous isotropic turbulence. In order to derive this spectrum, he made some key assumptions that have come to underlie turbulence theory: (i) statistical properties of turbulence, such as the energy spectrum, are universal at scales in between the injection and dissipation scale; (ii) the energy transfer from large to small scales happens locally in wavenumber space; (iii) no energy is lost at the intermediate scales, in other words, the flux of energy through each scale is independent of the scale.

Under these assumptions the energy density spectrum can be derived as follows: let u_λ be a velocity fluctuation at the length-scale λ. The (constant) flux of energy ϵ through the scale λ is then given by,

$$\frac{u_\lambda^2}{\tau_\lambda} \sim \epsilon, \tag{1.9}$$

where τ_λ^{-1} is the energy cascade rate at scale λ. Since the energy transfer to smaller scales is local, the cascade rate must be a function of quantities that depend on λ. Since u_λ and λ are the only physical quantities available, the cascade rate can be estimated as,

$$\tau_\lambda \sim \frac{\lambda}{u_\lambda}. \tag{1.10}$$

Therefore,

$$u_\lambda^2 \sim (\epsilon\lambda)^{2/3}. \tag{1.11}$$

Hence, the energy spectrum is a power law $k^{-\alpha}$. For $u_\lambda^2 \propto \lambda^g$, the spectral exponent α is calculated as $\alpha = g + 1$ [14]. Therefore, from Eq. (1.11), the energy spectrum for turbulence in the fluid limit is $k^{-5/3}$.

The power law spectrum is characteristic of broadband fluctuations, which may be thought of as a signature of turbulent systems.

1.2.2 Kinetic turbulence

In this section, we shall move away from the discussion about neutral fluid turbulence, and discuss the general properties of turbulence in weakly collisional plasmas. In addition to the fluid-like turbulent cascade in real space, weakly collisional systems also allow for transfer of energy to small velocity space scales by phase mixing. This makes the nature of dissipation for such systems a contentious issue [15]. Even though phase mixing damps perturbations in the plasma, the process is reversible in the collisionless limit, *i.e.*, it does not generate entropy. Therefore, phase mixing is not dissipative in the true sense. Irreversible heating for these sys-

Figure 1.6: Collisions in neutral fluids (left) result in sharp changes in velocity. Whereas, a particle (ion or electron) in a plasma undergoes many small-angle collisions (right). Therefore, collisions can be modeled as a diffusive operator in the velocity co-ordinate.

tems is only possible through collisions [1,16]. Collisions in plasmas are of a different character than the ones in neutral fluids (see Fig. 1.6). Unlike neutral fluids, particles (ions or electrons) in a plasma undergo numerous long-range collisions, which individually do not alter the velocity of the particle by much. Therefore, collisions can be modeled as a diffusive operator in velocity space: $\sim \nu\, \partial_v^2$ [1,17], where ν is the frequency with which a particle velocity is changed by $\pi/2$ radians. For systems with vanishingly small ν, energy has to be transferred to small scales in velocity space, before it can dissipate via collisions. As a result, in the weakly collisional limit, the cascade of energy occurs in the phase space (real and velocity space) [1, 8, 16]—the spatial cascade is the usual fluid-like nonlinear refinement of scales, whereas the cascade in velocity space is due to phase mixing.

The systems studied in this thesis are assumed to be weakly collisional, and allow for the above mentioned phase space cascade.

1.3 Magnetized plasmas

In addition to assuming that the plasma is weakly collisional, it is also assumed to be strongly magnetized. A strongly magnetized plasma is threaded by a mean magnetic field such that the ion Larmor radius is much smaller than the system size. Additionally, it is assumed that the magnitude of the background magnetic field is much larger than the turbulent electromagnetic fluctuations. For magnetic confinement fusion devices, this is a given, as a guide field is necessary for confinement of the burning plasma. For space and astrophysical plasmas, the large scale magnetic fluctuations behave as a background magnetic field for the small scale turbulence (Kraichnan hypothesis [18]).

The background magnetic field makes these systems very anisotropic [19,20]—the perpendicular length scales (λ) are much smaller than the parallel length scales (l). For such anisotropic systems, the Kolmogorov derivation for the energy spectrum is no longer possible, since the timescale at a given scale cannot be determined uniquely. There is a perpendicular, nonlinear timescale λ/u_λ, and a parallel, linear timescale associated with the Alfvén waves l/v_A, where v_A is the Alfvén velocity. In the magnetohydrodynamic limit, Goldreich and Sridhar [19, 20] proposed a way forward by assuming that the turbulence, at sufficiently small scales, arranges itself in such a way that the linear and nonlinear timescales are comparable to each other [21, 22]. This assumption, taken scale by scale is known as *critical balance*.

One can then estimate the cascade time as

$$\tau_\lambda \sim \frac{\lambda}{u_\lambda} \sim \frac{l}{v_A}, \tag{1.12}$$

which once again gives,

$$u_\lambda \sim (\epsilon\lambda)^{1/3}. \tag{1.13}$$

This again corresponds to a $k_\perp^{-5/3}$ spectrum, but now the spectrum is in the perpendicular direction, as opposed to the isotropic spectrum derived earlier for neutral fluids. The critical balance assumption also relates the parallel and perpendicular length scales:

$$l \sim l_0^{1/3}\lambda^{2/3}, \tag{1.14}$$

where $l_0 = v_A^3/\epsilon$; l_0 is the parallel length scale where the velocity fluctuation is comparable to the Alfvén velocity, and can be thought of as a natural outer scale. Therefore, the velocity fluctuation scaling with respect to l is given by

$$u_\lambda \sim \left(\frac{\epsilon^{1/3}}{l_0^{1/6}}\right) l^{1/2}. \tag{1.15}$$

This corresponds to a parallel spectrum of $k_\parallel^{-2}$. The relationship given by Eq. (1.14) between the parallel and perpendicular length scales looks like $k_\parallel \sim k_\perp^{2/3}$ in terms of the wavenumbers, *i.e.*, as the cascade moves forward to smaller spatial scales, it gets increasingly anisotropic.

In addition to the spatial scale separation, the background magnetic field also

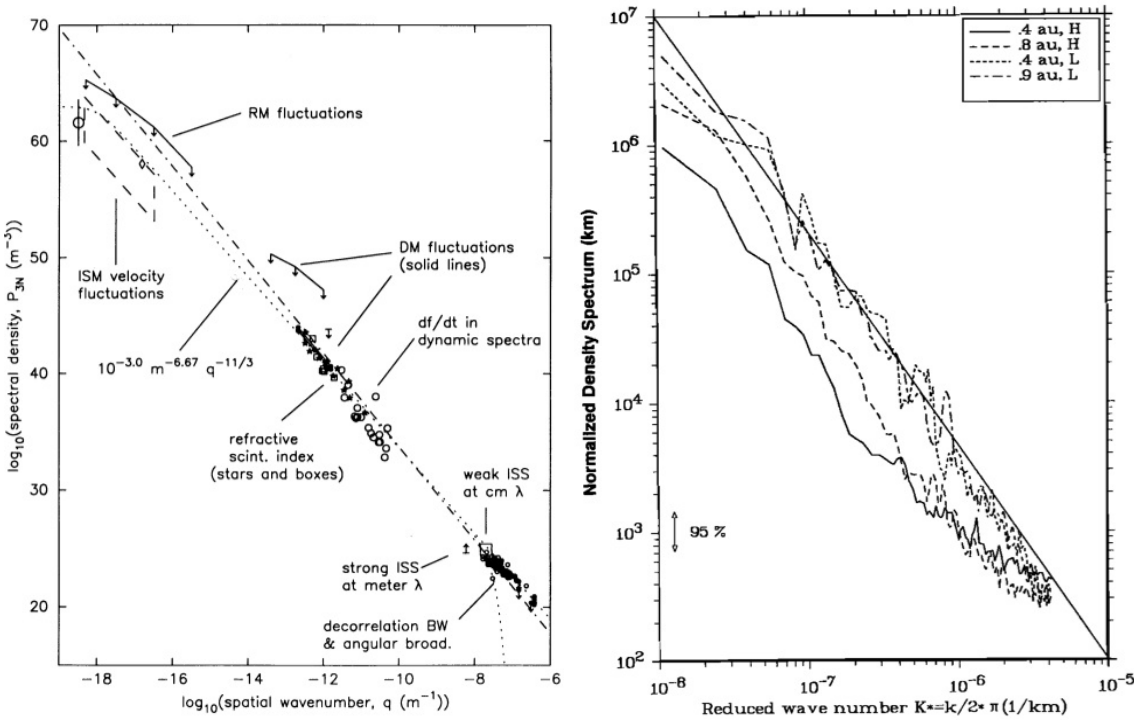

Figure 1.7: Density fluctuation spectra in the interstellar medium (left, taken from [2]) and the solar wind (right, taken from [3]). These power law spectra span multiple decades, even at scales where these fluctuations are expected to be strongly damped.

separates timescales. The cyclotron motion may be assumed to be much faster than any timescale of interest in the system—this allows for reduced descriptions of kinetic plasmas, which are discussed further in Sec. 1.5 and appendix A.

1.4 Phase mixing in turbulent magnetized plasmas: Questions

In Secs. 1.1 and 1.2 we discussed how phase mixing and turbulent cascade dictate the turbulent characteristics of a plasma individually. It is however unclear, as to what happens to phase mixing in a nonlinear turbulent system. Understanding how phase mixing works in presence of turbulence is an important problem in kinetic plasma turbulence.

A simple way to incorporate phase mixing in a model for a turbulent plasma would be to introduce it as a sink of energy to small velocity scales, at each spatial scale, in essence superimposing phase mixing on to the turbulent cascade [23–25]. For the cascade of a macroscopic quantity like density fluctuations, this would show up as a scale-by-scale dissipative term, where the rate of dissipation is proportional to the parallel wavenumber. Such dissipation would violate the constant-flux-through-scales assumption of Kolmogorov. Extraction of energy at each scale at a rate proportional to the wavenumber would imply that the energy spectrum should be an exponential decay instead of a power law. However, power law energy spectra are commonly observed in weakly collisional turbulent magnetized plasmas. A striking example is that of compressive fluctuations in astrophysical systems. Electron density fluctuations in the interstellar medium extend over twelve decades of scales, famously known as "the Great Power Law in the Sky" [2, 26, 27]. In the solar wind, these fluctuations are observed for roughly three decades [3, 28–37] (see Fig. 1.7). These observations are at scales where the plasma is weakly collisional. Linear theory predicts that compressive fluctuations should be strongly damped in the weakly collisional limit [38], which makes these observed power law spectra surprising. This suggests that when the system is nonlinear, the linear predictions need to be modified. A possible explanation for such power law spectra, though not specifically for these plasmas, was given recently by Plunk *et al.* [39, 40], where they argue that phase mixing is suppressed due to what is in essence, an "impedance mismatch" with the nonlinear turbulent frequency. However, in their study, they do not include the nonlinear cascade. Instead, they consider a single Fourier mode, and add

a random source term as a stand-in for turbulence—this approach is quite different from the one we adopt here.

In this thesis, the interplay between the nonlinear cascade and phase mixing is studied. This is done by considering nonlinear models which incorporate both these effects[§]. The first nonlinear model allows for a turbulent cascade in the direction perpendicular to the guide field, but does not allow for a transfer of energy to small spatial scales parallel to the background field. In this scenario, when the turbulent cascade rate is comparable to or larger than the phase mixing rate, energy gets swept up to small spatial scales before it can phase mix. As a result a fluid-like turbulent cascade, *i.e.* a power law spectrum is observed. In the other, more interesting model, where the turbulent cascade proceeds in both perpendicular and parallel directions, a turbulent analog of the plasma echo is observed, which unravels the velocity space structure generated by phase mixing. This *stochastic plasma echo* suppresses phase mixing, which again results in a fluid-like turbulent cascade at scales where, in the linear limit, perturbations would be strongly damped due to phase mixing. Hence, regardless of whether or not there is a parallel cascade, power law energy spectra are observed for turbulent fluctuations at these "kinetic" scales.

[§]This is different from what is generally referred to as nonlinear Landau damping (see [41] and references therein for a detailed analysis of this problem from a mathematician's perspective) in the literature. The question there is what happens to the validity of Landau's results if the perturbations have finite amplitudes. In our work, all perturbations are assumed small compared to the equilibrium.

1.5 Kinetic Reduced MHD

1.5.1 Basic framework

The basic mathematical framework used in this work is known as Kinetic Reduced MagnetoHydroDynamics (KRMHD). KRMHD is the long wavelength limit of gyrokinetics [1, 17, 42–51]. It is derived in thorough detail in Schekochihin *et al.* [1], by expanding "δf gyrokinetics" in small $k_\perp \rho_i$ ($k_\perp$ is the perpendicular wavenumber, ρ_i is the ion Larmor radius). In this limit, the Alfvénic component of the cascade decouples from the compressive fluctuations. The dynamics of the system are completely determined by the Alfvénic fluctuations, which evolve according to reduced MHD [52, 53]. The compressive fluctuations, on the other hand, are described by a kinetic equation for a passive scalar that is nonlinearly advected by the background Alfvénic turbulence. These equations provide an efficient framework within which one may study the turbulent cascade of density and field strength fluctuations in weakly collisional turbulent magnetized plasmas like the solar wind.

The passive nature of compressive fluctuations in this model neatly ties in with a popular approach used to study turbulent cascade in fluid systems, namely that of passive scalar turbulence [14, 54–78]. This gives us the opportunity to study the general problem of *kinetic* passive scalar turbulence, while having a physically relevant system to compare with. General results regarding kinetic passive scalar turbulence are presented in Chapters 3, 4 and 5, by considering simplified versions of KRMHD. The full KRMHD equations are numerically solved in Chapter 6.

The derivation of KRMHD given in Schekochihin *et al.* [1] is extremely de-

tailed, and we do not attempt to better it in this thesis. Instead, we give an outline of the derivation of KRMHD in appendix A, and give a summary of the final equations here.

The KRMHD model assumes a homogeneous equilibrium, with a Maxwellian as the background distribution function. A perturbation of this equilibrium is evolved in time. The Alfvén cascade is described by reduced MHD, which in its simplest form is written in terms of Elsasser variables [79]:

$$\frac{\partial \nabla_\perp^2 \xi^\pm}{\partial t} \mp v_A \frac{\partial \nabla_\perp^2 \xi^\pm}{\partial z} = -\frac{1}{2}\left[\{\xi^+, \nabla_\perp^2 \xi^-\} + \{\xi^-, \nabla_\perp^2 \xi^+\} \mp \nabla_\perp^2 \{\xi^+, \xi^-\}\right], \quad (1.16)$$

where the background magnetic field $\mathbf{B}_0 = B_0 \hat{\mathbf{z}}$ is in the $\hat{\mathbf{z}}$ direction, $\hat{\mathbf{x}}$ and $\hat{\mathbf{y}}$ are the transverse directions, $\xi^\pm = \Phi \pm \Psi$, $v_A = B_0/\sqrt{4\pi m_i n_{0i}}$ is the Alfvén velocity, and Φ and Ψ are stream and flux functions respectively, which are related to the electrostatic potential (φ) and the magnetic vector potential ($A_\parallel$) by:

$$\Phi = \frac{c}{B_0}\varphi, \quad \Psi = -\frac{A_\parallel}{\sqrt{4\pi m_i n_{0i}}}, \quad (1.17)$$

where c is speed of light, m_i is the ion mass, and n_{0i} is the background ion density. The braces denote the Poisson bracket:

$$\{P, Q\} = \frac{\partial P}{\partial x}\frac{\partial Q}{\partial y} - \frac{\partial P}{\partial y}\frac{\partial Q}{\partial x}. \quad (1.18)$$

The left hand side of Eq. (1.16) describes Alfvén wave packets, traveling up or down the field line. The nonlinear interaction between these wave packets is

captured by the right hand side. Observe that only counter-propagating Alfvén waves interact nonlinearly; these counter-propagating Alfvén waves give rise to the turbulent cascade by transferring energy to smaller spatial scales.

The compressive fluctuations are described in terms of two Elsasser-like variables g^+ and g^-:

$$\frac{dg^\pm}{dt} + v_\parallel \nabla_\parallel g^\pm = \frac{v_\parallel F_0(v_\parallel)}{\Lambda^\pm} \hat{\mathbf{b}} \cdot \nabla \int dv_\parallel g^\pm, \tag{1.19}$$

where $F_0(v_\parallel) = \exp(-v_\parallel^2/v_{\rm th}^2)/\sqrt{\pi} v_{\rm th}$ is a one-dimensional Maxwellian ($v_{\rm th} = \sqrt{2T_i/m_i}$ is the thermal velocity of ions, T_i is the ion temperature, m_i is the ion mass), and

$$\Lambda^\pm = -\frac{\tau}{Z} + \frac{1}{\beta_i} \pm \sqrt{\left(1 + \frac{\tau}{Z}\right)^2 + \frac{1}{\beta_i^2}}, \tag{1.20}$$

where τ is the ion to electron temperature ratio, Z is the ion charge in units of the electron charge, and $\beta_i = 8\pi n_{0i} T_i / B_0^2$ is the ion plasma beta. We observe from Eq. (1.20), that the range of $\Lambda^\pm$ is restricted to: $\Lambda^+ > 1$, and $\Lambda^- < 0$. The derivatives d/dt and $\nabla_\parallel$ in Eq. (1.19) are convective derivatives:

$$\frac{d}{dt} = \frac{\partial}{\partial t} + \{\Phi, \ldots\}, \quad \nabla_\parallel = \frac{\partial}{\partial z} + \frac{1}{v_A}\{\Psi, \ldots\}. \tag{1.21}$$

The relationship between the perturbed ion distribution function and $g^\pm$ is given in appendix A (see Eqs. (A.35) and (A.38)). Eqs. (1.16) and (1.19) together constitute the KRMHD model.

1.5.2 Conserved quantities

The energies in each of the Elsasser variables $(\xi^{\pm}, g^{\pm})$ are conserved independently in KRMHD:

$$W = W^{+}_{\mathrm{AW}} + W^{-}_{\mathrm{AW}} + W^{+}_{\mathrm{compr}} + W^{-}_{\mathrm{compr}}, \tag{1.22}$$

where

$$W^{\pm}_{\mathrm{AW}} = \int d^3\mathbf{r} \frac{m_i n_{0i}}{2} \left|\nabla_{\perp}\xi^{\pm}\right|^2 \tag{1.23}$$

are energies of the right and left-going Alfvénic fluctuations, and

$$W^{\pm}_{\mathrm{compr}} = \int d\mathbf{r} \frac{n_{0i}T_{0i}}{2} \left[\int dv_{\parallel} \frac{(g^{\pm})^2}{F_0} - \frac{1}{\Lambda^{\pm}} \left(\int dv_{\parallel} g^{\pm}\right)^2\right] \tag{1.24}$$

are energies of the + and − components of the compressive fluctuations[¶], as defined in the previous section, respectively; W is the total free energy.

[¶]Both the terms in Eq. (1.24) are positive for the "−" mode, since $\Lambda^{-} < 0$. For the "+" mode, W^{+}_{compr} can be shown to be positive using Cauchy-Schwarz inequality, and the condition $\Lambda^{+} > 1$.

Chapter 2

Gandalf

2.1 Introduction

We have developed a new code called *Gandalf*[*] to solve the KRMHD Eqs. (1.16) and (1.19). *Gandalf* is written in CUDA, a GPU computing platform and programming model invented by NVIDIA, and is an efficient numerical tool to study the long-wavelength asymptotic behavior of anisotropic magnetized plasmas.

2.2 Equations

Instead of directly solving Eq. (1.19), we first expand g in Eq. (1.19) (superscripts will be suppressed whenever no confusion would result) in terms of its Hermite moments. Evolving the moments of g instead of using a grid in velocity space makes the numerical scheme spectrally accurate in the $v_\parallel$ coordinate. Expanding Eq. (1.19) in terms of Hermite polynomials also provides an elegant analytical framework to study phase mixing (see Chapter 3 for details). The Hermite moments are defined as follows:

$$g(v_\parallel) = \sum_{m=0}^{\infty} \frac{H_m(v_\parallel/v_{\rm th})F_0}{\sqrt{2^m m!}} g_m, \quad g_m = \int \mathrm{d}v_\parallel \, \frac{H_m(v_\parallel/v_{\rm th})}{\sqrt{2^m m!}} \, g(v_\parallel), \tag{2.1}$$

[*]The code solves for *g-and-Alf*vén waves, hence the name.

where H_m is the Hermite polynomial of order m. Eq. (1.19) then becomes a fluid-like hierarchy of equations:

$$\frac{dg_0}{dt} + v_{\rm th}\nabla_\parallel \frac{g_1}{\sqrt{2}} = 0, \tag{2.2}$$

$$\frac{dg_1}{dt} + v_{\rm th}\nabla_\parallel \left(g_2 + \frac{(1-1/\Lambda)}{\sqrt{2}}\, g_0 \right) = 0, \tag{2.3}$$

$$\frac{dg_m}{dt} + v_{\rm th}\nabla_\parallel \left(\sqrt{\frac{m+1}{2}}\, g_{m+1} + \sqrt{\frac{m}{2}}\, g_{m-1} \right)$$

$$= C[g_m], \quad m \geq 2. \tag{2.4}$$

The first term on the right hand side of Eq. (1.19), being proportional to H_1, only appears in Eq. (2.3). The parallel streaming term couples each Hermite moment to the previous and the next moment[†]. Dynamical coupling of different Hermite moments is the mathematical manifestation of linear phase mixing in Hermite space.

The right hand side of Eq. (2.4) has a collision operator $C[g_m]$ that has been added to the kinetic Eq. (1.19). Collisions are included in order to regularize the system at small velocity space scales. More importantly, they are also physically required to generate entropy and heat the plasma—an exactly collisionless limit is unphysical. We choose a convenient collision operator, the Lenard–Bernstein collision operator [80], which in Hermite space looks like:

$$C[g_m] = -\nu m g_m, \tag{2.5}$$

where ν is the collision frequency. The collision operator acts only on the second and

[†]This is a result of the Hermite recurrence relation: $H_{m+1}(v) = 2vH_m(v) - 2mH_{m-1}(v)$.

higher Hermite moments, and hence, conserves particle number and momentum. This particular collision operator is also manifestly most effective for the highest moments retained, since $C[g_m] \propto m$.

Eq. (1.16) and Eqs. (2.2–2.4) are the equations that are implemented in *Gandalf*.

2.3 Normalization

We normalize the perpendicular spatial co-ordinates x, y and the parallel spatial co-ordinate z, to independent arbitrary length scales ρ and L, respectively (with the assumption $L \gg \rho$). By normalizing parallel and perpendicular co-ordinates independently, we can simulate highly anisotropic fluctuations with a numerical box that is roughly a cube. In addition, since the ratio L/ρ is arbitrary, a single run simulates a whole range of problems with varying degrees of anisotropy. Time is normalized to L/v_A. The Elsasser fields $\xi^{\pm}$ are normalized to ρv_A (gradients of the Elsasser fields have units of velocity—see Eq. (1.17)). The Hermite moments g_m of the perturbed distribution function g are in arbitrary units. The Elsasser fields $\xi^{\pm}$, and the distribution function moments g_m are scaled up by a factor of L/ρ so that all normalized terms have unity order of magnitude.

The normalized equations can then be written as,

$$\frac{\partial \nabla_\perp^2 \xi^{\pm}}{\partial t} \mp \frac{\partial \nabla_\perp^2 \xi^{\pm}}{\partial z} = -\frac{1}{2}\left[\{\xi^{+}, \nabla_\perp^2 \xi^{-}\} + \{\xi^{-}, \nabla_\perp^2 \xi^{+}\} \mp \nabla_\perp^2 \{\xi^{+}, \xi^{-}\}\right], \qquad (2.6)$$

$$\frac{dg_0}{dt} + \sqrt{\beta_i}\nabla_\parallel \frac{g_1}{\sqrt{2}} = 0, \tag{2.7}$$

$$\frac{dg_1}{dt} + \sqrt{\beta_i}\nabla_\parallel \left(g_2 + \frac{1 - 1/\Lambda}{\sqrt{2}}\, g_0 \right) = 0, \tag{2.8}$$

$$\frac{dg_m}{dt} + \sqrt{\beta_i}\nabla_\parallel \left(\sqrt{\frac{m+1}{2}}\, g_{m+1} + \sqrt{\frac{m}{2}}\, g_{m-1} \right)$$

$$= -\nu m g_m, \quad m \geq 2, \tag{2.9}$$

where

$$\frac{d}{dt} = \frac{\partial}{\partial t} + \{\Phi, \ldots\}, \quad \nabla_\parallel = \frac{\partial}{\partial z} + \{\Psi, \ldots\}, \tag{2.10}$$

$$\Phi = \frac{\xi^+ + \xi^-}{2}, \quad \Psi = \frac{\xi^+ - \xi^-}{2}, \tag{2.11}$$

and $\beta_i = 8\pi n_{0i} T_i / B_0^2$ is the ion plasma beta, n_{0i} is the equilibrium ion density, T_i is the equilibrium ion temperature, and B_0 is the magnitude of the background magnetic field.

2.4 Algorithm

We solve Eqs. (2.6–2.9) using a pseudo-spectral scheme. The Elsasser fields $\xi^\pm$, and the Hermite moments g_m are expressed in terms of Fourier modes. The nonlinear term is calculated in the real space by taking fast Fourier transforms using the CUDA FFT library. After transforming back to Fourier space, the nonlinear term is dealiased according to the Orszag $2/3^{\text{rd}}$ dealiasing rule [81]. The time integration for the linear term in Eq. (2.6) is done analytically using an integrating factor technique (discussed below); the nonlinear term is integrated using second-order Runge-Kutta

scheme[‡].

Consider the Fourier transform of Eq. (2.6),

$$\frac{\partial \xi^{\pm}}{\partial t} \mp i k_z \xi^{\pm} = \frac{1}{k_\perp^2} \left[\mathrm{NL}\right], \tag{2.12}$$

where [NL] are all the nonlinear terms. The $k_x = 0, k_y = 0$ mode is decoupled from all the other Fourier modes, and is not included in our simulations. Multiply throughout by $e^{-ik_z t}$,

$$\frac{\partial \left(\xi^{\pm} e^{\mp i k_z t}\right)}{\partial t} = e^{\mp i k_z t} \frac{1}{k_\perp^2} \left[\mathrm{NL}\right]. \tag{2.13}$$

Eqs. (2.13) and (2.4) are then discretized in time and solved as follows:

1. Take a half time-step:

$$\xi^{\pm,n+1/2} = e^{\pm i k_z \delta t/2} \xi^{\pm,n} + e^{\pm i k_z \delta t/2} \frac{1}{k_\perp^2} \left[\mathrm{NL}\right]^n, \tag{2.14}$$

$$g_0^{n+1/2} = g_0^n - \frac{\delta t}{2} \left[\{\Phi^n, g_0^n\} + \frac{i k_z \sqrt{\beta_i}}{\sqrt{2}} g_1^n + \sqrt{\beta_i} \left\{ \Psi^n, \frac{g_1^n}{\sqrt{2}} \right\} \right], \tag{2.15}$$

$$\begin{aligned} g_1^{n+1/2} = g_1^n - \frac{\delta t}{2} \Bigg[\{\Phi^n, g_1^n\} + i k_z \sqrt{\beta_i} \left(g_2^n + (1 - 1/\Lambda) \frac{g_0^n}{\sqrt{2}} \right) \\ + \sqrt{\beta_i} \left\{ \Psi^n, \left(g_2^n + (1 - 1/\Lambda) \frac{g_0^n}{\sqrt{2}} \right) \right\} \Bigg], \end{aligned} \tag{2.16}$$

[‡]This choice was made for ease of numerical implementation, and due to memory constraints on the GPU. The unconditionally unstable nature of RK2 is mollified by choosing a small time-step. The RK2 time-stepping scheme can be easily improved upon, which we hope to do in the near future.

$$g_m^{n+1/2} = g_m^n - \frac{\delta t}{2}\left[\{\Phi^n, g_m^n\} + ik_z\sqrt{\beta_i}\left(\frac{\sqrt{m+1}}{2}g_{m+1}^n + \frac{\sqrt{m}}{2}g_{m-1}^n\right)\right.$$
$$\left. + \sqrt{\beta_i}\left\{\Psi^n, \left(\frac{\sqrt{m+1}}{2}g_{m+1}^n + \frac{\sqrt{m}}{2}g_{m-1}^n\right)\right\}\right], \quad (2.17)$$

where the superscript denotes the time index.

2. Calculate nonlinear terms at the half time-step:

$$[\mathrm{NL}]^{n+1/2} = -\frac{1}{2}\left[\{\xi^{+,n+1/2}, \nabla_\perp^2 \xi^{-,n+1/2}\} + \{\xi^{-,n+1/2}, \nabla_\perp^2 \xi^{+,n+1/2}\}\right.$$
$$\left. \mp \nabla_\perp^2\{\xi^{+,n+1/2}, \xi^{-,n+1/2}\}\right]. \quad (2.18)$$

3. Take a full time-step using the nonlinear term calculated in the previous step:

$$\xi^{\pm,n+1} = e^{\pm ik_z\delta t}\xi^{\pm,n} + e^{\pm ik_z\delta t}\frac{1}{k_\perp^2}[\mathrm{NL}]^{n+1/2}. \quad (2.19)$$

$$g_0^{n+1} = g_0^n - \delta t\left[\left\{\Phi^{n+1/2}, g_0^{n+1/2}\right\} + \frac{ik_z\sqrt{\beta_i}}{\sqrt{2}}g_1^{n+1/2} + \sqrt{\beta_i}\left\{\Psi^{n+1/2}, \frac{g_1^{n+1/2}}{\sqrt{2}}\right\}\right], \quad (2.20)$$

$$g_1^{n+1} = g_1^n - \delta t\left[\left\{\Phi^{n+1/2}, g_1^{n+1/2}\right\} + ik_z\sqrt{\beta_i}\left(g_2^{n+1/2} + (1-1/\Lambda)\frac{g_0^{n+1/2}}{\sqrt{2}}\right)\right.$$
$$\left. + \sqrt{\beta_i}\left\{\Psi^{n+1/2}, \left(g_2^{n+1/2} + (1-1/\Lambda)\frac{g_0^{n+1/2}}{\sqrt{2}}\right)\right\}\right], \quad (2.21)$$

$$g_m^{n+1} = g_m^n - \frac{\delta t}{2}\left[\left\{\Phi^{n+1/2}, g_m^{n+1/2}\right\} + ik_z\sqrt{\beta_i}\left(\frac{\sqrt{m+1}}{2}g_{m+1}^{n+1/2} + \frac{\sqrt{m}}{2}g_{m-1}^{n}\right)\right.$$
$$\left. + \sqrt{\beta_i}\left\{\Psi^{n+1/2}, \left(\frac{\sqrt{m+1}}{2}g_{m+1}^{n+1/2} + \frac{\sqrt{m}}{2}g_{m-1}^{n+1/2}\right)\right\}\right]. \tag{2.22}$$

4. Integrate the dissipative terms (collisions and diffusion) using the same integrating factor technique as above:

$$\xi^{\pm} \to \xi^{\pm} \exp\left(-\eta k_\perp^2 \delta t\right), \tag{2.23}$$

$$g_0 \to g_0 \exp\left(-\eta k_\perp^2 \delta t\right), \quad g_1 \to g_1 \exp\left(-\eta k_\perp^2 \delta t\right), \tag{2.24}$$

$$g_m \to g_m \exp\left(-\eta k_\perp^2 \delta t - \nu m \delta t\right), \quad m \geq 2. \tag{2.25}$$

Since each Hermite moment is coupled to the next one, a suitable closure is required for the last retained Hermite moment, g_M. Two simple closures have been implemented: $g_{M+1} = 0$ and $g_{M+1} = g_{M-1}$. When the collisions are set high enough so that there is negligible energy in the last Hermite moment, the results are independent of the particular choice of closure. Throughout this thesis, we use the $g_{M+1} = 0$ closure, along with finite collisions.

Due to the explicit nature of the numerical scheme, the time step is restricted by a Courant-Friedrichs-Lewy condition:

$$\delta t = \frac{C}{\sqrt{M}} \times \text{Min}\left\{\frac{1}{k_{x,\max}\text{Max}\left\{|k_y\xi^{\pm}|\right\}}, \frac{1}{k_{y,\max}\text{Max}\left\{|k_x\xi^{\pm}|\right\}}\right\}, \tag{2.26}$$

where C is a positive constant less than one, specified by the user.

2.5 Additional features

2.5.1 Forcing

A Gaussian white noise source has been implemented in order to study driven turbulence. The two Elsasser fields are driven using the same source—this ensures that only the velocity field $\mathbf{u}_\perp = \hat{\mathbf{z}} \times \nabla\Phi$ is forced, and there is no artifical large-scale reconnection. The slow modes are driven independently by forcing the zeroth and/or the first moment. The slow modes can also be be driven by injecting energy into the field strength fluctuations—this physically corresponds to an external antenna that drives a perpendicular current in the plasma. The slow modes are driven at specified wavenumbers (k_x, k_y, k_z)[§].

2.5.2 Hyper-dissipation

Theories of turbulence generally give predictions for wavenumbers far from forcing and disipation scales, *i.e.*, in the inertial range. The range of such wavenumbers may be estimated roughly as the ratio between the forcing and the dissipation scales, and hence is limited by resolution constraints. To maximize this range, we employ hyper-diffusion ($-\eta k_\perp^{2r}$) and hyper-collisions ($-\nu m^{2n}$) instead of regular diffusion ($-\eta k_\perp^2$) or collisions ($-\nu m$); r and n are positive integers. Such

[§]Due to the Alfvénic turbulence, the total magnetic field is not the same as the background magnetic field, $\mathbf{B} = B_0\hat{\mathbf{z}} + \delta\mathbf{B}_\perp$. As a result, the wavenumber k_z is not necessarily same as the wavenumber along the total field $k_\parallel$. The implemented forcing routine does not check for what $k_\parallel$ values are being forced.

hyper-dissipation operators restrict the dissipation range to a very narrow set of wavenumbers, and help the user simulate a large inertial range at a lower computational cost [82–86]. Typically, in this thesis, $r = 4$ and $n = 4$ were used. For the KRMHD simulations in Chapter 6, $r = 8$ was used.

2.5.3 Diagnostics

Gandalf writes out the following diagnostic data every few time-steps:

- For the Alfvénic fluctuations, we calculate the kinetic $|k_\perp^2 \Phi^2|$ and magnetic $|k_\perp^2 \Psi^2|$ energy spectra as functions of $k_\perp$ and $k_\parallel$. For slow modes, the energy spectrum $|g_m^2|$ is a function of $k_\perp$, $k_\parallel$ and m.

  Energy at a particular perpendicular wavenumber $k_\perp = \sqrt{k_x^2 + k_y^2}$ is calculated by summing over shells. A mode at k_x, k_y contributes to the spectrum at $k_\perp$, if and only if, $k_\perp - 0.5 \leq \sqrt{k_x^2 + k_y^2} < k_\perp + 0.5$. The wavenumber $k_\parallel$, is the parallel wavenumber calculated along the local mean field. That is to say, $k_\parallel$ includes the perpendicular perturbation:

$$\hat{\mathbf{b}} \cdot \nabla = \frac{\partial}{\partial z} + \{\Psi, \ldots\}\,, \tag{2.27}$$

  and is not same as k_z. The distinction between k_z and $k_\parallel$ is important, because the two terms in Eq. (2.27) appear at the same order in the gyrokinetic ordering. Since particles are not aware of the split between the background and fluctuating magnetic fields, and always experience the total magnetic field, $k_\parallel$ is the more physical choice for a parallel wavenumber. We calculate the

$k_\parallel$ dependence of the spectra by following the exact field lines through our numerical box, and interpolating fluctuations along these field lines. This is done as follows:

1. Transform all the fluctuations from Fourier space to real space.

2. Pick an initial position x_0, y_0 at one end of the box, say $z_0 = -Lz/2$, where L_z is the length of the box in the z direction.

3. Calculate the perturbations $\mathbf{u}_\perp = \hat{\mathbf{z}} \times \Phi$, $\delta\mathbf{B}_\perp = \hat{\mathbf{z}} \times \Psi$ and g_m at $x = x_0, y = y_0, z = z_0$, using bilinear interpolation[¶].

4. Take a half step forward along the field line:

$$x_{1/2} = x_0 + \delta B_x \, \Delta z/2, \quad y_{1/2} = y_0 + \delta B_y \, \Delta z/2, \quad z_{1/2} = z_0 + \Delta z/2, \tag{2.28}$$

   where $\Delta z = L_z/k_{z,max}$ is the spacing-in-z between nearby grid points in real space.

5. Calculate the magnetic field perturbation $\delta\mathbf{B}_\perp$ at $x_{1/2}, y_{1/2}, z_{1/2}$ using bilinear interpolation.

6. Take a full step forward along the field line using the value of the magnetic field at $x_{1/2}, y_{1/2}, z_{1/2}$:

$$x_1 = x_0 + \delta B_x \, \Delta z, \quad y_1 = y_0 + \delta B_y \, \Delta z, \quad z_1 = z_0 + \Delta z. \tag{2.29}$$

[¶]This choice of interpolation scheme is sufficient for our purposes. A better scheme, like cubic splines could be easily implemented.

7. If $z_1 < L_z/2$, copy over the positions: $x_0 \leftarrow x_1$, $y_0 \leftarrow y_1$, $z_0 \leftarrow z_1$, and repeat from step 3.

8. Once the fluctuations $\mathbf{u}_\perp$, $\delta\mathbf{B}_\perp$ and g_m are known along the exact field lines, transform them back to Fourier space. The parallel wavenumber is this space is, in fact, $k_\parallel$.

9. Calculate the spectra as functions of $k_\perp$ and $k_\parallel$ by summing over shells, as discussed above.

A related, somewhat subtle issue is that of periodicity of the magnetic field lines. It is observed that the magnetic field lines that are initially periodic—say, for a driven simulation—naturally become aperiodic due to the turbulence. It can be shown that the $k_\parallel = 0$ mode plays a crucial role in giving rise to this aperiodicity. However, we do not discuss this point further in this thesis.

- The flux of energy $\Gamma_{m,\mathbf{k}}$ from the m^{th} to the $(m+1)^{\text{st}}$ Hermite moment is calculated as

$$\Gamma_{m,\mathbf{k}} = -k_\parallel \sqrt{2(m+1)}\, \text{Im}\left[g_{m+1} g_m^\star\right]. \tag{2.30}$$

The derivation of this expression is discussed in detail in Sec. 3.4.4.

- For large values of m, a slow mode perturbation can be split into a phase mixing component that propagates from small to large m, and an phase unmixing component that propagates from large to small m (see Sec. 3.4.5). In *Gandalf*, we also calculate the spectra for these phase mixing and phase unmixing modes.

2.6 Code verification

2.6.1 Kinetic fluctuation-dissipation relations

In Chapter 3, we calculate the saturated amplitudes of a driven kinetic field that evolves according to the linearized Vlasov equation. The analytical predictions are compared with the numerical results obtained from *Gandalf* in Figs. 3.1 and B.1. The comparison shows good agreement.

Fig. 3.3 plots the phase mixing and phase unmixing spectra of the kinetic field versus m. The numerical spectra calculated using *Gandalf* agree with the analytical prediction. The dotted lines in Fig. 3.3 are not fits to the numerical spectra, but are the exact expressions from Eqs. (3.37) and (3.58), *i.e.*, the agreement between the numerics and the analytical predictions is not just for the scaling in m, but also for the overall level of the spectra.

These comparisons provide a solid linear benchmark for *Gandalf*.

2.6.2 Orszag-Tang test case

We present results from the well-known Orszag-Tang test case [87] for MHD simulations. The initial condition for this test is given by

$$\Phi = -2\left(\cos\left(2\pi\frac{x}{L_x}\right) + \cos\left(2\pi\frac{y}{L_y}\right)\right), \tag{2.31}$$

$$\Psi = \left(\cos\left(4\pi\frac{x}{L_x}\right) + 2\cos\left(2\pi\frac{y}{L_y}\right)\right). \tag{2.32}$$

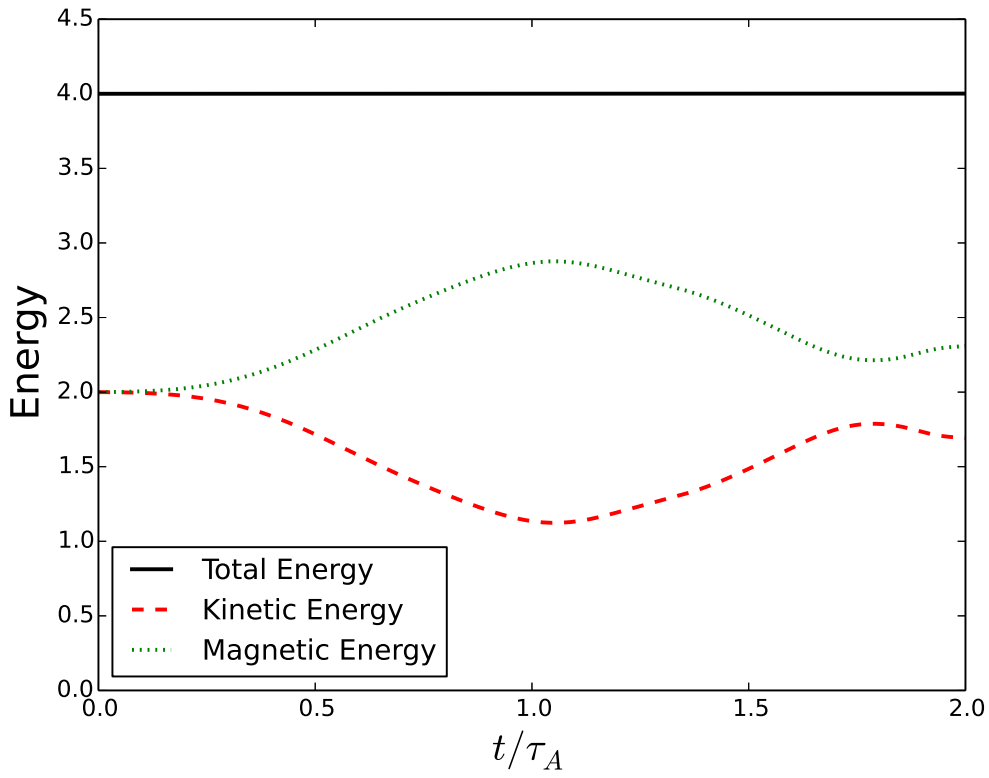

Figure 2.1: Time evolution of kinetic and magnetic energies for the Orszag-Tang test case.

We evolved this initial condition for two Alfvén times, using a $32^2 \times 1$ sized simulation domain. Fig. 2.1 plots the time evolution of kinetic and magnetic energies for the above initial condition, which is in qualitative agreement with the original results by Orszag and Tang.

2.6.3 Turbulent spectra for Alfvénic cascade

We simulated the reduced MHD equations for the simulation domains 64^3, and 128^3, with two different values for the hyper-diffusion exponent: $r = 4$ and $r = 8$. We ran these simulations till saturation, and then time-averaged the kinetic and magnetic energy spectra over two Alfvén times. These time-averaged spectra

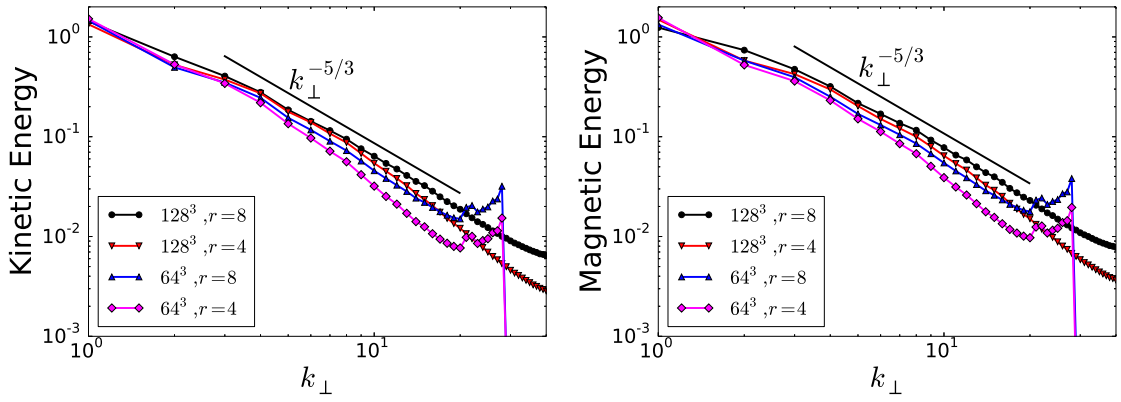

Figure 2.2: The kinetic (left) and magnetic (right) energy spectra for Alfvénic turbulent cascade. The four different lines correspond to four separate simulations—the first number is the resolution, and the second number is the exponent for the hyper-diffusion term (see Sec. 2.5.2). The spectra approach the critical-balance prediction of $k_\perp^{-5/3}$ for large resolution, and for large hyper-diffusion exponent.

are plotted in Fig. 2.2—they are in agreement with the critical-balance prediction of $k_\perp^{-5/3}$.

Chapter 3

Fluctuation-dissipation relations for a kinetic Langevin equation

3.1 Introduction

Fluctuation dissipation relations (FDR) predict the response of a dynamical system to an externally applied perturbation, based on the system's internal dissipation properties. The classical Langevin equation [88, 89] supplies the best known example of such FDR. The standard formulation is to consider a scalar φ forced by a Gaussian white-noise source χ and damped at the rate γ:

$$\begin{aligned} &\frac{\partial \varphi}{\partial t} + \gamma\varphi = \chi, \\ &\langle \chi(t)\chi(t')\rangle = \varepsilon\delta(t-t'), \end{aligned} \tag{3.1}$$

where angle brackets denote the ensemble average and $\varepsilon/2$ is the mean power injected into the system by the source:

$$\frac{\partial}{\partial t}\frac{\langle\varphi^2\rangle}{2} + \gamma\langle\varphi^2\rangle = \frac{\varepsilon}{2}. \tag{3.2}$$

The steady-state mean square fluctuation level is then given by the FDR, linking the injection and the dissipation of the scalar fluctuations:

$$\langle \varphi^2 \rangle = \frac{\varepsilon}{2\gamma}. \tag{3.3}$$

The simplest physical example of such a system is a Brownian particle suspended in liquid, with φ the velocity of the particle and γ the frictional damping. More generally, Eq. (3.1) may be viewed as a generic model for systems where some perturbed quantity is randomly stirred and decays via some form of linear damping, a frequently encountered situation in, e.g., fluid dynamics.

Nearly every problem in plasma physics involves a system with driven and damped linear modes. Here we consider the prototypical such case: the behavior of perturbations of a Maxwellian equilibrium in a weakly collisional plasma in one spatial and one velocity-space dimension. In such a system (and in weakly collisional or collisionless plasmas generally), damping of the perturbed electric fields occurs via the famous Landau mechanism [4]. Landau damping, however, is different in several respects from standard "fluid" damping phenomena. It is in fact a phase mixing process: electric—and, therefore, density—perturbations are phase mixed and thus are effectively damped (see Sec. 1.1). Their (free) energy is transferred to perturbations of the particle distribution function that develop ever finer structure in velocity space and are eventually removed by collisions or, in a formally collisionless limit, by some suitable coarse-graining procedure. The electrostatic potential φ in such systems cannot in general be rigorously shown to satisfy a "fluid" equation of

the form (3.1), with γ the Landau damping rate, although the idea that Eq. (3.1) or a higher-order generalization thereof is not a bad model underlies the so-called Landau-fluid closures [90–103].

It is a natural question to ask whether, despite the dynamical equations for φ (or, more generally, for the moments of the distribution function) being more complicated than Eq. (3.1), we should still expect the mean fluctuation level to satisfy Eq. (3.3), where γ is the Landau damping rate. And if that is not the case, then should the value of γ *defined* by Eq. (3.3) be viewed as the effective damping rate in a driven system, replacing the Landau rate? Plunk [39] recently considered the latter question and argued that the fact that the effective damping rate defined this way differs from the Landau rate suggests a fundamental modification of Landau response in a stochastic setting. Our take on the problem at hand differs from theirs somewhat in that we take the kinetic version of the Langevin equation (introduced in Sec. 3.2) at face value and derive the appropriate kinetic generalization of the FDR, instead of attaching a universal physical significance to the "fluid" version of it. Interestingly, the kinetic FDR does simplify to the classical fluid FDR when the Landau damping rate is small. Furthermore, we prove that in this limit (and when the system has no real frequency), the dynamics of φ is in fact described by Eq. (3.1) with γ equal precisely to the Landau rate (i.e., the simplest Landau fluid closure is a rigorous approximation in this limit). The latter result is obtained by treating the velocity-space dynamics of the system in Hermite space. We also show how phase mixing in our system can be treated as a free-energy flux in Hermite space, what form the FDR takes for the Hermite spectrum of the perturbations of the

distribution function, and how collisional effects can be included. The intent of this treatment is to provide a degree of clarity as to the behavior of a very simple plasma model and thus set the stage for modelling more complex, nonlinear phenomena.

In Sec. 3.2, we describe a simple model for a weakly collisional plasma, which we call the kinetic Langevin equation, and then, in Sec. 3.3, derive the FDR for the same, including the "fluid" limit mentioned above. In Sec. 3.4, Hermite-space dynamics are treated, including the limit where Landau-fluid closures hold rigorously. An itemized summary of our findings is given in Sec. 3.5. A version of the calculation with a different random source is presented in appendix B.

3.2 Kinetic Langevin equation

We consider the following (1+1)-dimensional model of a homogeneous plasma perturbed about a Maxwellian equilibrium:

$$\frac{\partial g}{\partial t} + \underbrace{v\frac{\partial g}{\partial z}}_{\text{phase mixing}} + \underbrace{vF_0\frac{\partial \varphi}{\partial z}}_{\text{electric field}} = \underbrace{\chi(t)F_0}_{\text{source}} + \underbrace{C[g]}_{\text{collisions}}, \tag{3.4}$$

$$\varphi = \alpha \int_{-\infty}^{\infty} \mathrm{d}v\, g, \tag{3.5}$$

$$\langle \chi(t)\chi(t')\rangle = \varepsilon\delta(t-t'),$$

where $g(z,v,t)$ is the perturbed distribution function and $F_0(v)$ is the Maxwellian equilibrium distribution $F_0 = e^{-v^2}/\sqrt{\pi}$. The velocity v (in the z direction) is normalized to the thermal speed $v_{\text{th}} = \sqrt{2T/m}$ (T and m are the temperature and mass of the particle species under consideration), spatial coordinate z is normalized

to an arbitrary length L, and time t to $L/v_{\rm th}$. Only one species (either electrons or ions) is evolved. The second species follows the density fluctuations of the first via whatever response a particular physical situation warrants: Boltzmann, isothermal, or no response—all of these possibilities are embraced by Eq. (3.5), which determines the (suitably normalized) scalar potential φ in terms of the perturbed density associated with g; the parameter α contains all of the specific physics. For example, if g is taken to be the perturbed ion distribution function in a low-beta magnetized plasma and electrons to have Boltzmann response, then $\alpha = ZT_e/T_i$, the ratio of the electron to ion temperatures (Z is the ion charge in units of electron charge e)—the resulting system describes (Landau-damped) ion-acoustic waves; Eq. (3.5) in this case is the statement of quasineutrality. Another, even more textbook example is damped Langmuir waves, the case originally considered by Landau [4]: g is the perturbed electron distribution function, ions have no response, so $\alpha = 2/k^2\lambda_D^2$, where λ_D is the Debye length and k is the wave number of the perturbation ($\partial/\partial z = ik$); Eq. (3.5) in this case is the Gauss-Poisson law.

A particularly astrophysically and space-physically relevant example (in the sense of being accessible to measurements in the solar wind [3,30,31,34,35,104]) is the compressive perturbations in a magnetized plasma—perturbations of plasma density and magnetic-field strength at scales long compared to the ion Larmor radius (see KRMHD equations in Sec. 1.5). The model given by Eqs. (3.4–3.5) can be obtained from KRMHD by setting the Alfvén fluctuations to zero, adding a source term, and defining the parameter $\alpha = -1/\Lambda$ (see Eq. (1.20)).

Thus, Eqs. (3.4) and (3.5) correspond a variety of interesting physical situa-

tions.

The energy injection in Eq. (3.4) is modelled by a white-in-time, Maxwellian-in-velocity-space source $\chi(t)F_0$ supplying fixed power $\propto \varepsilon$ to the perturbations (see below). This is a direct analog of the noise term in the "fluid" Langevin equation (3.1) and so this particular choice of forcing was made in order to enable the simplest possible comparison with the "fluid" case*. The energy injection leads to sharp gradients in the velocity space (phase mixing), which are removed by the collision operator $C[g]$. "The energy" in the context of a kinetic equation is the free energy of the perturbations [1, 16] (see Eq. (1.24)), given in this case by

$$W = \int \mathrm{d}v \, \frac{\langle g^2 \rangle}{2F_0} + \frac{\langle \varphi^2 \rangle}{2\alpha} \tag{3.6}$$

and satisfying

$$\frac{\mathrm{d}W}{\mathrm{d}t} = \frac{1+\alpha}{2}\,\varepsilon + \int \mathrm{d}v \, \frac{gC[g]}{F_0}. \tag{3.7}$$

The first term on the right-hand side is the energy injection by the source, the second, negative definite term is its thermalization by collisions. Note that the variance of φ is not by itself a conserved quantity:

$$\frac{\mathrm{d}}{\mathrm{d}t}\frac{\langle \varphi^2 \rangle}{2} + \alpha \left\langle \varphi \frac{\partial}{\partial z} \int \mathrm{d}v \, vg \right\rangle = \frac{\alpha^2}{2}\,\varepsilon. \tag{3.8}$$

*One might argue that this is not, however, the most physical form of forcing and that it would be better to inject energy by applying a random electric field to the plasma, rather than a source of density perturbations. In appendix B we present a version of our calculation for such a more physical source, and show that all the key results are similar. Note that the forcing in Eq. (3.4) does not violate particle conservation because we assume that spatial integrals of all perturbations vanish: $\int \mathrm{d}z \, g = 0$, $\int \mathrm{d}z \, \chi = 0$.

The power $\alpha^2\varepsilon/2$ injected into fluctuations of φ is transferred into higher moments of g via phase mixing. Phase mixing is precisely this process of draining free energy from the lower moments and transferring it into higher moments of the distribution function—without collisions, this is just a redistribution of free energy within Eq. (3.6), which, in the absence of source, would look like a linear damping of φ[†].

In the presence of a source, the system described by Eqs. (3.4) and (3.5) is a driven-damped system much like the Langevin equation (3.1). The damping of φ in the kinetic case is provided by Landau damping (phase mixing) as opposed to the explicit dissipation term in Eq. (3.1). It is an interesting question whether in the steady state, the second term on the left-hand side of Eq. (3.8) can be expressed as $\gamma_{\text{eff}}\langle\varphi^2\rangle$, leading an analogue of the FDR (Eq. (3.3)), and if so, whether the "effective damping rate" γ_{eff} in this expression is equal to the Landau damping rate γ_L. The answer is that an analogue of the FDR does exist, γ_{eff} is non-zero for vanishing collisionality, but in general, $\gamma_{\text{eff}} \neq \gamma_L$.

3.3 Kinetic Fluctuation-Dissipation Relations

Ignoring collisions in Eq. (3.4) and Fourier-transforming it in space in time, we get

$$g_{k\omega} = -\varphi_{k\omega}\frac{vF_0}{v-\omega/k} - \frac{i\chi_{k\omega}}{k}\frac{F_0}{v-\omega/k}. \tag{3.9}$$

[†]Note that $\alpha = -1$ corresponds to an effectively undriven system; the Landau damping rate for this case is zero (Eq. (3.16)). We will see in Sec. 3.4.1 that in this case the driven density moment decouples from the rest of the perturbed distribution function; see Eq. (3.27). For $\alpha < -1$ the system is no longer a driven-damped system; this parameter regime never occurs physically.

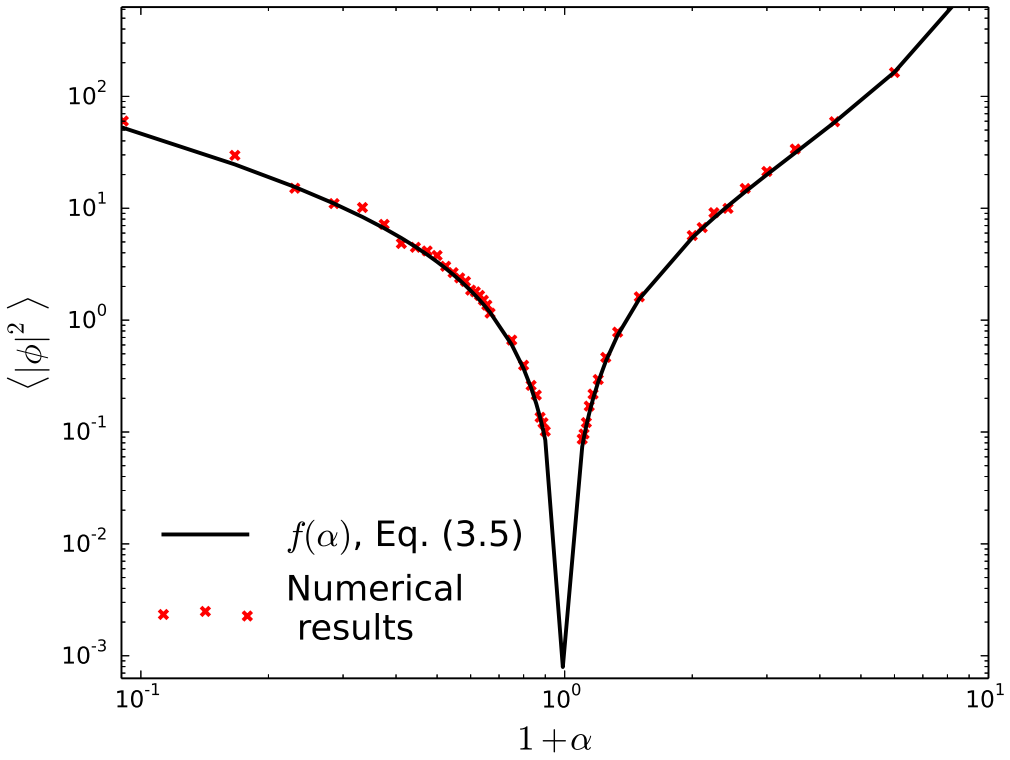

Figure 3.1: Normalized steady-state amplitude $2\pi|k|\langle|\varphi_k|^2\rangle/\varepsilon_k = f(\alpha)$ vs. $1+\alpha$: the solid line is the analytical prediction ($f(\alpha)$ as per Eq. (3.13)), the crosses are computed from the long-time limit of $\langle|\varphi_k|^2\rangle$ obtained via direct numerical solution of Eqs. (3.4) and (3.5).

Introducing the plasma dispersion function $Z(\zeta) = \int \mathrm{d}v F_0/(v-\zeta)$, where the integration is along the Landau countour [105], we find from Eqs. (3.9) and (3.5):

$$\varphi_{k\omega} = -\frac{i\chi_{k\omega}}{|k|}\frac{Z(\omega/|k|)}{D_\alpha(\omega/|k|)}, \tag{3.10}$$

$$D_\alpha\left(\frac{\omega}{|k|}\right) = 1 + \frac{1}{\alpha} + \frac{\omega}{|k|}Z\left(\frac{\omega}{|k|}\right). \tag{3.11}$$

Note that $D_\alpha(\omega/|k|) = 0$ is the dispersion relation for the classic Landau problem [4]. We now inverse Fourier transform Eq. (3.10) back into the time domain,

$$\varphi_k(t) = \int \mathrm{d}\omega\, e^{-i\omega t}\varphi_{k\omega} = -\frac{i}{|k|}\int \mathrm{d}\omega\, e^{-i\omega t}\chi_{k\omega}\frac{Z(\omega/|k|)}{D_\alpha(\omega/|k|)}, \tag{3.12}$$

and compute $\langle|\varphi_k|^2\rangle$ in the steady state. In order to do this, we use the fact that $\chi_{k\omega} \equiv \int \mathrm{d}t e^{i\omega t}\chi_k(t)/2\pi$ satisfies $\langle\chi_{k\omega}\chi^*_{k\omega'}\rangle = \varepsilon_k\delta(\omega-\omega')/2\pi$ because $\langle\chi_k(t)\chi^*_k(t')\rangle = \varepsilon_k\delta(t-t')$, where ε_k is the source power at wave number k. The result is

$$\langle|\varphi_k|^2\rangle = \frac{\varepsilon_k}{2\pi|k|}f(\alpha), \quad f(\alpha) = \int_{-\infty}^{+\infty}\mathrm{d}\zeta\left|\frac{Z(\zeta)}{D_\alpha(\zeta)}\right|^2, \tag{3.13}$$

where we have changed the integration variable to $\zeta = \omega/|k|$. This is the fluctuation-dissipation relation for our kinetic system that predicts the long-time behavior of the electrostatic potential. The function $f(\alpha)$, computed numerically as per Eq. (3.13), is plotted in Fig. 3.1, together with the results of direct numerical solution of Eqs. (3.4) and (3.5), in which $f(\alpha)$ is found by computing the saturated fluctuation level $\langle|\varphi_k|^2\rangle$.

Eq. (3.13) can be written in the form

$$\langle|\varphi_k|^2\rangle = \frac{\alpha^2\varepsilon_k}{2\gamma_{\rm eff}}, \quad \gamma_{\rm eff}(\alpha) = \frac{\pi\alpha^2}{f(\alpha)}|k|, \tag{3.14}$$

but the "effective damping rate" $\gamma_{\rm eff}$ is not in general the same as the Landau damping rate γ_L. This is illustrated in Fig. 3.2, where we plot the real (ω_L) and imaginary ($-\gamma_L$) parts of the slowest-damped root(s) of $D_\alpha(\omega/|k|) = 0$ together with $\gamma_{\rm eff}(\alpha)$ for $\alpha < 0$ and $\gamma_{\rm eff}(\alpha)/2$ for $\alpha > 0$. In the latter case, the linear modes of the system have real frequencies and the analogy with the Langevin equation (3.1) is not apt—a better mechanical analogy is a damped oscillator, as explained at the end of Sec. 3.3.2; the FDR in this case acquires an extra factor of 1/2, which is why we plot $\gamma_{\rm eff}/2$ (see Eq. (3.23)). Remarkably, $\gamma_{\rm eff}(\alpha)$ does asymptote to γ_L in the limit $1 + \alpha \ll 1$ and to $2\gamma_L$ in the limit $\alpha \to \infty$, i.e., when the damping is weak. These asymptotic results can be verified analytically.

3.3.1 Zero real frequency, weak damping ($\alpha \to -1$)

When $\alpha+1 \ll 1$, the solution of the dispersion relation will satisfy $\zeta = \omega/|k| \ll 1$. In this limit,

$$Z(\zeta) \approx i\sqrt{\pi}, \quad D_\alpha(\zeta) \approx 1 + \frac{1}{\alpha} + i\zeta\sqrt{\pi} \approx i\sqrt{\pi}\left(\zeta - i\frac{1+\alpha}{\sqrt{\pi}}\right). \tag{3.15}$$

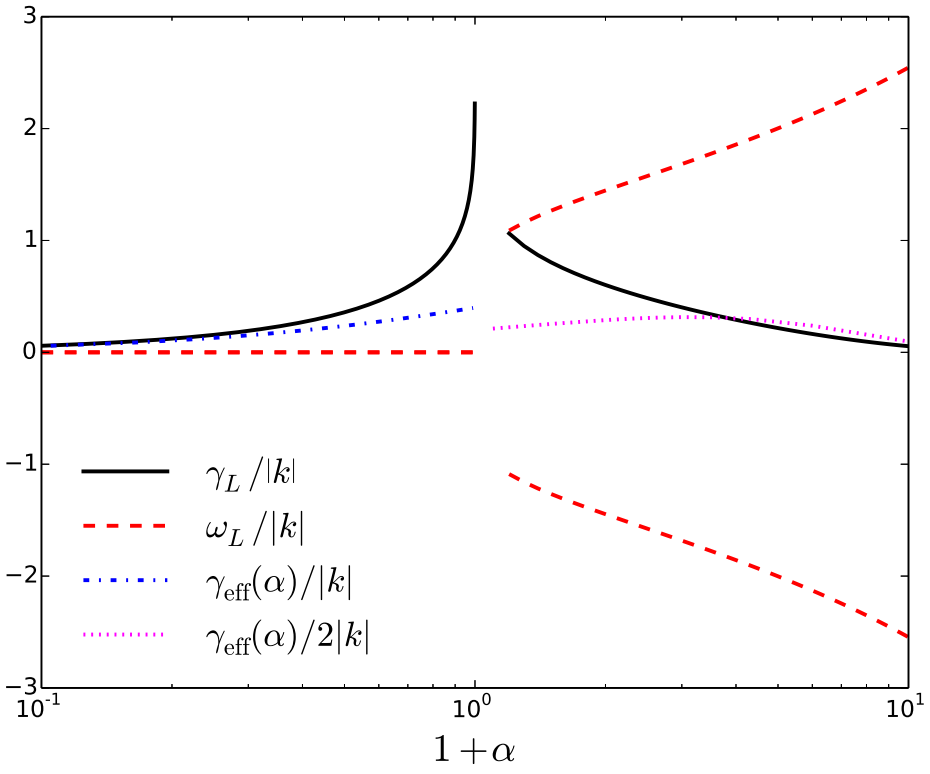

Figure 3.2: Slowest-damped solutions of the dispersion relation $D_\alpha(\omega/|k|) = 0$: normalized frequency $\omega_L/|k|$ (red dashed line) and damping rate $\gamma_L/|k|$ (black soloid line) vs. $1+\alpha$. Also shown are $\gamma_{\rm eff}(\alpha)$ for $\alpha < 0$ (blue dash-dotted line) and $\gamma_{\rm eff}(\alpha)/2$ for $\alpha > 0$ (magenta dotted line), as per Eq. (3.14). The two asymptotic limits in which these match γ_L are discussed in Secs. 3.3.1 and 3.3.2.

Therefore, the solution of $D_\alpha(\omega/|k|) = 0$ is

$$\omega \approx -i\gamma_L, \quad \gamma_L = \frac{1+\alpha}{\sqrt{\pi}}|k|. \tag{3.16}$$

A useful physical example of Landau damping in this regime is the Barnes damping [38] of compressive fluctuations in high-beta plasmas, where $1 + \alpha \approx 1/\beta_i$ (see Schekochihin et al [1], their eq. (190)).

Since the zeros of $D_\alpha(\zeta)$ and $D^*_\alpha(\zeta)$, which are poles of the integrand in the expression for $f(\alpha)$ (Eq. (3.13)), lie very close to the real line in this case, the integral is easily computed by using the approximate expressions (3.15) for $Z(\zeta)$ and $D_\alpha(\zeta)$ and applying Plemelj's formula, to obtain

$$f(\alpha) \approx \frac{\pi\sqrt{\pi}}{1+\alpha} = \frac{\pi|k|}{\gamma_L} \quad \Rightarrow \quad \langle|\varphi_k|^2\rangle \approx \frac{\sqrt{\pi}\varepsilon_k}{2(1+\alpha)|k|} = \frac{\varepsilon_k}{2\gamma_L}. \tag{3.17}$$

Noting that $\alpha^2 \approx 1$, this is the same as Eq. (3.14) with $\gamma_{\text{eff}} = \gamma_L$, so the "fluid" FDR is recovered. Note, however, that this recovery of the exact form of the "fluid" FDR is a property that is not universal with respect to the exact form of energy injection: as shown in appendix B, it breaks down for a different forcing (see Eq. (B.14)).

3.3.2 Large real frequency, weak damping ($\alpha \to \infty$)

Another analytically tractable limit is $\alpha \gg 1$, in which case the solutions of the dispersion relation have $\zeta = \omega/|k| \gg 1$. In this limit,

$$Z(\zeta) \approx i\sqrt{\pi}\, e^{-\zeta^2} - \frac{1}{\zeta} - \frac{1}{2\zeta^3}, \quad D_\alpha(\zeta) \approx \frac{1}{\alpha} - \frac{1}{2\zeta^2} + i\sqrt{\pi}\,\zeta e^{-\zeta^2}. \tag{3.18}$$

The solutions of $D_\alpha(\omega/|k|) = 0$ are

$$\omega \approx \pm\sqrt{\frac{\alpha}{2}}\,|k| - i\gamma_L, \quad \gamma_L = \sqrt{\pi}\,\frac{\alpha^2}{4}\,e^{-\alpha/2}|k|. \tag{3.19}$$

Two textbook examples of Landau-damped waves in this regime are ion acoustic waves at $\beta_i \ll 1$, $T_i \ll T_e$ (cold ions), for which $\alpha = ZT_e/T_i$, and long-wavelength Langmuir waves, for which $\alpha = 2/k^2\lambda_D^2$ [4].

In the integral in Eq. (3.13), the poles are again very close to the real line and so in the integrand, we may approximate, in the vicinity of one of the two solutions (3.19)

$$Z(\zeta) \approx \mp\sqrt{\frac{2}{\alpha}}, \quad D_\alpha(\zeta) \approx \pm\left(\frac{2}{\alpha}\right)^{3/2}\left(\zeta \mp \sqrt{\frac{\alpha}{2}} + i\,\frac{\gamma_L}{|k|}\right). \tag{3.20}$$

Using again Plemelj's formula and noting that equal contributions arise from each of the two roots, we find

$$f(\alpha) \approx 2\sqrt{\pi}\,e^{\alpha/2} = \frac{\pi\alpha^2|k|}{2\gamma_L} \quad \Rightarrow \quad \langle|\varphi_k|^2\rangle \approx \frac{\alpha^2\varepsilon_k}{4\gamma_L}, \tag{3.21}$$

which is the same as Eq. (3.14) with $\gamma_{\text{eff}} = 2\gamma_L$.

Despite the apparently discordant factor of 2, this, in fact, is again consistent with a non-kinetic, textbook FDR. However, since we are considering a system with a large frequency, the relevant mechanical analogy is not Eq. (3.1), but the equally standard (and more general) equation for a forced and damped oscillator:

$$\ddot{\varphi} + \gamma\dot{\varphi} + \omega^2\varphi = \dot{\chi}, \tag{3.22}$$

where overdots mean time derivatives.

We continue to consider χ a Gaussian white noise satisfying $\langle\chi(t)\chi(t')\rangle = \varepsilon\delta(t-t')$. For $\omega = 0$, Eq. (3.22) then precisely reduces to Eq. (3.1). For $\omega \neq 0$, it is not hard to show (by Fourier transforming in time, solving, then inverse Fourier transforming and squaring the amplitude) that the stationary mean square amplitude $\langle\varphi^2\rangle$ for Eq. (3.22) still satisfies Eq. (3.3). However, the relationship between the actual linear damping rate γ_L of φ and the parameter γ depends on the frequency: $\gamma_L = \gamma$ when $\omega \ll \gamma$ and $\gamma_L = \gamma/2$ when $\omega \geq \gamma/2$. In the latter case, which is the one with which we are preoccupied here, Eq. (3.3) becomes, in terms of γ_L:

$$\langle\varphi^2\rangle = \frac{\varepsilon}{4\gamma_L}. \tag{3.23}$$

The required extra factor of 2 is manifest.[‡]

[‡]As in Sec. 3.3.1, this very simple mechanical analogy also breaks down for a different choice of forcing; see appendix B (Eq. (B.15)).

3.4 Velocity-space structure

The kinetic FDR derived in the previous section was concerned with the rate of removal of free energy from the density moment of the perturbed distribution function. This free energy flows into higher moments, i.e., is "phase mixed" away. In this section, we diagnose the velocity-space structure of the fluctuations and extend the FDR to compute their amplitude.

3.4.1 Kinetic equation in Hermite space

The emergence of ever finer velocity-space scales is made explicit by recasting the kinetic equation (3.4) in Hermite space, a popular approach for many years [40, 106–114]. The distribution is decomposed into Hermite moments as follows

$$g(v) = \sum_{m=0}^{\infty} \frac{H_m(v) F_0}{\sqrt{2^m m!}} g_m, \quad g_m = \int \mathrm{d}v \, \frac{H_m(v)}{\sqrt{2^m m!}} \, g(v), \tag{3.24}$$

where $H_m(v)$ is the Hermite polynomial of order m. In terms of Hermite moments, Eq. (3.5) becomes

$$\varphi = \alpha g_0, \tag{3.25}$$

while Eq. (3.4) turns into a set of equations for the Hermite moments g_m, where phase mixing is manifested by the coupling of higher-m moments to the lower-m

ones:

$$\frac{\partial g_0}{\partial t} + \frac{\partial}{\partial z}\frac{g_1}{\sqrt{2}} = \chi, \tag{3.26}$$

$$\frac{\partial g_1}{\partial t} + \frac{\partial}{\partial z}\left(g_2 + \frac{1+\alpha}{\sqrt{2}}\, g_0\right) = 0, \tag{3.27}$$

$$\frac{\partial g_m}{\partial t} + \frac{\partial}{\partial z}\left(\sqrt{\frac{m+1}{2}}\, g_{m+1} + \sqrt{\frac{m}{2}}\, g_{m-1}\right) = -\nu m g_m, \quad m \geq 2, \tag{3.28}$$

where ν is the collision frequency and we have used the [80] collision operator, a natural modelling choice in this context because its eigenfunctions are Hermite polynomials.

The free energy (3.6) in these terms is

$$W = \frac{1+\alpha}{2}\langle g_0^2\rangle + \frac{1}{2}\sum_{m=1}^{\infty}\langle g_m^2\rangle \tag{3.29}$$

and satisfies

$$\frac{\mathrm{d}W}{\mathrm{d}t} = \frac{1+\alpha}{2}\,\varepsilon - \nu\sum_{m=2}^{\infty} m\langle g_m^2\rangle. \tag{3.30}$$

3.4.2 Fluctuation-Dissipation Relations in Hermite space

It is an obvious generalization of the FDR to seek a relationship between the fluctuation level in the m-th Hermite moment, $\langle |g_m|^2\rangle$ (the "Hermite spectrum"), and the injected power ε. This can be done in exactly the same manner as the kinetic FDR was derived in Sec. 3.3. Hermite-transforming Eq. (3.9) gives

$$g_{m,k\omega} = -\frac{i\chi_{k\omega}}{|k|}\frac{1+\alpha}{\alpha}\frac{(-\operatorname{sgn} k)^m}{\sqrt{2^m m!}}\frac{Z^{(m)}(\omega/|k|)}{D_\alpha(\omega/|k|)}, \quad m \geq 1, \tag{3.31}$$

where we have used

$$Z^{(m)}(\zeta) \equiv \frac{\mathrm{d}^m Z}{\mathrm{d}\zeta^m} = (-1)^m \int \mathrm{d}v \, \frac{H_m(v) F_0(v)}{v - \zeta} \tag{3.32}$$

and $Z^{(m)}(\omega/k) = (\operatorname{sgn} k)^{m+1} Z^{(m)}(\omega/|k|)$. The mean square fluctuation level in the statistical steady state is then derived similarly to Eq. (3.13):

$$C_{m,k} \equiv \langle |g_{m,k}|^2 \rangle = \frac{\varepsilon_k}{2\pi|k|} \left(\frac{1+\alpha}{\alpha} \right)^2 \frac{1}{2^m m!} \int_{-\infty}^{+\infty} \mathrm{d}\zeta \left| \frac{Z^{(m)}(\zeta)}{D_\alpha(\zeta)} \right|^2, \quad m \geq 1. \tag{3.33}$$

This is the extension of the kinetic FDR, Eq. (3.13), to the fluctuations of the perturbed distribution function. The "Hermite spectrum" $C_{m,k}$ characterizes the distribution of free energy in phase space.

3.4.3 Hermite spectrum

It is interesting to derive the asymptotic form of this spectrum at $m \gg 1$. Using in Eq. (3.32) the asymptotic form of the Hermite polynomials at large m [115],

$$e^{-v^2/2} H_m(v) \approx \left(\frac{2m}{e} \right)^{m/2} \sqrt{2} \cos\left(v\sqrt{2m} - \pi m/2 \right), \tag{3.34}$$

and remembering that the v integration is over the Landau contour (i.e., along the real line, cicumnavigating the pole at $v = \zeta$ from below), we find

$$Z^{(m)}(\zeta) \approx i^{m+1} \sqrt{2\pi} \left(\frac{2m}{e} \right)^{m/2} e^{-\zeta^2/2 + i\zeta\sqrt{2m}}, \tag{3.35}$$

provided $\zeta \ll \sqrt{2m}$ (this result is obtained by expressing the cosine in Eq. (3.34) in terms of exponentials, completing the square in the exponential function appearing in the integral (3.32) and moving the integration contour to $v = \pm i\sqrt{2m}$; the dominant contribution comes from the Landau pole). Finally, in Eq. (3.33),

$$\frac{|Z^{(m)}(\zeta)|^2}{2^m m!} \approx \sqrt{\frac{2\pi}{m}}\, e^{-\zeta^2}, \tag{3.36}$$

and so the Hermite spectrum has a universal scaling at $m \gg 1$:

$$C_{m,k} \approx \left[\frac{\varepsilon_k}{\sqrt{2\pi}|k|}\left(\frac{1+\alpha}{\alpha}\right)^2 \int_{-\infty}^{+\infty} \frac{\mathrm{d}\zeta\, e^{-\zeta^2}}{|D_\alpha(\zeta)|^2}\right] \frac{1}{\sqrt{m}} = \frac{\varepsilon_k(1+\alpha)}{\sqrt{2}|k|}\frac{1}{\sqrt{m}}. \tag{3.37}$$

The universal $1/\sqrt{m}$ scaling was derived in a different way by Zocco et al. [112] (see Sec. 3.4.4; [111, 114]). The integral in (3.37) was evaluated using the Kramers–Kronig relations [116, 117] for the function $h(\zeta) = 1/D_\alpha(\zeta) - \alpha$ (which is analytic in the upper half plane and decays at least as fast as $1/|\zeta|^2$ at large ζ):

$$\int_{-\infty}^{+\infty} \frac{\mathrm{d}\zeta\, e^{-\zeta^2}}{|D_\alpha(\zeta)|^2} = -\sqrt{\pi}\left[\frac{1}{\pi}\,\mathcal{P}\int_{-\infty}^{+\infty} \frac{\mathrm{d}\zeta\, \mathrm{Im}\, h(\zeta)}{\zeta - \zeta'}\right]_{\zeta'=0} = -\sqrt{\pi}\,\mathrm{Re}\, h(0) = \frac{\alpha^2}{1+\alpha}\sqrt{\pi}. \tag{3.38}$$

Note that in the limit of high frequency ($\alpha \gg 1$, Sec. 3.3.2), the approximation (3.35) requires $\omega_L/|k| \ll \sqrt{2m}$, or $\alpha \ll 4m$, but there is also a meaningful intermediate range of m for which $1 \le m \ll \alpha/4$. In this range, we can approximate $Z(\zeta) \approx -1/\zeta$

and, since $\zeta \approx \pm\sqrt{\alpha/2}$, we have in Eq. (3.33):

$$\frac{|Z^{(m)}(\zeta)|^2}{2^m m!} \approx \frac{2m!}{\alpha^{m+1}} \quad \Rightarrow \quad C_{m,k} \approx \frac{\varepsilon_k}{\sqrt{\pi}|k|}\frac{m!}{\alpha^m}\, e^{\alpha/2}. \tag{3.39}$$

This spectrum decays with m up to $m \sim \alpha$, where it transitions into the universal spectrum (3.37).

3.4.4 Free-energy flux, the effect of collisions and the FDR for the total free energy

Observe that the total free energy in our system, with its $1/\sqrt{m}$ Hermite spectrum, is divergent. The regularization in Hermite space (removal of fine velocity-space scales) is provided by collisions. If ν is infinitesimal, these are irrelevant at finite m, but eventually become important as $m \to \infty$. To take account of their effect and to understand the free-energy flow in Hermite space, we consider Eq. (3.28), which it is convenient to Fourier transform in z and rewrite in terms of $\tilde{g}_{m,k} \equiv (i\,\mathrm{sgn}\,k)^m g_{m,k}$:

$$\frac{\partial \tilde{g}_{m,k}}{\partial t} + \frac{|k|}{\sqrt{2}}\left(\sqrt{m+1}\,\tilde{g}_{m+1,k} - \sqrt{m}\,\tilde{g}_{m-1,k}\right) = -\nu m \tilde{g}_{m,k}. \tag{3.40}$$

The Hermite spectrum $C_{m,k} = \langle |g_{m,k}|^2 \rangle = \langle |\tilde{g}_{m,k}|^2 \rangle$ therefore satisfies

$$\frac{\partial C_{m,k}}{\partial t} + \Gamma_{m+1/2,k} - \Gamma_{m-1/2,k} = -2\nu m C_{m,k}, \tag{3.41}$$

where $\Gamma_{m+1/2,k} = |k|\sqrt{2(m+1)}\mathrm{Re}\langle\tilde{g}_{m+1,k}\tilde{g}^*_{m,k}\rangle$ is the free-energy flux in Hermite space. If we make an assumption (verified in Sec. 3.4.5) that for $m \gg 1$ the Hermite moments $\tilde{g}_{m,k}$ are continuous in m, i.e., $\tilde{g}_{m+1,k} \approx \tilde{g}_{m,k}$, then

$$\Gamma_{m+1/2,k} \approx |k|\sqrt{2(m+1)}\, C_{m+1,k} \tag{3.42}$$

and Eq. (3.41) turns into a closed evolution equation for the Hermite spectrum [112]:

$$\frac{\partial C_{m,k}}{\partial t} + |k|\frac{\partial}{\partial m}\sqrt{2m}\, C_{m,k} = -2\nu m C_{m,k}. \tag{3.43}$$

The universal $C_{m,k} \propto 1/\sqrt{m}$ spectrum derived in Sec. 3.4.3 is now very obviously a constant-flux spectrum, reflecting steady pumping of free energy towards higher m's (phase mixing). The full steady-state solution of Eq. (3.43) including the collisional cutoff is

$$C_{m,k} = \frac{A_k}{\sqrt{m}}\, \exp\left(-\frac{2\sqrt{2}}{3}\frac{\nu}{|k|}m^{3/2}\right), \tag{3.44}$$

where A_k is an integration constant, which must be determined by matching this high-m solution with the Hermite spectrum at low m. This we are now in a position to do: for $1 \ll m \ll (\nu/|k|)^{-2/3}$, $C_{m,k} \approx A_k/\sqrt{m}$ and comparison with Eq. (3.37) shows that the constant A_k is the same as the constant $A_k(\alpha)$ in that equation. Thus, Eq. (3.44) with A_k given by Eq. (3.37) provides a uniformly valid expression for the Hermite-space spectrum, including the collisional cutoff (modulo the Hermite-space continuity assumption (3.42), which we will justify in Sec. 3.4.5).

As a check of consistency of our treatment, let us calculate the collisional

dissipation rate of the free energy. This is the second term on the right-hand side of Eq. (3.30). Since $C_{m,k} \propto 1/\sqrt{m}$ before the collisional cutoff is reached, the sum over m will be dominated by $m \sim (\nu/|k|)^{-2/3}$ and can be approximated by an integral:

$$\nu \sum_{m,k} m C_{m,k} \approx \sum_k \nu \int_0^\infty \mathrm{d}m \, m C_{m,k} = \sum_k \frac{A_k |k|}{\sqrt{2}}. \tag{3.45}$$

On the other hand, in steady state, Eq. (3.30) implies

$$\nu \sum_{m,k} m C_{m,k} = \frac{1+\alpha}{2} \, \varepsilon. \tag{3.46}$$

If energy injection is into a single k mode, $\varepsilon = \varepsilon_k$, comparing these two expressions implies

$$A_k = \frac{\varepsilon_k (1+\alpha)}{\sqrt{2}|k|}, \tag{3.47}$$

which, of course, is consistent with Eq. (3.37).

Finally, we use Eq. (3.44) to calculate (approximately) the total steady-state amount of free energy across the phase space:

$$\frac{1}{2} \sum_{m=1}^{\infty} C_{m,k} = \frac{\Gamma(1/3)}{\sqrt{2}\, 3^{2/3}} \frac{A_k}{(\nu/|k|)^{1/3}} = \frac{\Gamma(1/3)}{2 \cdot 3^{2/3}} \frac{1+\alpha}{\nu^{1/3} |k|^{2/3}} \, \varepsilon_k \tag{3.48}$$

(we have again approximated the sum with an integral, assumed energy injection into a single k and used Eq. (3.47)). Eq. (3.48) can be thought of as the FDR for the total free energy. The fact that this diverges as $\nu \to 0$ underscores the principle that the "true" dissipation (in the sense of free energy being thermalized) is always

collisional—a consequence of Boltzmann's H theorem.

3.4.5 Continuity in Hermite space

In this section, we make a somewhat lengthy formal digression to justify the assumption of continuity of Hermite moments in m at large m, which we need for the approximation (3.42). The formalism required for this will have some interesting features which are useful in framing one's thinking about energy flows in Hermite space.

Returning to Eq. (3.40) and considering $1 \ll m \ll (\nu/|k|)^{-2}$, we find that to lowest approximation, the $\sqrt{m}$ terms are dominant and must balance, giving $\tilde{g}_{m+1,k} \approx \tilde{g}_{m-1,k}$. This is consistent with continuity in m, viz., $\tilde{g}_{m+1,k} \approx \tilde{g}_{m,k}$, but there is also a solution allowing the consecutive Hermite moments to alternate sign: $\tilde{g}_{m+1,k} \approx -\tilde{g}_{m,k}$. Thus, there are, formally speaking, two solutions: one for which $\tilde{g}_{m,k}$ is continuous and one for which $(-1)^m \tilde{g}_{m,k}$ is. To take into account both of them, we introduce the following decomposition [118]:

$$\tilde{g}_{m,k} = \tilde{g}^{+}_{m,k} + (-1)^m \tilde{g}^{-}_{m,k}, \tag{3.49}$$

where the "+" ("continuous") and the "−" ("alternating") modes are

$$\tilde{g}^{+}_{m,k} = \frac{\tilde{g}_{m,k} + \tilde{g}_{m+1,k}}{2}, \quad \tilde{g}^{-}_{m,k} = (-1)^m \frac{\tilde{g}_{m,k} - \tilde{g}_{m+1,k}}{2}. \tag{3.50}$$

The Hermite spectrum and the flux of the free energy can be expressed in terms of

the spectra of these modes as follows:

$$C_{m,k} \equiv \langle |\tilde{g}_{m,k}|^2 \rangle = C^+_{m,k} + C^-_{m,k}, \tag{3.51}$$

$$\Gamma_{m+1/2,k} \equiv |k|\sqrt{2(m+1)}\mathrm{Re}\langle \tilde{g}_{m+1,k}\tilde{g}^*_{m,k}\rangle \approx |k|\sqrt{2m}\left(C^+_{m,k} - C^-_{m,k}\right), \tag{3.52}$$

where $C^\pm_{m,k} \equiv \langle |\tilde{g}^\pm_{m,k}|^2 \rangle$ and the last expression in Eq. (3.52) is an approximation valid for $m \gg 1$.

The functions $\tilde{g}^\pm_{m,k}$ can both be safely treated as continuous in m for $m \gg 1$. Treating them so in Eq. (3.40) and working to lowest order in $1/m$, we find that they satisfy the following *decoupled* evolution equations:

$$\frac{\partial \tilde{g}^\pm_{m,k}}{\partial t} \pm \sqrt{2}|k| m^{1/4} \frac{\partial}{\partial m} m^{1/4} \tilde{g}^\pm_{m,k} = -\nu m \tilde{g}^\pm_{m,k}, \tag{3.53}$$

or, for their spectra,

$$\frac{\partial C^\pm_{m,k}}{\partial t} \pm |k| \frac{\partial}{\partial m}\sqrt{2m}\, C^\pm_{m,k} = -2\nu m C^\pm_{m,k}. \tag{3.54}$$

Manifestly, the "+" mode propagates from lower to higher m and the "−" mode from higher to lower m—they are the "phase-mixing" and the "un-phase-mixing" collisionless solutions, respectively.[§]

Taking the collisional term into account and noting that energy is injected

[§]The existence of un-phase-mixing solutions has been known for a long time: e.g., [108] treated them as forward and backward propagating waves in a mechanical analogy of Eq. (3.40) with a row of masses connected by springs. The un-phase mixing solutions are also what allows the phenomenon of plasma echo [9], including in stochastic nonlinear systems [118].

into the system at low, rather than high, m, the solution satisfying the boundary condition $\tilde{g}_{m,k} \to 0$ as $m \to \infty$ has $\tilde{g}^-_{m,k} = 0$ and so $\tilde{g}_{m,k} = \tilde{g}^+_{m,k}$. Thus, $\tilde{g}_{m,k}$ is continuous in m. With $C^-_{m,k} = 0$, Eq. (3.52) is the same as our earlier approximation (3.42) (to lowest order in the $m \gg 1$ expansion).

As $\tilde{g}^+_{m,k}$ and $\tilde{g}^-_{m,k}$ are decoupled at large m, if we start with a $\tilde{g}^-_{m,k} = 0$ solution, no $\tilde{g}^-_{m,k}$ will be produced. However, both the decoupling property and the interpretation of $\tilde{g}^\pm_{m,k}$ as the phase-mixing and un-phase-mixing modes are only valid to lowest order in $1/m$. It is useful to know how well this approximation holds.

Let us use Eq. (3.31) to calculate (in the collisionless limit)

$$R_{m+1} \equiv \frac{\tilde{g}_{m+1,k\omega}}{\tilde{g}_{m,k\omega}} = i \operatorname{sgn} k \, \frac{g_{m+1,k\omega}}{g_{m,k\omega}} = -\frac{i}{\sqrt{2(m+1)}} \frac{Z^{(m+1)}(\zeta)}{Z^{(m)}(\zeta)}. \tag{3.55}$$

Taking $m \gg 1, \zeta^2/4$ and using Eq. (3.35), we find[¶]

$$R_{m+1} = 1 + \frac{i\zeta}{\sqrt{2m}} - \frac{1}{4m} + O\left(\frac{1}{m^{3/2}}\right). \tag{3.56}$$

Therefore, to lowest order in $1/\sqrt{m}$,

$$\tilde{g}^-_{m,k\omega} = (-1)^m \tilde{g}_{m,k\omega} \, \frac{1 - R_{m+1}}{2} \approx (-1)^{m+1} \, \frac{i\zeta}{2\sqrt{2m}} \, \tilde{g}_{m,k\omega}. \tag{3.57}$$

[¶]The same lowest-order expression can be found by Fourier-transforming Eq. (3.40) in time, ignoring collisions, writing $R_{m+1} = R_m^{-1}\sqrt{m/(m+1)} + i\zeta\sqrt{2/(m+1)}$, approximating $R_m \approx R_{m+1}$, solving the resulting quadratic equation for R_{m+1}, expanding in powers of $1/\sqrt{m}$ and choosing the solution for which $R_{m+1} = 1$ to lowest order. This last step is the main difference between the two methods: if we work with Eq. (3.40) in the manner just described, we have to make an explicit choice between the continuous and alternating solutions ($R_{m+1} = 1$ and $R_{m+1} = -1$); on the other hand, Eq. (3.31) already contains the choice of the former (which is ultimately traceable to Landau's prescription guaranteeing damping rather than growth of the perturbations).

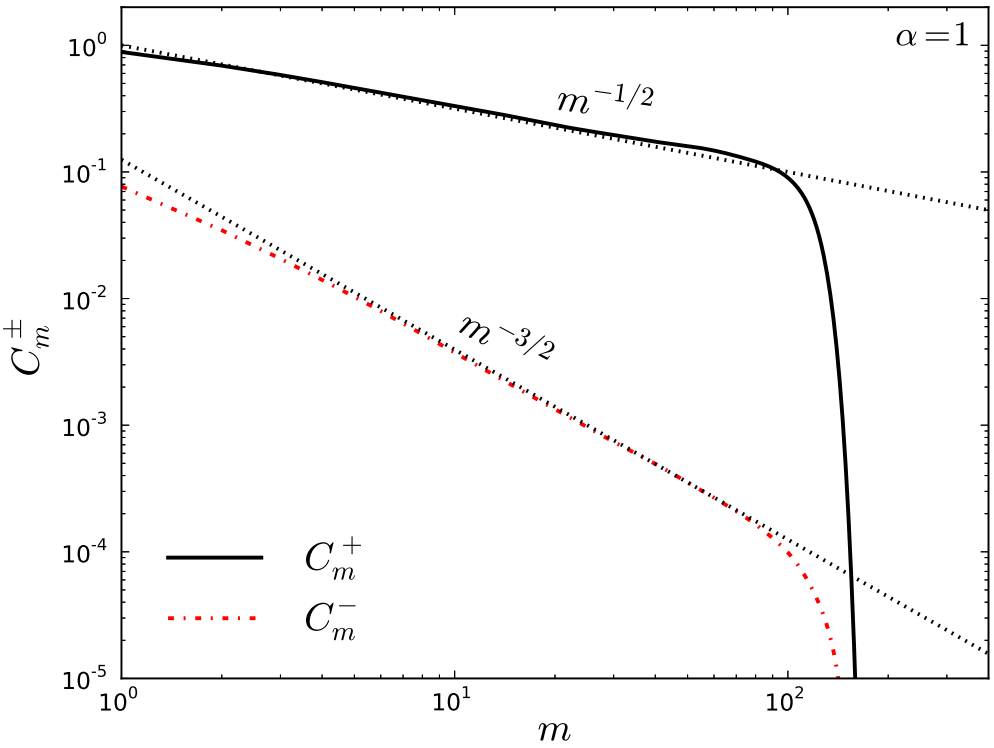

Figure 3.3: The free-energy spectra $C_m^{\pm}$ obtained via direct numerical solution of Eqs. (3.26–3.28) with $\alpha = 1.0$ followed by decomposing the solution according to Eq. (3.50). In the code, rather than using the Lenard–Bernstein collision operator (as per Eq. (3.28)), hypercollisional regularization, $-\nu m^6 g_{m,k}$, was used to maximize the utility of the velocity-space resolution, hence the very sharp cut off. The dotted lines show the collisionless approximation: Eq. (3.37) for $C_{m,k}^+$ (the phase-mixing "+" mode predominates, so $C_{m,k} \approx C_{m,k}^+$) and Eq. (3.58) for $C_{m,k}^-$.

Following the same steps as those that led to Eq. (3.37)[‖], we get

$$C^-_{m,k} \approx \left[\frac{\varepsilon_k}{8\sqrt{2\pi}|k|}\left(\frac{1+\alpha}{\alpha}\right)^2 \int_{-\infty}^{+\infty} \frac{\mathrm{d}\zeta\, \zeta^2 e^{-\zeta^2}}{|D_\alpha(\zeta)|^2}\right] \frac{1}{m^{3/2}} = \frac{\varepsilon_k (1+\alpha)^2}{16\sqrt{2}|k|} \frac{1}{m^{3/2}}, \qquad (3.58)$$

so both the energy (~ 1, while the total is $\sim \nu^{-1/3}$; see Eq. (3.48)) and the dissipation ($\sim \nu \sum_m m C^-_{m,k} \sim \nu^{2/3}$) associated with the "$-$" modes is small.

The steady-state spectra $C^\pm_{m,k}$ obtained via direct numerical solution of Eqs. (3.4) and (3.5) are shown in Fig. 3.3, where they are also compared with the analytical expressions (3.37) and (3.58).

Note that we could have, without further ado, simply taken Eq. (3.56) to be the proof of continuity in Hermite space. We have chosen to argue this point via the decomposition (3.49) because it provided us with a more intuitive understanding of the connection between this continuity and the direction of the free-energy flow (phase mixing rather than un-phase mixing).

3.4.6 The simplest Landau-fluid closure

Simplistically described, the idea of Landau-fluid closures is to truncate the Hermite hierarchy of Eqs. (3.26–3.28) at some finite m and to replace in the last retained equation

$$g_{m+1,k}(t) = -(i \operatorname{sgn} k) R_{m+1} g_{m,k}(t), \qquad (3.59)$$

[‖]The integral is again calculated via Kramers–Kronig relations, this time for the function $h(\zeta) = \zeta^2/D_\alpha(\zeta) - \alpha\zeta^2 - \alpha^2/2$, so $\int_{-\infty}^{+\infty} \mathrm{d}\zeta\, \zeta^2 e^{-\zeta^2}/|D_\alpha(\zeta)|^2 = \alpha^2\sqrt{\pi}/2$.

where R_{m+1}, which in general depends on the complex frequency ζ (Eq. (3.55)), is approximated by some suitable frequency-independent expression leading to the correct recovery of the linear physics from the truncated system. A considerable level of sophistication has been achieved in making these choices and we are not proposing to improve on the existing literature [90–93, 95, 98, 99, 102]. It is, however, useful, in the context of the result of Sec. 3.3.1 that the "fluid" version of FDR is recovered in the limit of low frequency and weak damping, to show how the same conclusion can be arrived at via what is probably the simplest possible Landau-fluid closure.

In the limit $\zeta \to 0$, the ratio R_{m+1}, given by Eq. (3.55), becomes independent of ζ and so a closure in the form (3.59) becomes a rigorous approximation. It is not hard to show that

$$Z^{(m)}(0) = \frac{i^{m+1}\sqrt{\pi}\, m!}{\Gamma(m/2+1)}. \tag{3.60}$$

Therefore, for $\zeta \ll 1$ and $m \geq 1$,**

$$R_{m+1} = \frac{m}{\sqrt{2(m+1)}} \frac{\Gamma(m/2)}{\Gamma((m+1)/2)}. \tag{3.61}$$

If we wish to truncate at $m = 1$, then $R_2 = \sqrt{\pi}/2$, and so in Eq. (3.27),

$$g_{2,k} = -i \operatorname{sgn} k \, \frac{\sqrt{\pi}}{2} \, g_{1,k}. \tag{3.62}$$

**The same result can be obtained by inferring $R_{m+1} \approx R_m^{-1}\sqrt{m/(m+1)}$ from Eq. (3.40) (provided $m \ll 1/\zeta^2$), then iterating this up to some Hermite number M such that $1 \ll M \ll 1/\zeta^2$, and approximating $R_M \approx 1$ (Eq. (3.56)). The condition $m, M \ll 1/\zeta^2$ is necessary so that the ζ terms in R_{m+1} are not just small compared to unity but also compared to the next-order $1/m$ terms (see Eq. (3.56)).

On the basis of Eq. (3.26), we must order $g_{1,k} \sim O(\zeta) g_{0,k}$. Thefore, $\partial g_{1,k}/\partial t \sim O(\zeta^2) g_{0,k}$ must be neglected in Eq. (3.27), from which we then learn that

$$g_{1,k} \approx -i \operatorname{sgn} k \sqrt{\frac{2}{\pi}} (1+\alpha)\, g_{0,k}. \tag{3.63}$$

Finally, substituting this into Eq. (3.26), we get

$$\frac{\partial g_{0,k}}{\partial t} + \frac{1+\alpha}{\sqrt{\pi}} |k| g_{0,k} = \chi_k. \tag{3.64}$$

This is a Langevin equation (3.1) with a damping rate that is precisely the Landau damping rate γ_L in the limit $1+\alpha \ll 1$ (and so $\zeta \ll 1$), given by Eq. (3.16). In this limit, $\varphi = -g_0$ (Eq. (3.25), $\alpha \approx -1$) and we recover the standard "fluid" FDR (Eq. (3.17)). As we discussed in Sec. 3.2, a useful application of this regime is to compressive fluctuations in high-beta plasmas: in this case $1+\alpha \approx 1/\beta_i \ll 1$ and the damping is the Barnes damping (also known as transit-time damping) [38], well known in space and astrophysical contexts [1, 119, 120].

3.5 Conclusions and discussion

We have provided a reasonably complete treatment of the simplest generalization of the Langevin problem to plasma kinetic systems. While we have focused on the simplest Langevin problem, in which the source term is a white noise, there is an obvious route towards generalizing this by considering source terms with more coherent time dependence (longer correlation times, prescribed frequency spectra;

see [39]). One such calculation was recently undertaken by Plunk [40], who considered a coherent oscillating source and found that when the frequency of the source is large, the amount of energy that can be absorbed by the kinetic system is exponentially small. Another straightforward generalization (or variation) of our model (as treated in this chapter) is energy injection into momentum, rather than density fluctuations—which can be interpreted as forcing by an externally imposed random electric field. Whereas some of the more literal parallels with the Langevin problem are lost in this case, the results are fundamentally the same (appendix B). Let us itemize the main results and conclusions.

- Eq. (3.13) is the fluctuation-dissipation relation for the kinetic system (Eqs. (3.4) and (3.5)), expressing the relationship between the fluctuation level $\langle|\varphi_k|^2\rangle$ and the injected power. This can be expressed in terms of an "effective" damping rate γ_{eff} in a way that resembles the standard "fluid" version of the fluctuation-dissipation relation (Eq. (3.14)), but γ_{eff} is not in general equal to the Landau damping rate γ_L. We stress that this result is not a statement of any kind of surprising "modification" of Landau damping in a system with a random source, but rather a clarification of what the linear response in the statistical steady state of such a system actually is. The system, in general, is not mathematically equivalent to the Langevin equation (3.1) and so the fluctuation-dissipation relation for it need not have the same form.

- In the limit of zero real frequency and weak Landau damping, the effective and

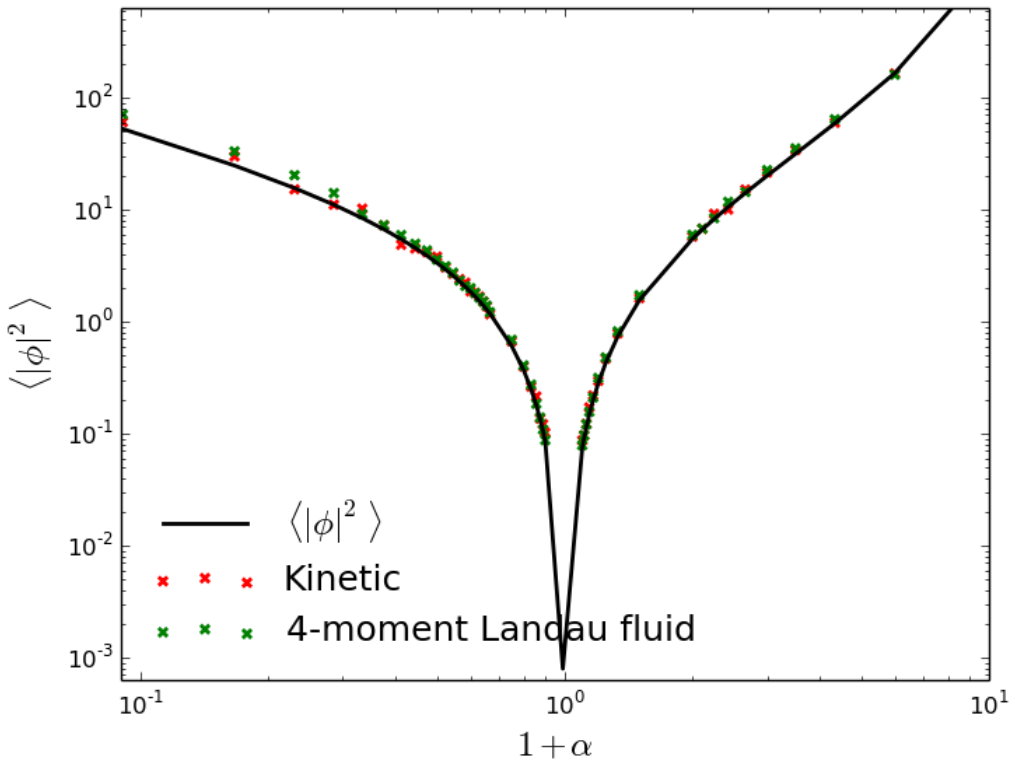

Figure 3.4: Reproduction of Fig. 3.1 along with the normalized saturated amplitude calculated using a 4-moment Landau fluid model (green crosses).

the Landau damping rates do coincide (Eq. (3.17)). Another way to view this result is by noting that this is a regime in which the simplest possible Landau-fluid closure becomes a rigorous approximation and the evolution equation for the electrostatic potential can be written as a Langevin equation with the Landau damping rate γ_L (Eq. (3.64)). It is crucial to note, however, that a more realistic 4-moment Landau-fluid model reproduces the kinetic results with near-perfect accuracy as can be seen in Fig. 3.4.

- Another limit in which the fluctuation-dissipation relation for the kinetic system can be interpreted in "fluid" (in fact, mechanical) terms is one of high real

frequency and exponentially Landau small damping, although the correct analogy is not the Langevin equation but a forced-damped oscillator (Sec. 3.3.2; this analogy, however, ceases to hold in such a simple form for a different choice of forcing, as shown in appendix B).

- The damping of the perturbations of φ (which are linearly proportional to the density perturbations) occurs via phase mixing, which transfers the free energy originally injected into φ away from it and into higher moments of the perturbed distribution function. This process can be described as a free-energy flow in Hermite space. The generalization of the FDR to higher-order Hermite moments takes the form of an expression for the Hermite spectrum $C_{m,k}$ (Eq. (3.33)), which at high Hermite numbers $m \gg 1$ has a universal scaling $C_{m,k} \propto 1/\sqrt{m}$ (Eq. (3.37)). This scaling corresponds to a constant free-energy flux from low to high m (Eq. (3.42)). Analysis of the solutions of the kinetic equation making use of a formal decomposition of these solutions into phase mixing and un-phase mixing modes underscores the predominance of the former (Sec. 3.4.5).

- A solution for the Hermite spectrum including the collisional cutoff is derived (Eq. (3.44)). The fluctuation-dissipation relation for the total free energy stored in the phase space (Eq. (3.48)) shows that it diverges $\propto \nu^{-1/3}$ in the limit of vanishing collisionality ν, a result that underscores the fact that ultimately all dissipation (i.e., all entropy production in the system) is collisional.

In the process of deriving these results, we have made an effort to explain the simple connections between the Landau formalism (solutions of the kinetic equation expressed via the plasma dispersion function) and the Hermite-space one. We are not aware of any work where the results presented here are adequately explained—although implicitly they underlie the thinking behind both Landau-fluid closures [90–93,95,98,99,102] and Hermite-space treatments for plasma kinetics [40,106–114].

Besides providing a degree of clarity on an old topic in the linear theory of collisionless plasmas, our findings lay the groundwork for a study of the much more complicated nonlinear problem of the role of Landau damping and phase mixing in turbulent collisionless plasma systems [118,121], which is carried out in the following chapters.

Chapter 4

Kinetic passive scalar advection by 2D velocity

4.1 Introduction

Advection of a passive scalar by a turbulent velocity field is a fundamental and well studied problem in hydrodynamic turbulence [14, 54–78]. Investigations into passive scalar turbulence have helped develop the basic ideas underlying hydrodynamic turbulence theory (Refs. [69, 77, 78] give thorough reviews of this topic). Recently, a few authors have carried out numerical investigations of passive scalar advection in magnetohydrodynamic turbulence [122–125]. However, to the best of our knowledge, kinetic passive scalar turbulence has not been studied before.

A kinetic passive scalar is slaved to a turbulent cascade while simultaneously being phase mixed. Since the particle distribution functions for such systems may develop non-trivial velocity space structure, it is unclear if the results regarding passive scalar advection derived in the fluid limit will still be valid in the kinetic regime. In the fluid limit, the passive scalar acquires the same energy spectrum as the advecting velocity field. However, in the kinetic limit, if phase mixing turns out to be the dominant process, the turbulent cascade of the scalar will terminate. This will result in an exponentially attenuated spectrum. The key question then is whether a kinetic passive scalar has a power law spectrum, or an exponentially decaying spectrum.

The answer to this question has significant implications regarding how the system chooses to dissipate the energy contained in the scalar. There are two available dissipation mechanisms: phase mixing transfers energy to smaller velocity space scales, which eventually gets dissipated by collisions; on the other hand, the turbulent cascade transfers energy to small scales in real space, which is then dissipated by a diffusive term*. In the context of KRMHD, all energy that is dissipated by collisions will end up heating ions, whereas the energy that survives in the low velocity moments until the cascade reaches the diffusive cutoff may end up heating either ions or electrons. Therefore, knowing how the injected energy gets partitioned between collisions and diffusion will shed some light on the differential heating of ions and electrons.

In this chapter, we consider a simple model for a kinetic passive scalar g, which can be obtained from the KRMHD equation by making certain simplifying assumptions† :

1. Electrostatic approximation: set $\delta\mathbf{B}_\perp = \hat{\mathbf{z}} \times \nabla A_\parallel = 0$.

2. Assume the Kraichnan model [59] for the velocity field, i.e., let $\mathbf{u}_\perp$ be an Ornstein-Uhlenbeck process [126–133] evaluated by solving the Langevin equation [88]:

$$\frac{\partial \Phi}{\partial t} + \gamma \Phi = \kappa, \quad \mathbf{u}_\perp = \hat{\mathbf{z}} \times \nabla \Phi, \tag{4.1}$$

where Φ is the stream function for the velocity field; κ is a white noise source,

*Diffusion here is a stand-in for a more complicated cutoff like finite Larmor radius effects. One may also consider it to be classical diffusion.

†This should be thought of as a first step towards solving the full KRMHD equations. Study of a simpler model such as this one helps develop understanding of how the full system behaves.

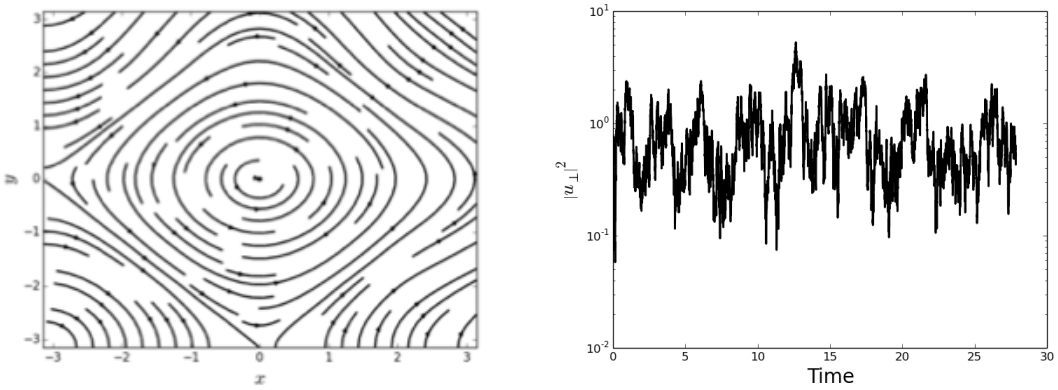

Figure 4.1: The velocity field $\mathbf{u}_\perp$ is independent of z. The structure of the velocity field with respect to x and y is plotted on the left. The time evolution of the kinetic energy is plotted on the right.

$\langle \kappa(t)\kappa(t')\rangle = \epsilon\delta(t-t')$. The amplitude of the advecting velocity (which can be thought of as the strength of the turbulence) is controlled by changing ϵ. Depending on the value of ϵ, γ is chosen such that the Kubo number (a dimensionless parameter characterizing the correlation time of the velocity field) $\mathrm{Ku} = p_\perp u_\perp/\gamma$, where $p_\perp$ is the perpendicular wavenumber of the velocity is held constant. We set $\mathrm{Ku} = 1$.

3. Additionally, assume that the velocity field $\mathbf{u}_\perp$ is a 2D, single-scale velocity field, i.e., the energy containing wavenumbers $\mathbf{p}$ have $p_\perp \neq 0, p_\parallel = 0$. Further assume that the scale given by $p_\perp$ corresponds to the largest scale (smallest magnitude wavenumber) in the system[‡]—this is akin to the Batchelor limit [56] in hydrodynamic turbulence. A cross section of the velocity field at constant z, along with the time evolution of the kinetic energy is plotted in Fig. 4.1.

[‡]In our numerical box, this corresponds to $p_\perp = 1$.

Under these assumptions the kinetic scalar Eq. (1.19) in KRMHD reduces to:

$$\partial_t g + \mathbf{u}_\perp \cdot \nabla_\perp g + v_\parallel \nabla_\parallel (g + \varphi F_0) = C^h[g] + \eta \nabla_\perp^8 g + \chi, \tag{4.2}$$

$$\varphi = \alpha \int_{-\infty}^{\infty} dv_\parallel g(v_\parallel), \tag{4.3}$$

where α is defined in the same way as Chapter 3, $\alpha = -1/\Lambda$ (see Eq. (1.20)); the electrostatic potential φ is same as the one used in Chapter 3 (see Eq. (3.5)). $C^h[g]$ is the hyper-collision operator which in Hermite space looks like $-\nu m^8 g_m$ for the m^{th} Hermite moment; $\eta k_\perp^8 g$ is a hyper-diffusion term that extracts energy from the system at small perpendicular scales in real space, and χ is a delta-correlated-in-time source term which drives g. Since Eq. (4.2) is homogeneous in g, the strength of χ can be set to one without any loss of generality.

4.2 Nonlinear Cascade and timescales

Since the velocity $\mathbf{u}_\perp$ does not vary in the z, the passive scalar g does not undergo a parallel cascade. This can be seen by considering a three mode interaction where modes with wavenumbers $\mathbf{p}$ and $\mathbf{q}$ couple to give a mode with the wavenumber $\mathbf{k} = \mathbf{q} + \mathbf{p}$. The parallel wavenumber remains unchanged, $k_\parallel = q_\parallel$. If the source χ injects energy into the system with a parallel wavenumber $k_{\parallel 0}$ then the timescale associated with phase mixing is given by $(k_{\parallel 0} v_{\text{th}})^{-1}$. Since $p_\perp$ is non-zero, the passive scalar does get mixed in the perpendicular plane. The rate at which the scalar cascades to small perpendicular scales can be roughly estimated as $\sim |p_\perp u_\perp|$.

Since we have assumed that the scale of the velocity field is the largest scale in the system, we are in the so-called Batchelor limit [56]; this implies that if g were a fluid passive scalar instead of a kinetic one, it would have had a $1/k_\perp$ spectrum. On the other hand, if there were no velocity field, i.e., no turbulent cascade for the scalar, then the problem gets reduced to the one from Chapter 3, where the spectrum in velocity space is given by $1/\sqrt{m}$. In this sense, if the nonlinear cascade dominates over linear phase mixing, that corresponds to the "fluid" limit, whereas in the "kinetic" limit phase mixing is the dominant process.

4.3 Numerical setup

We solved Eqs. (4.2–4.3) using *Gandalf*[§]. The velocity field was driven at wavenumbers $\mathbf{p}$ such that $p_\perp = 1$, $p_\parallel = 0$. The passive scalar g was driven by injecting energy into the first Hermite moment at perpendicular wavenumbers between one and two, and parallel wavenumber $k_{\parallel 0} = 1$. For these runs, we chose $\alpha = 2$. As shown in Chapter 3, the particular value of α does not have any bearing on the Hermite space dynamics for $m \geq 1$. It only determines the relationship between g_0 and g_1. The resolution was 64^2 in the perpendicular plane, single wavenumber in the parallel direction and 100 Hermite moments. We chose values for hyper-collision frequency ν and the hyper-difussion coefficient η, such that the collisional dissipation microscale was $m_c \sim 66$, and the diffusion microscale was $k_{\perp,\eta} \sim 21$[¶]. All the

[§] *Gandalf* has an option where instead of solving reduced MHD equations, it can be made to solve the Langevin equation to evaluate the velocity field $\mathbf{u}_\perp$. In this scenario ϵ and γ are user-provided inputs which allow the user to control the strength of the velocity field.

[¶] Due to the "hyper" nature of the dissipation, the dissipation microscales give a better sense of the numerical setup, instead of the values of ν and η.

simulations in this chapter are in the "strongly nonlinear" regime, *i.e.*, in the limit where the nonlinear timescale is comparable to, or greater than the phase mixing timescale. In the opposite limit, phase mixing dominates and the problem reduces to the one discussed in Chapter 3.

We change the Hermite space variable from m to $s = \sqrt{m}$. In terms of the new variables $(s, k_\perp, k_\parallel)$, the energy spectrum is given by $F_{s,\mathbf{k}} = s|g_{m,k}|^2$. The numerical results presented in this chapter use this definition for the energy spectrum.

4.4 Results

We observe in our simulations, that when the nonlinear timescale is faster than the linear timescale, the passive scalar does not get phase-mixed. This is shown in Fig. 4.2, where we see the spread of the spectrum in s to be strongly dependent on the strength of the nonlinearity. Figs. 4.3 and 4.4 show this dependence—the spectrum decays exponentially in s at a rate proportional to $|p_\perp \mathbf{u}_\perp| / k_{\parallel 0} v_{\rm th}$. This is further confirmed by Fig. 4.5, where the passive scalar is shown to have a perpendicular spectrum consistent with the fluid limit.

In Fig. 4.6 we plot the dissipation due to collisions normalized to the total dissipation (collisional and diffusion) as a function of $|p_\perp \mathbf{u}_\perp| / k_{\parallel 0} v_{\rm th}$, where we see that the dissipation due to collisions decreases exponentially as the nonlinear advection rate is increased with respect to the linear frequency, i.e., once nonlinear, the system preferentially dissipates via diffusion.

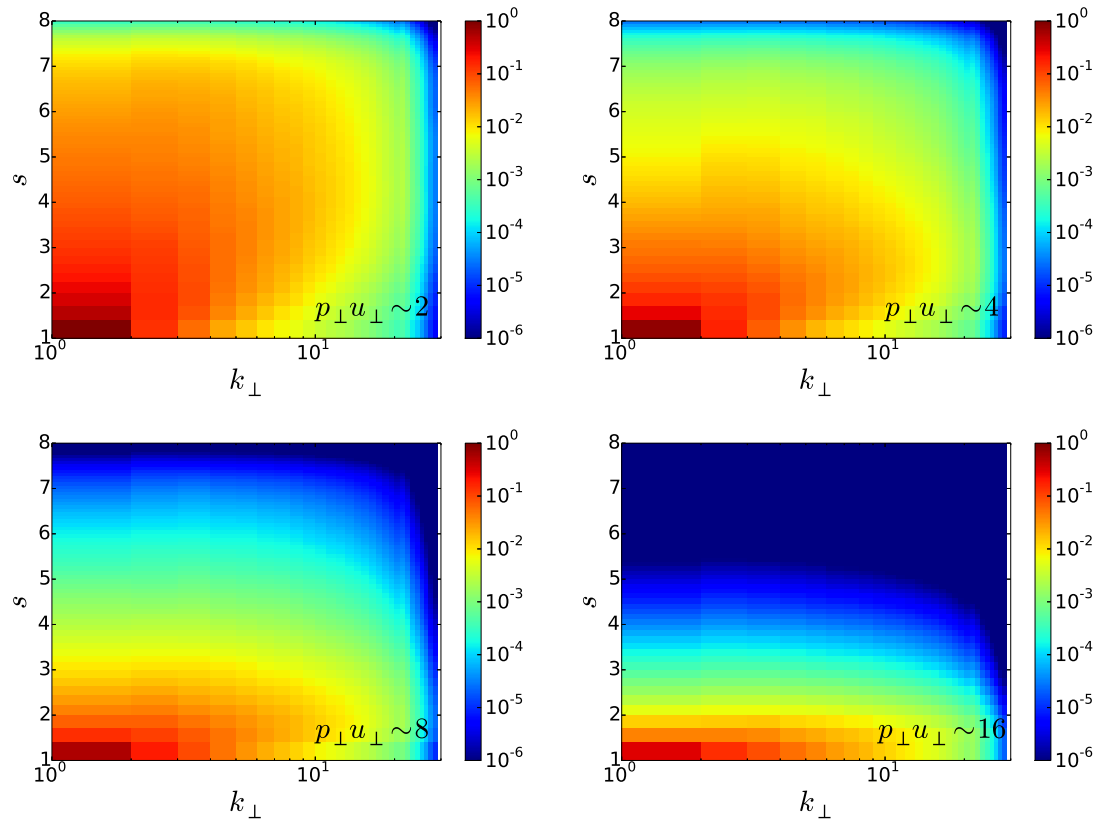

Figure 4.2: The spectrum $F_{s,\mathbf{k}}$ vs $s - k_\perp$ at $k_\parallel = 1$, for four different $|p_\perp \mathbf{u}_\perp|$. For larger values of $|p_\perp \mathbf{u}_\perp|$, the spectrum does not extend far into Hermite space, as expected.

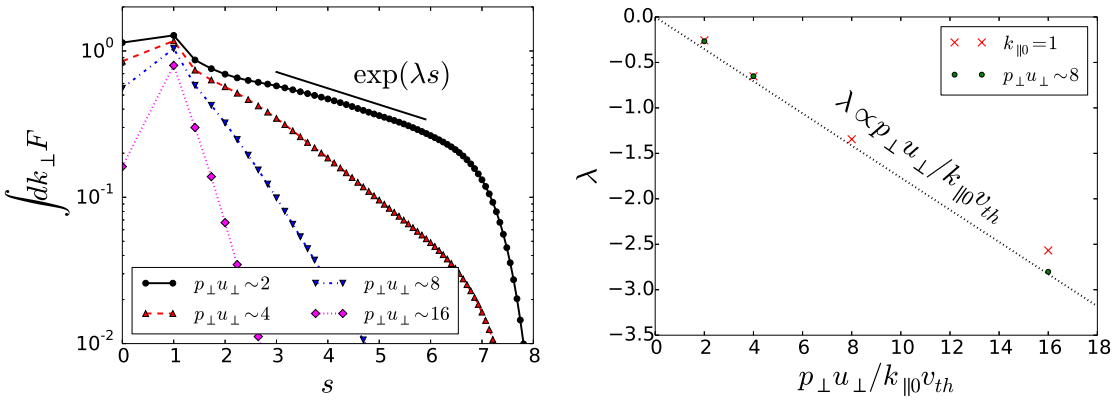

Figure 4.3: The 1D spectrum $\int dk_\perp F_{s,\mathbf{k}}$ vs s (left) is seen to be an exponential decay at a rate λ proportional to $|p_\perp \mathbf{u}_\perp| / k_{\parallel 0} v_{\text{th}}$. The decay rate is plotted versus $|p_\perp \mathbf{u}_\perp| / k_{\parallel 0} v_{\text{th}}$ on the right—the red crosses are runs with fixed $k_{\parallel 0} = 1$ and varying $|p_\perp \mathbf{u}_\perp|$, whereas the green circles are runs with fixed $|p_\perp \mathbf{u}_\perp| \sim 8$ and varying $k_{\parallel 0}$.

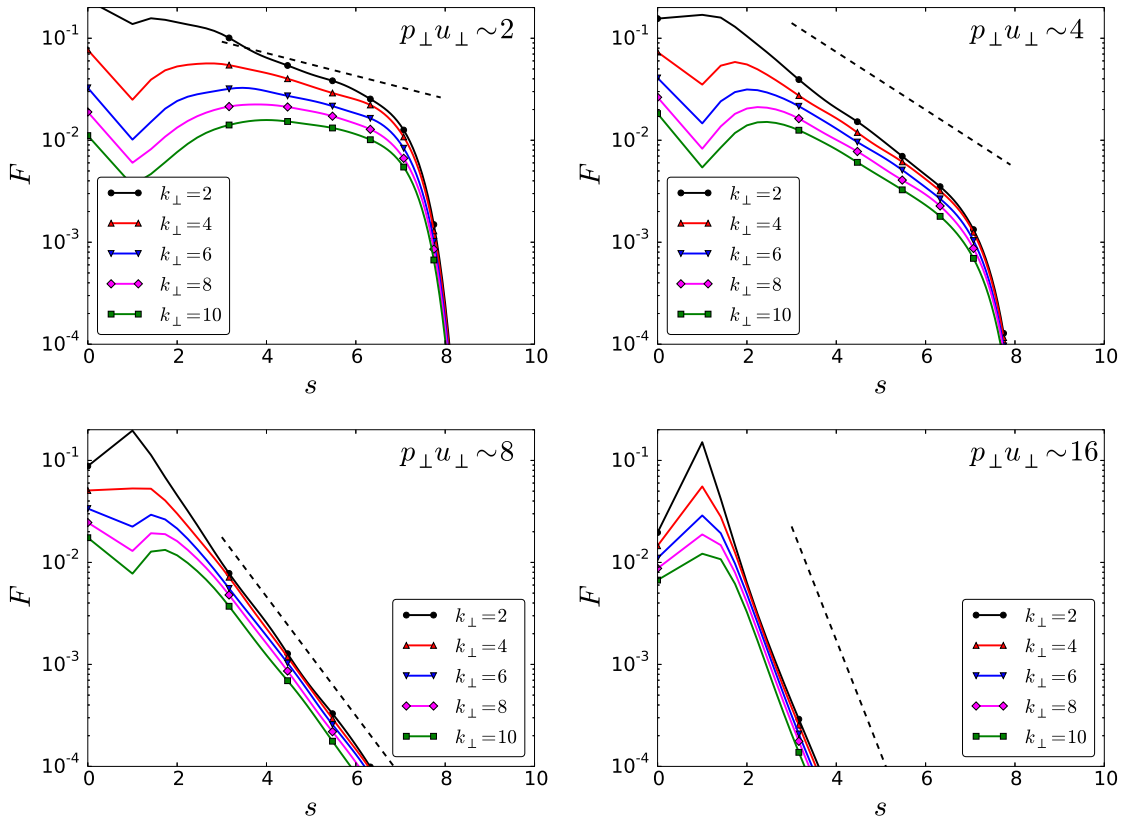

Figure 4.4: Spectrum F at fixed $k_\perp$ vs s for four different values of $|p_\perp \mathbf{u}_\perp|$. After an initial "transient" in s, the spectrum decays exponentially at a rate $\propto |p_\perp \mathbf{u}_\perp| / k_{\parallel 0} v_{\rm th}$—the dashed line depicts the expected spectrum.

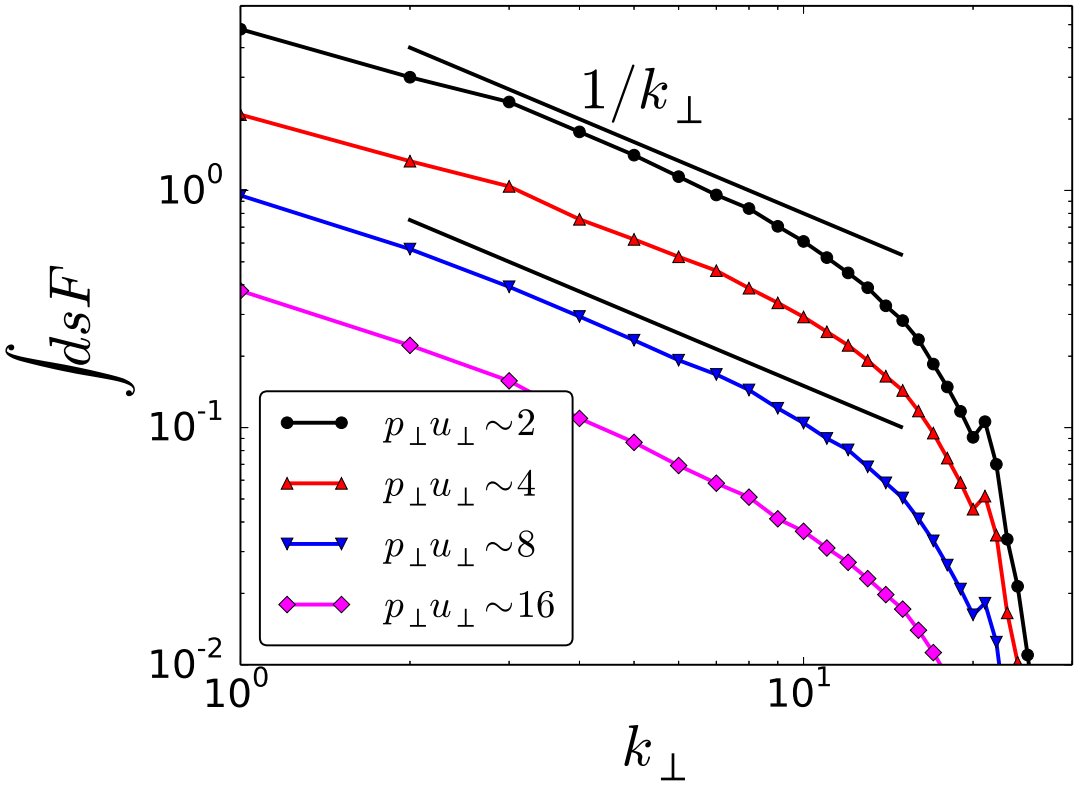

Figure 4.5: 1D spectrum $\int dsF_{s,\mathbf{k}}$ vs $k_\perp$. The spectrum becomes increasingly fluid-like ($\sim 1/k_\perp$), as $|p_\perp \mathbf{u}_\perp|$ is increased.

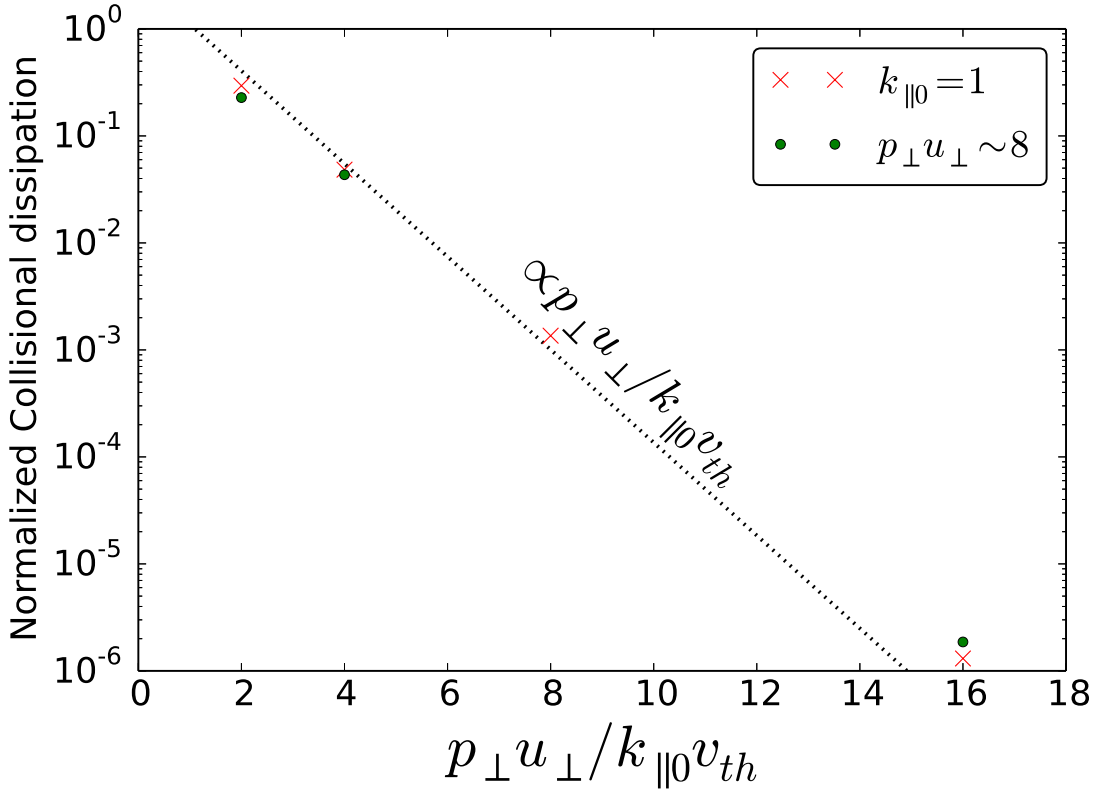

Figure 4.6: Collisional dissipation normalized to the total dissipation vs $|p_\perp \mathbf{u}_\perp| / k_{\parallel 0 v_{\rm th}}$. As the system becomes more nonlinear, most of the energy is dissipated by the diffusive cutoff, and vanishingly small amount of energy is dissipated via the collisional channel.

4.5 Discussion

We showed by numerically solving Eqs. (4.2–4.3), that if a kinetic passive scalar is being advected by a 2D velocity field, in the strongly nonlinear regime, the steady-state behavior is fluid-like. The nonlinear cascade transfers the energy to finer perpendicular scales, not allowing the scalar to phase mix. As a result, the perpendicular spectrum for such a system in the Batchelor limit is the well-known fluid spectrum: $1/k_\perp$. The spectrum in Hermite space decays exponentially at the rate $|p_\perp \mathbf{u}_\perp| / k_{\parallel 0} v_{\rm th}$, which is consistent with the fluid-like behavior of the system. The dissipation for such a system happens almost completely through diffusion, since negligible amount of energy is transferred to small scales in velocity space, which makes collisions inaccessible.

It has been suggested that the compressive fluctuations in the solar wind do not undergo a parallel cascade [1] (see Sec. 6.1 for a detailed discussion). If this is assumed to be true, then the results presented in this chapter help explain the observed power law spectra of density fluctuations. In KRMHD, the nonlinear cascade rate associated with the background Alfvénic turbulence increases with the perpendicular wavenumber; whereas, in absence of a parallel cascade, the linear phase mixing rate of the compressive fluctuations remains unchanged. As a result, beyond a certain scale the nonlinear cascade dominates, and disallows the slow modes to phase mix, resulting in a fluid-like turbulent cascade, *i.e.*, power law spectra.

The results discussed in this chapter are the kinetic generalization of the Batch-

elor spectrum for a passive scalar, where the advecting velocity is 2D and the scalar does not undergo a parallel cascade. We discuss the effects of parallel cascade in the next chapter, by considering a 3D advecting velocity field.

Chapter 5

Kinetic passive scalar advection by 3D velocity

5.1 Introduction

We saw in earlier chapters that phase mixing damps electromagnetic fluctuations and drives sharp velocity space gradients in the perturbed distribution function, which are eventually smoothed by collisions. The regularization of velocity gradients by collisions produces entropy and heats the plasma. For a linear system with a single Fourier mode, this is seen as a damping solution to the dispersion relation (see Fig. 3.2). However, the behavior of Landau damping in nonlinear turbulent systems, where multiple Fourier modes are coupled with each other is not fully understood. Some phenomenological models model the turbulent cascade by assuming that if the linear damping rate is comparable to, or larger than the nonlinear cascade rate scale-by-scale, a part of the energy is pumped into small velocity space scales at each spatial scale [23–25]. This, in essence, superimposes the linear damping physics on to the nonlinear turbulent cascade. However, such scale-by-scale extraction of energy results in an exponentially decaying energy spectrum [134, 135], which is not seen in numerical simulations [136–138] or in observations [3, 30–36, 104, 139–145]. Understanding how Landau damping (or, more generally, phase mixing) operates in a turbulent environment is essential in addressing this discrepancy.

In Chapter 4, we approached this problem by considering a model for a passive

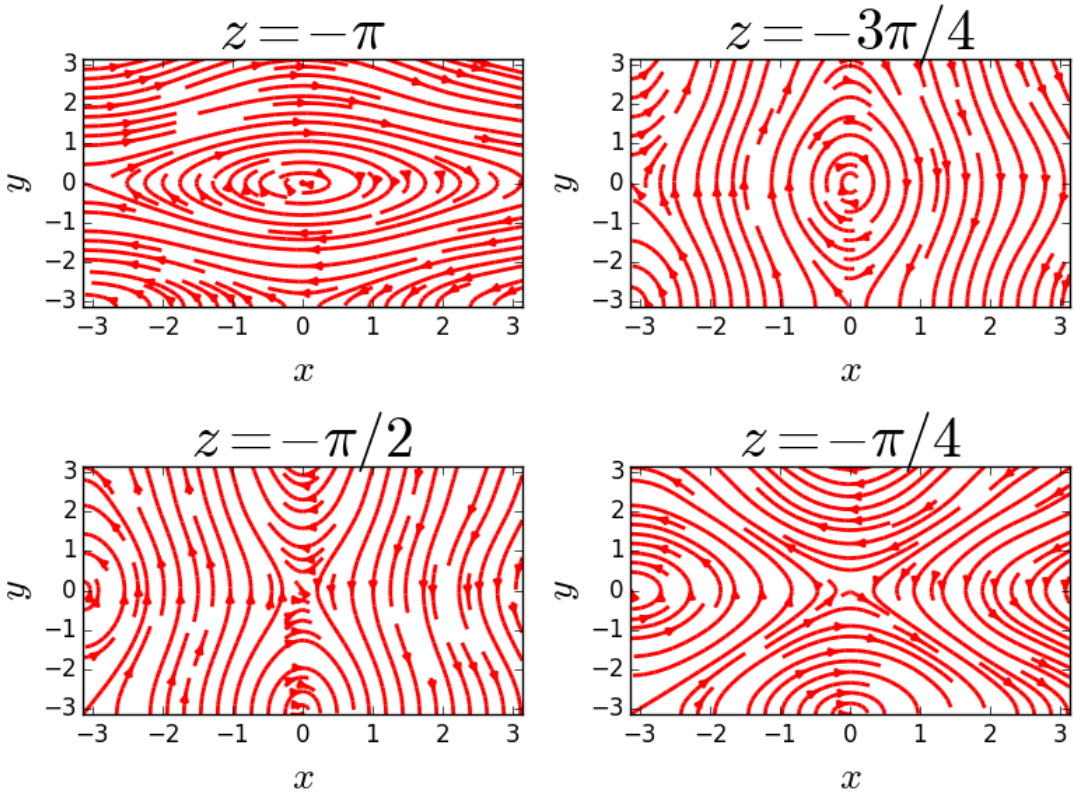

Figure 5.1: The velocity field $\mathbf{u}_\perp$ vs x and y for different values of z.

kinetic scalar being advected by a 2D chaotic velocity. There, the phase mixing rate for the scalar was fixed by its initial wavenumber. Therefore, for strongly nonlinear systems, the scalar spectrum with respect to s was a sharp exponential decay. In this chapter, we extend the analysis from Chapter 4 to a 3D advecting velocity field (see Fig. 5.1). Due to the 3D structure of the velocity, the scalar now undergoes a parallel cascade in addition to the perpendicular one. Hence, unlike the 2D velocity case, the scalar now has access to larger $k_{\parallel}$, and may phase mix more efficiently. Interestingly, we do not observe increased phase mixing efficiency in our numerical simulations. Instead, we see that the energy gets scattered in the phase space in such a way, that it generates a significant amount of return flux of energy from small to large velocity scales. We identify this effect as the stochastic analog of the plasma echo in a turbulent system. As a result, the net flux to small velocity scales is suppressed, effectively reducing the phase mixing efficiency. Suppression of phase mixing by the turbulent plasma echo helps explain the power law energy spectra at kinetic scales in turbulent plasmas, even when the scalar has a parallel cascade*.

5.2 Kinetic model

We consider a homogeneous magnetized plasma close to a Maxwellian equilibrium threaded by a background magnetic field $\mathbf{B_0} = B_0\hat{\mathbf{z}}$; with all fluctuations low-frequency compared to the cyclotron frequency. We assume that it suffices to describe only one particle species (ions or electrons) kinetically, and calculate the

*The case of no parallel cascade was discussed in Chapter 4, where it was shown that in the nonlinear limit energy in the scalar is swept up to small spatial scales before it can phase mix—resulting in power law spectra.

evolution of the other species using an appropriate Boltzmann response. We further assume all wavelengths to be large compared to the kinetic species' Larmor radius. Such a system is described using a (3+1)D model, with three spatial co-ordinates x, y, z and one velocity co-ordinate $v_\parallel$ parallel to the background magnetic field; the remaining velocity co-ordinates are integrated out. The perturbed distribution function g of the kinetic species satisfies a "drift-kinetic" equation[†]:

$$\partial_t g + \mathbf{u}_\perp \cdot \nabla_\perp g + v_\parallel \nabla_\parallel (g + \varphi F_0) = C[g] + \eta \nabla_\perp^2 g + \chi, \tag{5.1}$$

$$\varphi = \alpha \int_{-\infty}^{\infty} dv_\parallel g(v_\parallel). \tag{5.2}$$

Here $\mathbf{u}_\perp$ is a "fluid" drift velocity that mixes the perturbed distribution function perpendicular to the magnetic field, $v_\parallel \nabla_\parallel g$ is the parallel streaming term that phase-mixes the distribution function, i.e. generates $v_\parallel$ structure, $C[g]$ is a collision operator (diffusive in $v_\parallel$) that smooths this structure in an irreversible manner, $\eta \nabla_\perp^2 g$ is a diffusive term that extracts energy from the system at small perpendicular scales (and stands in for a possibly more complicated cutoff associated with finite-Larmor-radius physics). The equilibrium distribution function $F_0 = e^{-v_\parallel^2/v_{\text{th}}^2}/\sqrt{\pi} v_{\text{th}}$ is a Maxwellian, where $v_{\text{th}} = \sqrt{2T/m}$, T is the temperature and m the mass of the reference species, and the equilibrium density is assumed to be unity. $-\nabla_\parallel \varphi$ is the normalized (by the parameter α) parallel electric field, and χ is a source that injects energy into the system.

[†]This equation could have also been derived from KRMHD in the same way as Chapter 4. By giving an alternate presentation here, we emphasize the general applicability of this equation beyond KRMHD.

Eqs. (5.1–5.2) describe qualitatively or, in some cases, quantitatively, a multitude of plasmas, for *e.g.* ion-acoustic perturbations in a proton-electron plasma, in which case $\alpha = T_e/T_i$ (T_e and T_i are temperatures of electrons and ions respectively) and $\mathbf{u}_\perp = v_{thi}\hat{z} \times \rho_i \nabla\varphi/2$ (ρ_i is the ion Larmor radius) is the $\mathbf{E} \times \mathbf{B}$ drift velocity. In this electrostatic system, the fluctuating electric field, and hence the drift velocity, is set by the density fluctuations of the perturbed distribution function g. In contrast, compressive fluctuations in electromagnetic plasmas decouple from the Alfvénic turbulence in the long wavelength limit, and are passively advected by the velocity fluctuations due to the Alfvénic turbulence [1]. For such a system, the velocity $\mathbf{u}_\perp$ is independent of the perturbed distribution function g; the parameter α depends on plasma beta, T_i/T_e and the ion charge[‡].

5.2.1 Hermite space dynamics

The linear Hermite space formalism developed in Sec. 3.4 can be generalized to the nonlinear model at hand as follows. Eq. (5.2) becomes

$$\varphi = \alpha g_0, \tag{5.3}$$

whereas the kinetic equation (Eq. (5.1)) turns into a set of fluid-like equations (similar to Eqs. (3.26–3.28)) in which phase mixing is manifested as a coupling between

[‡]See eqs. 181 and 182 of Schekochihin et al. [1], α is related to their Λ as $\alpha = -1/\Lambda$.

neighboring Hermite moments:

$$\frac{dg_0}{dt} + v_{\rm th}\nabla_\parallel \frac{g_1}{\sqrt{2}} = \eta\nabla_\perp^2 g_0 + \chi_0, \tag{5.4}$$

$$\frac{dg_1}{dt} + v_{\rm th}\nabla_\parallel \left(g_2 + \frac{1+\alpha}{\sqrt{2}}\, g_0 \right) = \eta\nabla_\perp^2 g_1 + \chi_1, \tag{5.5}$$

$$\frac{dg_m}{dt} + v_{\rm th}\nabla_\parallel \left(\sqrt{\frac{m+1}{2}}\, g_{m+1} + \sqrt{\frac{m}{2}}\, g_{m-1} \right)$$

$$= -\nu m g_m + \eta\nabla_\perp^2 g_m, \quad m \geq 2. \tag{5.6}$$

Here $d/dt = (\partial_t + \mathbf{u}_\perp \cdot \nabla)$ is the convective derivative, $-\nu m g_m$ is the Hermite transform of the Lenard-Bernstein collision operator [80], and ν is the collision frequency. Energy is injected into the system by driving g_0 and/or g_1 using the source terms χ_0 and χ_1. The energy then propagates to higher m. We will later see that a perturbation at high m can be coupled back to low m through the nonlinear interaction—this is the "phase-unmixing" component, the stochastic turbulent analog of the plasma echo.

Upon Fourier transforming Eq. (5.6) in space, $(x, y, z) \to \mathbf{k}$ and defining $\tilde{g}_{m,k} = \left(i\,\mathrm{sgn}\, k_\parallel\right)^m g_{m,k}$, where $k_\parallel$ is the component of $\mathbf{k}$ parallel to $\mathbf{B}_0$, one finds

$$\frac{\partial \tilde{g}_{m,k}}{\partial t} + \frac{|k_\parallel| v_{\rm th}}{\sqrt{2}} \left(\sqrt{m+1}\tilde{g}_{m+1,\mathbf{k}} - \sqrt{m}\tilde{g}_{m-1,\mathbf{k}} \right) =$$

$$\sum_{\mathbf{p},\mathbf{q}} M_{\mathbf{kpq}} \left[\mathrm{sgn}\, \left(k_\parallel q_\parallel \right) \right]^m \Phi_{\mathbf{p}} \tilde{g}_{m,\mathbf{q}} - \nu m \tilde{g}_{m,k}$$

$$-\eta k_\perp^2 \tilde{g}_{m,k}, \tag{5.7}$$

where Φ is the stream function for the drift velocity, $\mathbf{u}_\perp = \hat{\mathbf{z}} \times \nabla\Phi$ and $M_{\mathbf{kpq}} =$

$-\hat{z}\cdot(\mathbf{p}\times\mathbf{q})\,\delta_{\mathbf{k},\mathbf{p}+\mathbf{q}}$.

If we assume weak collisions $\nu \ll |k_\parallel| v_{\rm th}$, large values of m, $1 \ll m \ll (|k_\parallel| v_{\rm th}/\nu)^2$, remain undamped. For such large m, the second term on the left hand side of Eq. (5.7) is dominant. This implies $\tilde{g}_{m+1} \approx \tilde{g}_{m-1}$, i.e., $\tilde{g}_{m+1} \approx \pm\tilde{g}_m$. Hence, there are two solutions: one where $\tilde{g}_m$ is continuous, and the other where $(-1)^m\tilde{g}_m$ is. Thus $\tilde{g}^+_m = (\tilde{g}_m + \tilde{g}_{m+1})/2$ and $\tilde{g}^-_m = (-1)^m(\tilde{g}_m - \tilde{g}_{m+1})/2$ are both continuous in m (see also Sec. 3.4.5)[§]. We would like to approximate the second term on the left hand side of Eq. (5.7) as a derivative in m. Since $\tilde{g}^\pm_{m,k}$ are continuous in m, we can derive approximate evolution equations[¶] (valid to $O(1/\sqrt{m})$) for $\tilde{g}^\pm_{m,k}$ from Eq. (5.7), by expanding in the small parameter $1/\sqrt{m}$

$$\frac{\partial \tilde{g}^\pm_{m,k}}{\partial t} \pm \sqrt{2}|k_\parallel| v_{\rm th} m^{1/4} \frac{\partial}{\partial m} m^{1/4} \tilde{g}^\pm_{m,k} + \nu m \tilde{g}^\pm_{m,k} = \sum_{\mathbf{p},\mathbf{q}} M_{\mathbf{kpq}} \Phi_{\mathbf{p}} \left(\delta^+_{k_\parallel,q_\parallel} \tilde{g}^\pm_{m,\mathbf{q}} + \delta^-_{k_\parallel,q_\parallel} \tilde{g}^\mp_{m,\mathbf{q}} \right) - \eta k_\perp^2 \tilde{g}^\pm_{m,k}, \tag{5.8}$$

where $\delta^\pm_{k_\parallel,q_\parallel} = 1$ if $k_\parallel$ and $q_\parallel$ have the same/opposite sign and 0 otherwise (the sign of $k_\parallel = 0$ is taken to be positive). There are three separate physical effects manifest in Eq. (5.8): (i) phase mixing/unmixing—the left hand side of Eq. (5.8) is an advection equation in m, where "+" (phase-mixing) modes propagate from small m to large, and "−" (phase-unmixing) modes propagate from large m back to small; (ii) turbulent cascade—the first term on the right hand side describes nonlinear coupling of modes with different wavenumbers, which generates fluctuations at small spatial scales; (iii) plasma echo—the second term on the right hand side couples the

[§]Note that the "+" and "−" fields here are not the same as the ones in Eq. (1.19).

[¶]Except for the nonlinear terms on the right hand side, this is the same equation as Eq. (3.53).

phase-mixing and phase-unmixing components via nonlinear interaction with the drift velocity. This allows for a phase-mixing mode propagating to large m to be converted to an phase-unmixing mode which would propagate back to small m, and vice versa.

In the absence of nonlinear advection ($\Phi = 0$), there is no turbulent cascade, and the phase-mixing and phase-unmixing components are decoupled. In this "linear" limit it can be proven analytically that $\tilde{g}_m^- = 0$ to lowest order in $1/\sqrt{m}$, i.e., there is no plasma echo (see [146], Chapter 3). Another instance where a complete lack of an echo can be shown, is when the drift velocity is 2D ($p_\parallel = 0$). Then, the resonance condition $k_\parallel = q_\parallel + p_\parallel = q_\parallel$ does not allow $k_\parallel$ and $q_\parallel$ to have opposite signs, which according to Eq. (5.8) is a necessary condition for coupling between phase-mixing and phase-unmixing modes. Unlike the linear or the 2D drift velocity limit, a 3D drift velocity ($p_\parallel \neq 0$) has all three aforementioned effects existing simultaneously in the system.

5.2.2 Energetics

In order to understand the relative importance of these three effects, we diagnose how the free energy of perturbations, $W = \int d\mathbf{r} \left(\int dv_\parallel \langle g^2 \rangle / 2F_0 + \langle \varphi^2 \rangle / 2\alpha \right) = \int d\mathbf{r} \left[\sum_m |g_m|^2 + |g_0|^2 (1+\alpha) \right]$ gets distributed in the phase space by the dynamics of the system. W is conserved by Eqs. (5.1–5.2) in absence of dissipation (see Refs. [1, 16, 146] and Sec. 1.5.2). Phase mixing transfers W from small m to large, phase unmixing brings it back from large m to small. Nonlinear advection cascades

W to small spatial scales.

The contribution of individual Hermite moments to the total free energy W, is given by $F_{s,\mathbf{k}} = \sqrt{m} k_\perp \, |\tilde{g}_{m,k}|^2$, where we have changed the Hermite space variable from m to $s = \sqrt{m}$. At large s, $F_{s,\mathbf{k}}$ can be split into the phase-mixing ($F^+_{s,\mathbf{k}}$) and phase-unmixing components ($F^-_{s,\mathbf{k}}$), where $F^\pm_{s,\mathbf{k}} = \sqrt{m} k_\perp \, |\tilde{g}^\pm_{m,k}|^2$ (see Eq. (5.8)). To derive evolution equations for $F^\pm_{s,\mathbf{k}}$, multiply Eq. (5.8) by $\sqrt{m} \; k_\perp \; \tilde{g}^{\pm\star}_{m,k}$ (the asterisk denotes complex conjugate), to obtain

$$\frac{\partial F^\pm_{s,\mathbf{k}}}{\partial t} \pm \frac{\left|k_\parallel\right| v_{\rm th}}{\sqrt{2}} \frac{\partial F^\pm_{s,\mathbf{k}}}{\partial s} + 2\nu s^2 F^\pm_{s,\mathbf{k}} + 2\eta k_\perp^2 F^\pm_{s,\mathbf{k}} = \textit{Nonlinear terms.} \tag{5.9}$$

We can now define the flux of energy from low to high s in the large s limit: $\Gamma_{s,\mathbf{k}} = \left|k_\parallel\right| v_{\rm th} \left(F^+_{s,\mathbf{k}} - F^-_{s,\mathbf{k}}\right)/\sqrt{2}$. The efficiency of phase mixing is then given by the normalized flux $\sqrt{2}\Gamma_{s,\mathbf{k}}/|k_\parallel| v_{\rm th} F_{s,\mathbf{k}} = (F^+_{s,\mathbf{k}} - F^-_{s,\mathbf{k}})/(F^+_{s,\mathbf{k}} + F^-_{s,\mathbf{k}})$—phase mixing is completely suppressed when this quantity is zero, whereas when it is one, the amount of phase mixing is same as that for the linear system. An exact expression for the flux that is valid at all s can be calculated directly from Eq. (5.7): $\Gamma_{s,\mathbf{k}} = \left|k_\parallel\right| v_{\rm th} \sqrt{(m+1)/2} \, {\rm Re}\langle \tilde{g}_{m+1,\mathbf{k}} \tilde{g}^\star_{m,k} \rangle$.

5.3 Numerical setup

We solve Eqs. (5.4–5.6) numerically using *Gandalf*. To simplify the analysis we assume that the distribution function is passive, i.e., the drift velocity $\mathbf{u}_\perp$ is independent of g. The velocity $\mathbf{u}_\perp = \hat{\mathbf{z}} \times \nabla\Phi$ is calculated by solving the Langevin equation $\partial_t \Phi + \gamma\Phi = \kappa$, where $\gamma > 0$ and κ is Gaussian white noise ($\langle \kappa(t)\kappa(t') \rangle =$

$\epsilon\delta(t-t')$) which drives Φ with power ϵ; γ is chosen such that the Kubo number is held constant at one (see Sec. 4.1). The drift velocity was restricted to a single scale (all wavenumbers $\mathbf{p}$ such that $p_\perp = 1, p_\parallel = 1$), the largest scale in our numerical box. The saturated root mean square amplitude of the drift velocity can be calculated using the fluctuation-dissipation theorem [89]: $\langle u_\perp^2 \rangle = p_\perp^2 \epsilon / 2\gamma$. In light of these simplifications, one can estimate the turbulent cascade rate as $\tau_C^{-1} \sim |p_\perp \mathbf{u}_\perp|$, which we control in our simulations by changing ϵ.

The source term in Eq. (5.4), χ_0, is assumed to be delta-correlated in time, and χ_1 is set to zero. Since Eq. (5.1) is homogeneous in g, the power with which χ_0 injects energy into the system can be set to unity without loss of generality.

Instead of using the Lenard-Bernstein collision operator or regular viscosity as in Eq. (5.6), we use hypercollisions ($-\nu m^8 g_m$) and hyperviscosity ($-\eta k_\perp^8 g_m$) to efficiently utilize computational resources. The dissipation microscales for these operators can be estimated as $s_c = \sqrt{m_c} = \left(p_\parallel v_{\mathrm{th}}/\nu\right)^{1/17}$ and $k_{\perp,\eta} = \left(|u_\perp|/\eta\right)^{1/8}$, where s_c is the collisional cutoff for modes with parallel wavenumber $p_\parallel$; $k_{\perp,\eta}$ is the viscous cutoff. A simulation is fully characterized by 3 parameters: the nonlinear advection rate τ_C^{-1}, the collisional cutoff s_c and the viscous cutoff $k_{\perp,\eta}$. All the results included in this chapter are from a simulation with parameters $\tau_C \simeq 1.5$, $s_c \simeq 21.3$ and $k_{\perp,\eta} \simeq 18.8$.

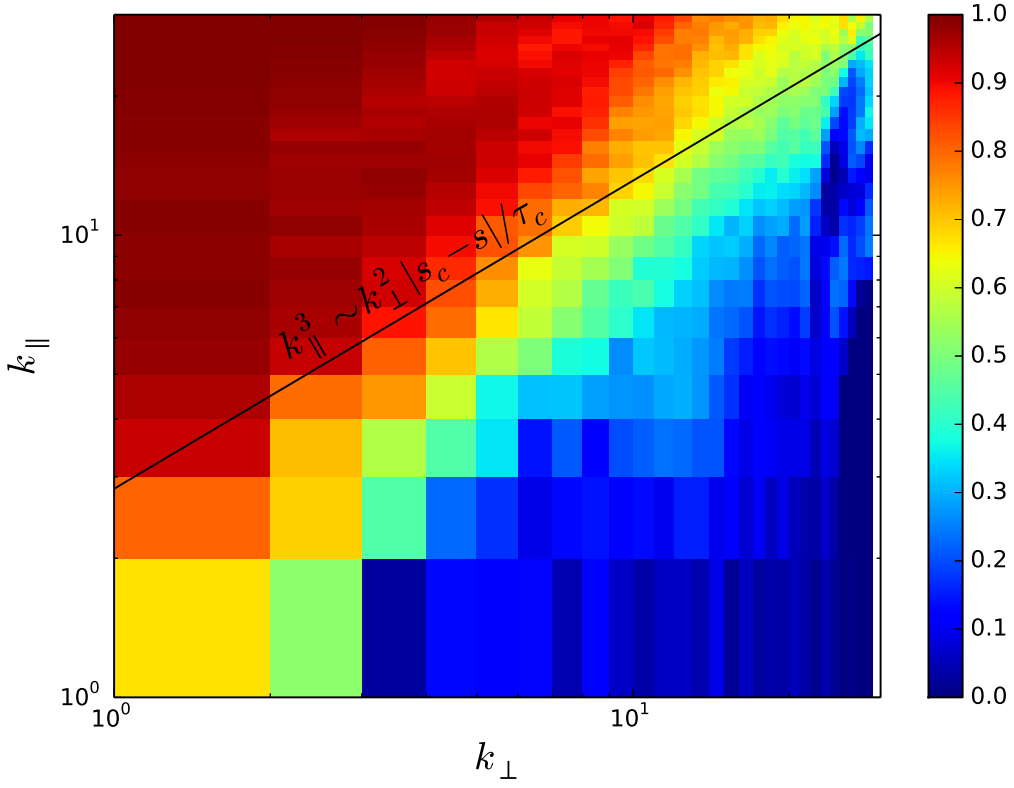

Figure 5.2: Normalized flux (defined after Eq. (5.9)) through $s = 10$ vs $k_\perp - k_\parallel$. Phase mixing is nearly completely suppressed for $k_\parallel^3 \leq k_\perp^2 \left|s_c - s\right| / \tau_C$.

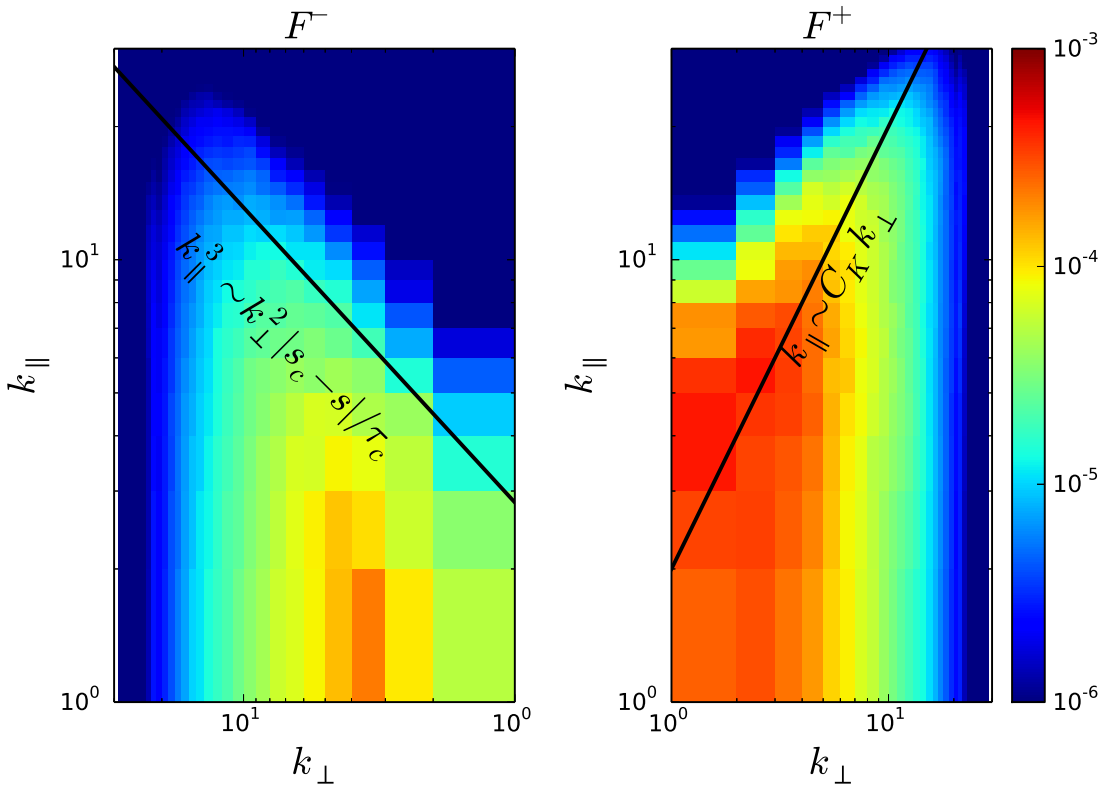

Figure 5.3: $F^{\pm}_{s,\mathbf{k}}$ (defined before Eq. (5.8)) at $s = 10$ vs $k_\perp - k_\parallel$; F^- is plotted on the left, F^+ on the right. The horizontal axis for F^- is reversed, so as to facilitate comparison with the F^+ plot. For $k_\parallel^3 \geq k_\perp^2 \left|s_c - s\right| / \tau_C$, there is negligible $F^-_{s,\mathbf{k}}$. $F^+_{s,\mathbf{k}}$ is seen to cascade to large wavenumbers along the $k_\parallel \sim C_K k_\perp$ line.

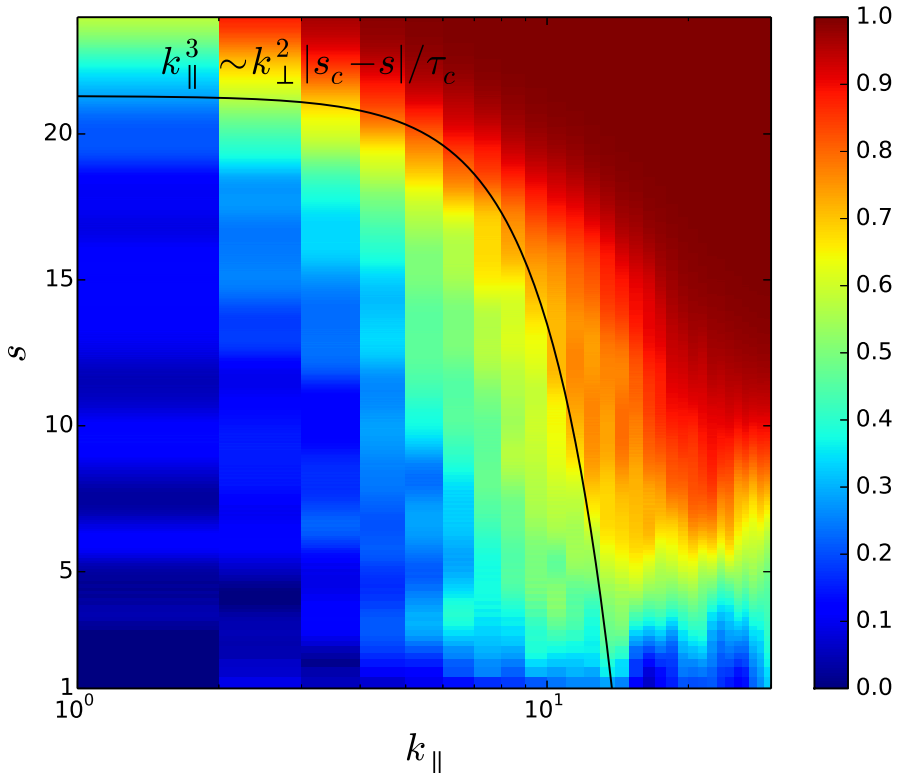

Figure 5.4: Normalized flux (defined after Eq. (5.9)) at $k_\perp = 8$ vs $k_\parallel - s$. Phase mixing is nearly completely suppressed for $k_\parallel^3 \leq k_\perp^2 |s_c - s| / \tau_C$.

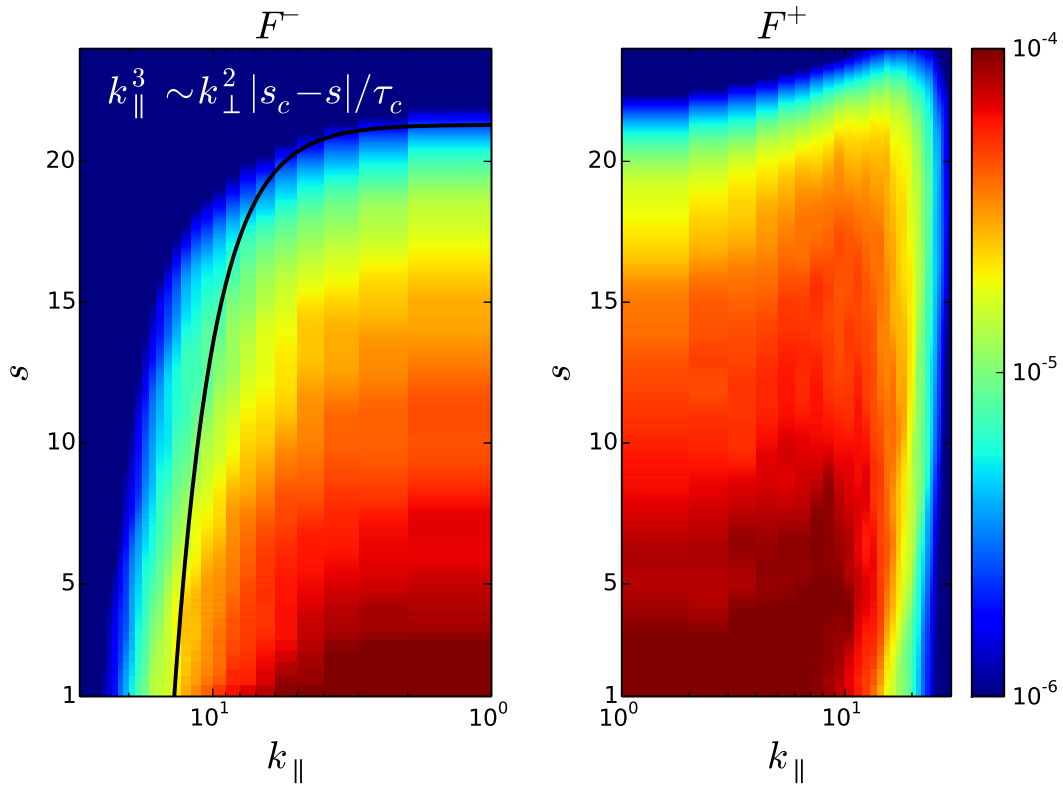

Figure 5.5: $F^{\pm}_{s,\mathbf{k}}$ (defined before Eq. (5.8)) at $k_\perp = 8$ vs $k_\parallel - s$; F^- is plotted on the left, F^+ on the right. The horizontal axis for F^- is reversed, so as to facilitate comparison with the F^+ plot. For $k_\parallel^3 \geq k_\perp^2 |s_c - s| / \tau_C$, there is negligible $F^-_{s,\mathbf{k}}$.

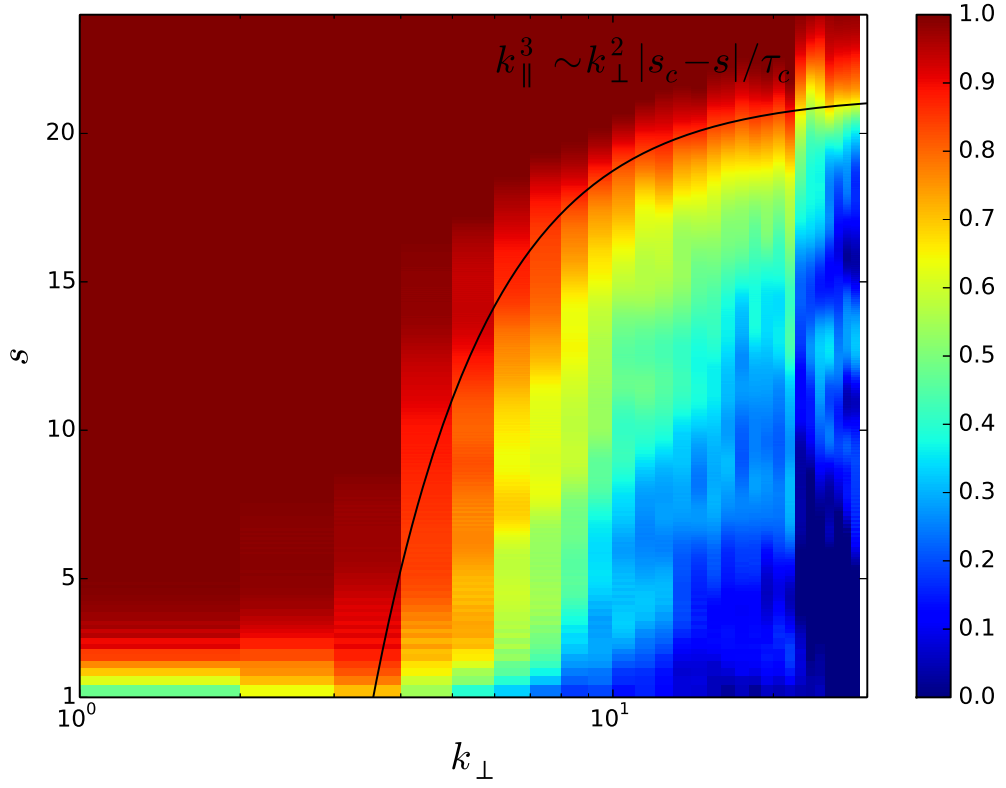

Figure 5.6: Normalized flux (defined after Eq. (5.9)) at $k_\parallel = 8$ vs $k_\perp - s$. Phase mixing is nearly completely suppressed for $k_\parallel^3 \leq k_\perp^2 |s_c - s| / \tau_C$.

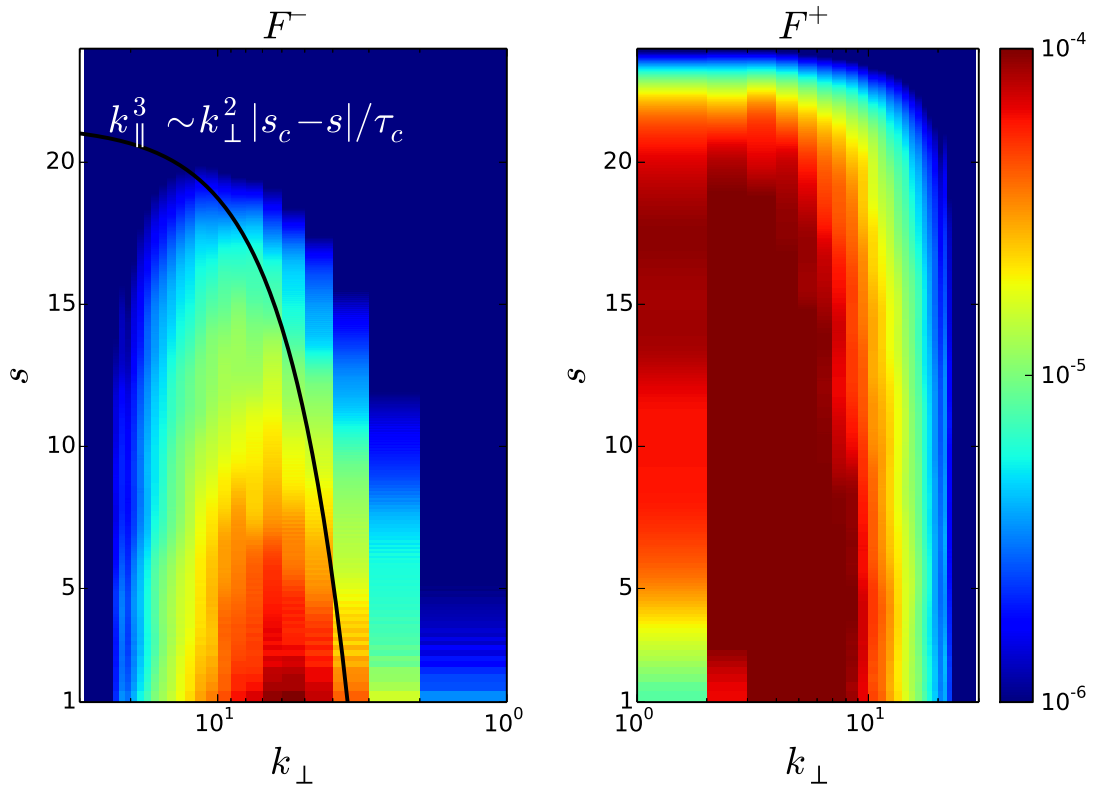

Figure 5.7: $F^{\pm}_{s,\mathbf{k}}$ (defined before Eq. (5.8)) at $k_\parallel = 8$ vs $k_\perp - s$; F^- is plotted on the left, F^+ on the right. The horizontal axis for F^- is reversed, so as to facilitate comparison with the F^+ plot. For $k_\parallel^3 \geq k_\perp^2 |s_c - s| / \tau_C$, there is negligible $F^-_{s,\mathbf{k}}$.

5.4 Results

5.4.1 Phase mixing efficiency

Since we chose the drift velocity to be a single scale velocity field with $p_\parallel = 1$, the nonlinear term couples modes whose parallel wavenumbers differ from each other by one. A phase mixing mode at $s = 1$, with a parallel wavenumber $k_\parallel$, is converted to an phase-unmixing mode only if the two have oppositely signed parallel wavenumbers (see Eq. (5.8)). Hence, such a phase-mixing mode has to go through at least $k_\parallel$ nonlinear interactions in order to reach $k_\parallel = 0$, before it can be converted to an phase-unmixing mode. While this phase-mixing mode cascades to $k_\parallel = 0$, it also gets transferred to a larger s due to phase mixing. If this value of s is comparable to the collisional cutoff s_c, a part of the energy is lost to collisions, and only the remaining energy gets converted to an phase-unmixing mode—this sets a bound on the extent of the plasma echo in the phase space. We observe in our simulations that the plasma echo is restricted to the $k_\parallel^3 \leq k_\perp^2 \left|s_c - s\right| / \tau_C$ region of the phase space as seen in figs. (5.2–5.7). As a result of the echo, phase mixing is significantly suppressed for $k_\parallel^3 \leq k_\perp^2 \left|s_c - s\right| / \tau_C$.

5.4.2 Spectra vs $(s, k_\perp, k_\parallel)$

In the previous section we saw that the phase space is split into a suppressed and an unsuppressed region by the $k_\parallel^3 \sim k_\perp^2 \left|s_c - s\right| / \tau_C$ line. In this section we discuss how the spectra look like in the $(s, k_\perp, k_\parallel)$ phase space.

From Fig. 5.3, we see that the phase-mixing component cascades to small

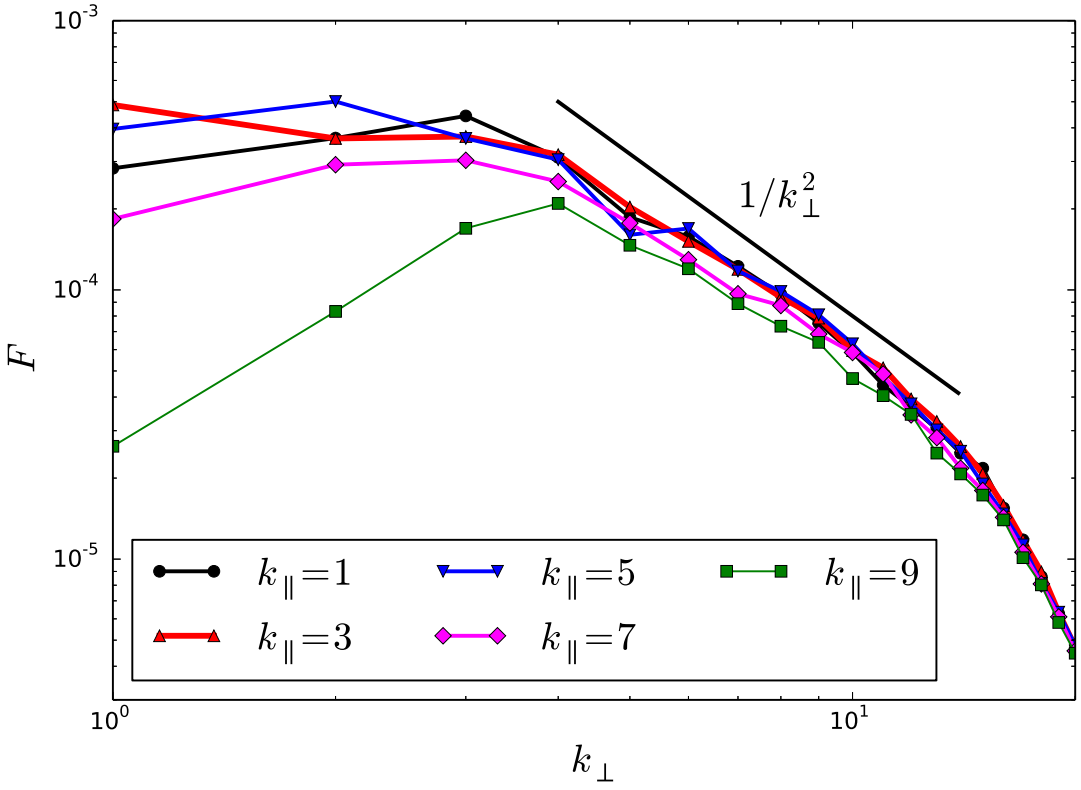

Figure 5.8: $F_{s,\mathbf{k}}$ vs $k_\perp$ for $s = 10$. $F_{s,\mathbf{k}}$ increases for $k_\perp \leq k_\parallel/C_K$, and then is $\sim 1/k_\perp^2$.

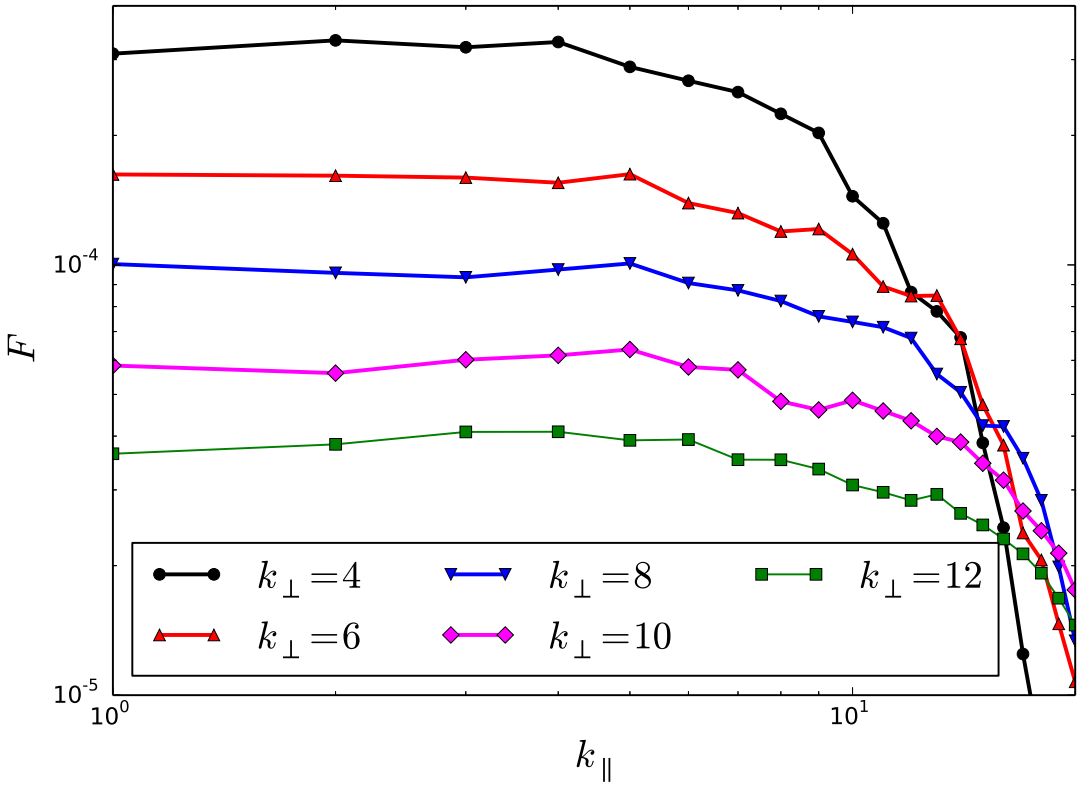

Figure 5.9: $F_{s,\mathbf{k}}$ vs $k_\parallel$ for $s = 10$. $F_{s,\mathbf{k}}$ is a constant $k_\parallel \leq C_K k_\perp$, and then steeply rolls off.

spatial scales along the $k_\parallel \sim C_K k_\perp$ line[‖], where C_K is a constant (we observe $C_K \approx 2$). This relationship between the parallel and the perpendicular wavenumber can also be seen from the 1D spectra plotted in Figs. 5.8 and 5.9: the perpendicular spectra increase till $k_\perp \leq k_\parallel / C_K$, and then are approximately $\sim 1/k_\perp^2$, whereas the parallel spectra are constant till $k_\parallel \leq C_K k_\perp$ and then roll off steeply.

In order to understand these spectra, we add the "+" and "−" equations in Eq. (5.9), to derive an equation for the spectrum $F_{s,\mathbf{k}}$:

$$\frac{\partial F_{s,\mathbf{k}}}{\partial t} + \frac{\partial \Gamma_{s,\mathbf{k}}}{\partial s} + 2\nu s^2 F_{s,\mathbf{k}} + 2\eta k_\perp^2 F_{s,\mathbf{k}} = \textit{Nonlinear terms.} \tag{5.10}$$

For the suppressed region of the phase space, $\Gamma_{s,\mathbf{k}} \approx 0$, i.e., the steady state spectrum is a zero flux solution. Setting $\Gamma_{s,\mathbf{k}} = 0$ in Eq. (5.10) reduces the problem to the fluid limit. It can be shown in this limit that the spectrum is given by $F_{s,\mathbf{k}} \propto k_\perp / \left(k_\parallel^2 + C_K^2 k_\perp^2\right)^{3/2}$; this is consistent with the spectra observed in Figs. 5.8 and 5.9.

The spectra versus s in the suppressed region are observed to decay exponentially at a rate proportional to $1/k_\perp$, and independent of $k_\parallel$ (see Figs. 5.10, 5.11 and 5.12). In the unsuppressed (phase-mixed) region, the s spectrum is constant (see Figs. 5.11, 5.12 and 5.13), which is the same spectrum as that for the Landau-damped solution[**] [111, 112, 114, 146].

[‖]This may be thought of as the analog of a critical-balance style relationship between parallel and perpendicular wavenumbers in our model; C_K is the equivalent Kolmogorov-constant.

[**]Since the spectrum plotted in this chapter is $F_{s,\mathbf{k}} = \sqrt{m} k_\perp |\tilde{g}_{m,k}|^2$, a constant-in-$s$ spectrum is same as the $|g_m|^2 \sim 1/\sqrt{m}$ spectrum from Chapter 3.

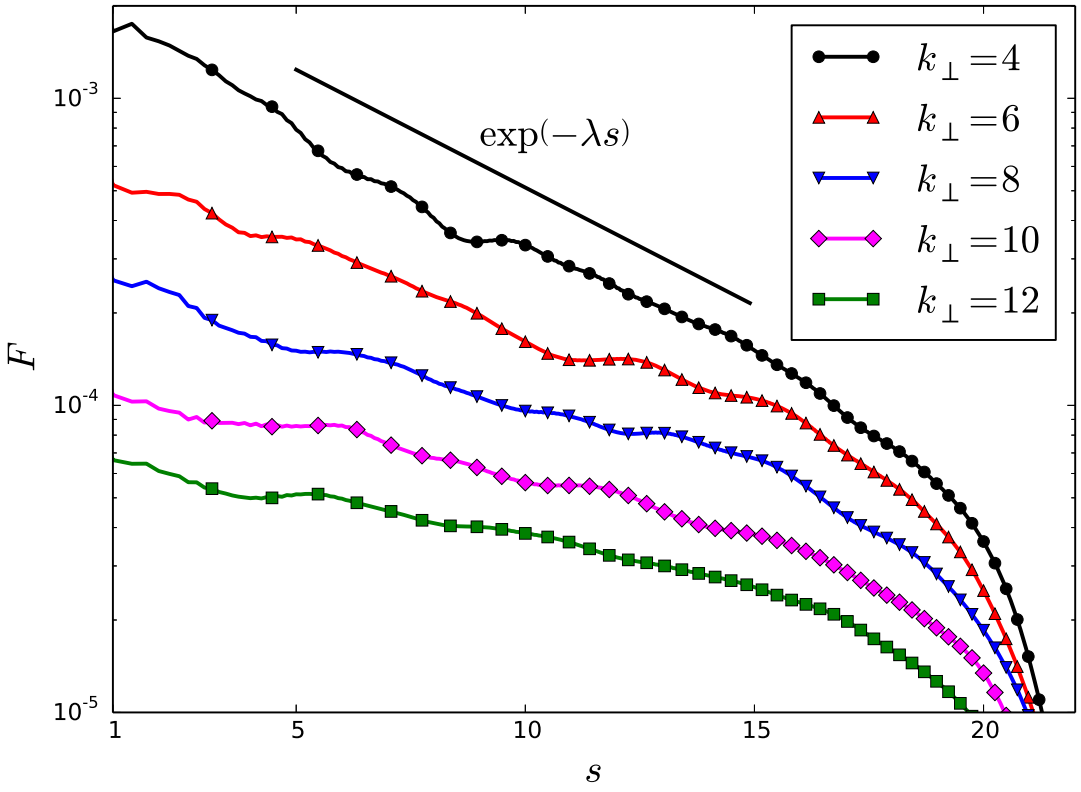

Figure 5.10: $F_{s,\mathbf{k}}$ vs s for $k_\parallel = 2$. The spectrum decays in s at a rate $\lambda \propto 1/k_\perp$ (see Fig. 5.11) in the region where phase-mixing is suppressed (see figs. (5.2–5.7)).

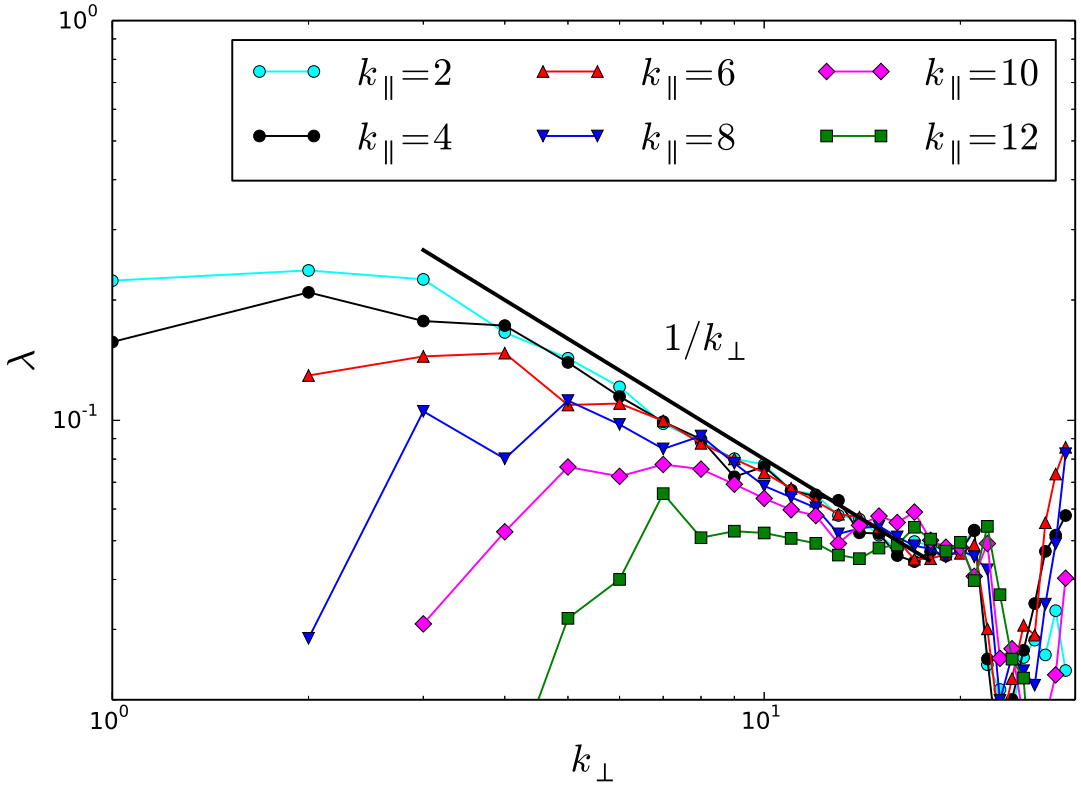

Figure 5.11: The rate λ at which spectrum $F_{s,\mathbf{k}}$ decays in s (see Fig. 5.10) vs $k_\perp$. We observe that $\lambda \propto 1/k_\perp$ in the suppressed region; in the unsuppressed region $\lambda \approx 0$.

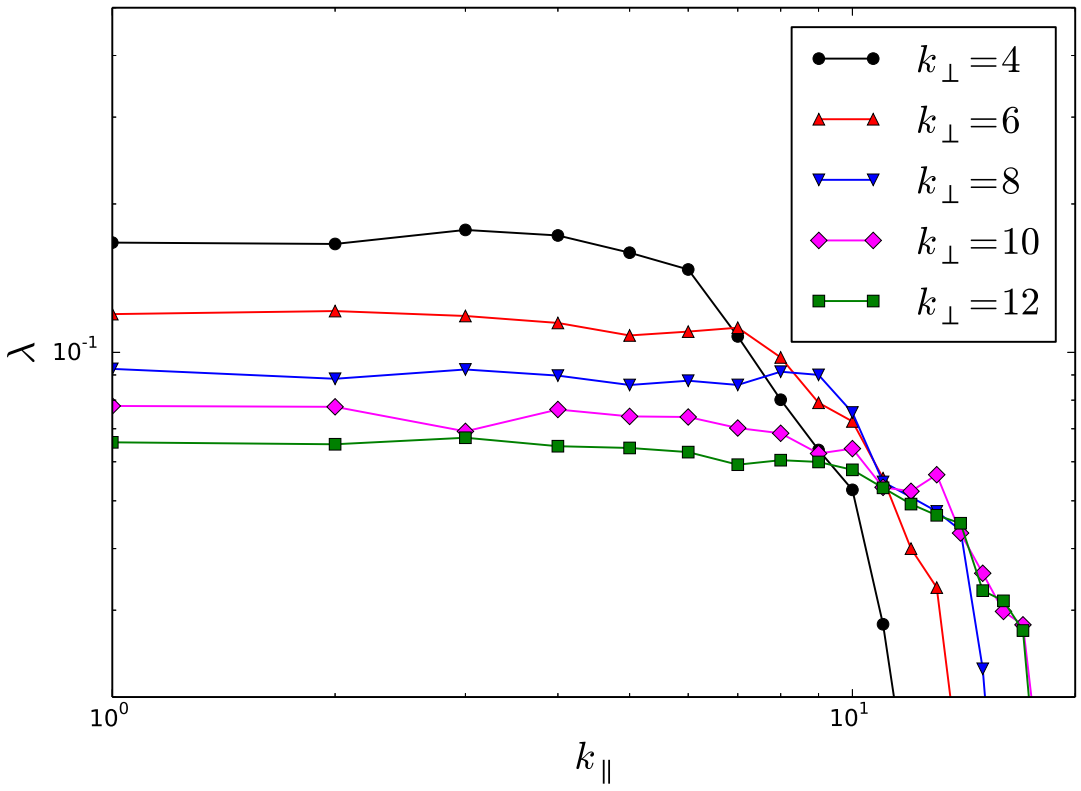

Figure 5.12: The rate λ at which spectrum $F_{s,\mathbf{k}}$ decays in s (see Fig. 5.10) vs $k_\parallel$. λ is independent of $k_\parallel$ in the suppressed region; in the suppressed region $\lambda \to 0$.

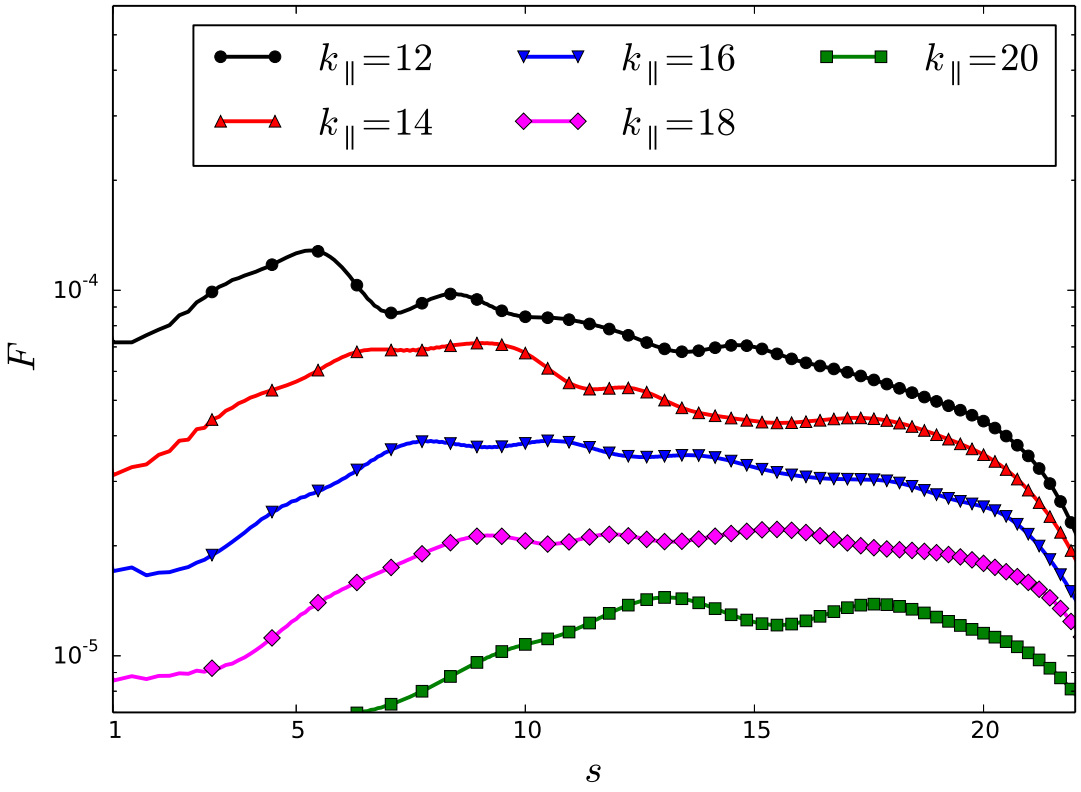

Figure 5.13: $F_{s,\mathbf{k}}$ vs s for $k_\perp = 6$. In the unsuppressed region the spectrum vs s is constant.

5.5 Conclusions and discussion

We demonstrated with a simplified model for kinetic passive scalar turbulence that Landau damping, or more generally phase mixing can be suppressed significantly in turbulent systems for a part of the phase space. Energy is scattered in the phase space such that the net flux to higher Hermite moments of the distribution function is reduced due to the stochastic plasma echo. We showed using direct numerical simulations that phase mixing is suppressed significantly in the region $k_\parallel^3 \leq |p_\perp \mathbf{u}_\perp| \, k_\perp^{2/3} s_c$. Therefore, in the collisionless limit ($s_c \to \infty$), phase mixing would be suppressed in the whole inertial range. Perpendicular and parallel spectra were shown to be the same as fluid spectra in the suppressed region. The suppression of Landau damping by the stochastic plasma echo helps explain why power law energy spectra survive at scales where fluctuations are expected to be strongly damped, by linear theory.

Here, we conclude our treatment of the kinetic passive scalar (chapters 3, 4 and 5), and give a summarized list of our results so far:

- We analytically derived the fluctuation-dissipation relations in the linear limit for the kinetic passive scalar.

- We constructed an analytical framework to diagnose the efficiency of phase mixing by considering the flow of energy in the Hermite space. Within this framework, we proved that in the linear limit, the steady state solution to the system is a constant-flux solution, and that the energy solely flows from small to large Hermite moments for large values of $\sqrt{m}$.

- When the passive scalar is being mixed by a 2D velocity field, the spectrum in the Hermite space is exponentially attenuated in the strong turbulence regime, and the behavior of the kinetic system is essentially fluid-like. This is a result of the energy in the passive scalar being swept up to small spatial scales by the advecting velocity field, before it can phase mix.

- On the other hand, if the scalar is being mixed by a 3D velocity, there is a stochastic analog of the plasma echo which suppresses the efficiency of phase mixing in a part of the phase space, the extent of which is determined by the collisionality of the system, and the amplitude of the advecting velocity.

In the next chapter, we use these ideas, and the diagnostic tools developed here to study the compressive fluctuations cascade in the kinetic reduced MHD limit.

Chapter 6

Compressive fluctuations in the solar wind

6.1 Introduction

In situ measurements of turbulence in the solar wind [135, 147–151] make it a remarkable laboratory to study kinetic plasma turbulence. It is generally agreed upon that the turbulence in the solar wind comprises mostly of Alfvénic fluctuations [152] (about 90% of the energy), with an admixture of compressive modes. The Alfvén-wave cascade has been studied in great detail using fluid [122, 153–167] and kinetic [136, 168, 169] models. Numerical studies of the compressive cascade have mostly been done in the fluid limit [120, 170–174]. However, since the solar wind is a nearly collisionless plasma, a kinetic treatment is required. The compressive perturbations in the solar wind are mostly slow and entropy modes with negligible amounts of energy in the fast mode [175], hence a low frequency description like kinetic reduced MHD (which orders the fast mode out) can be used.

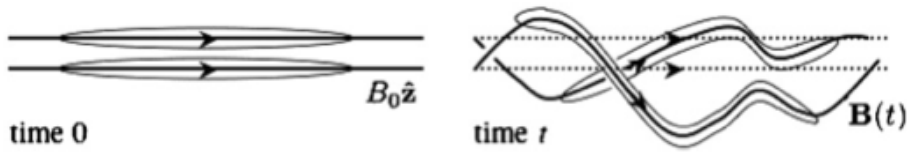

Figure 6.1: The compressive fluctuations are passively cascaded by the Alfvénic turbulence, and may remain correlated along the perturbed fieldlines (figure taken from Schekochihin et al. [1]).

In a weakly collisional system like the solar wind, slow modes are subject to strong kinetic damping. This is at odds with the observed power law spectra for density and field strength fluctuations. Power law spectra suggest that compressive fluctuations undergo a Kolmogorov-style turbulent cascade. A possible explanation for this apparent discrepancy is that even though slow modes develop fine scales in the plane perpendicular to the local magnetic field as they are passively mixed by the background Alfvénic turbulence, they remaining correlated in the parallel direction [1]. This leads to highly anisotropic structures with the parallel wavelength set by the initial conditions, which results in weak damping since the damping rate is proportional to the parallel wavenumber (see Fig. 6.1). However, this argument ignores dissipation. Lithwick and Goldreich [120] argued against this suggestion, by noticing that when the cascade reaches the ion Larmor radius in the perpendicular plane, these highly anisotropic fluctuations would decorrelate due to finite Larmor radius effects (which in our model show up as a diffusive term at small perpendicular scales), and acquire the same parallel correlation lengths as the Alfvén waves. Recent observations of the solar wind seem to support the idea that there is no parallel cascade [104]. However, these results are somewhat inconclusive. In Chen *et al.* [104], they construct a representative eddy for the field strength fluctuations, and find it to be much more anisotropic than the Alfvénic eddy (see their figures 4 and 6), which on its surface seems to have settled the issue. But in the same paper, they also observe a power law spectrum in the direction of the local magnetic field, with a spectral exponent between -1.42 and -1.58 (see their figure 5)—a shallower spectrum than that for Alfvénic fluctuations (though severely limited by

resolution). In fact they use this shallow spectrum to construct the eddy in the first place. A possible conciliation between these two mutually contradictory results is that the compressive fluctuations are anisotropic at the outer scale itself, and then cascade to smaller perpendicular and parallel scales [176]—i.e., an anisotropic structure observed at small scales does not imply a lack of parallel cascade, and might be a result of the initial conditions. This however, still leaves two questions unanswered — (a) is there a parallel cascade for the compressive fluctuations? (b) If there is a parallel cascade, why are the compressive fluctuations undamped?

We show, using direct numerical simulations of kinetic reduced MHD, that the compressive fluctuations undergo a parallel cascade*, but they remain undamped due to suppression of phase mixing by the turbulent plasma echo discussed in Chapter 5.

6.2 Numerics

We solve Eqs. (1.16) and (1.19) using *Gandalf*. Alfvén waves were driven by injecting random velocity fluctuations using a Gaussian white noise source; compressive fluctuations were sourced independently by driving $\delta B_\parallel$, i.e. the zeroth velocity moment of g_B (see Eq. (A.35)). The ion charge (Z), ion to electron temperature ratio (τ) and the ion plasma beta (β_i) were all set to one—these choices are representative of the usual solar wind parameters. The resolution in the real space was chosen to be 128^3, 144 Hermite moments of the perturbed distribution function were evolved, hypercollisions (νm^8) and hyperviscosity ($\eta k_\perp^{16}$) were used to

*The observed parallel cascade may be a result of our forcing—this requires further investigation. However, the results from Chapter 4 explain the observed power law density fluctuation spectra for the case where there is no parallel cascade.

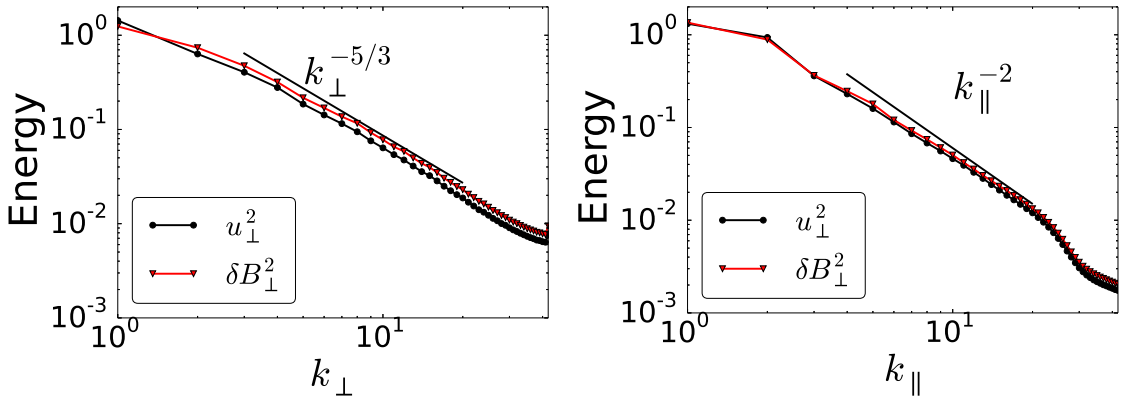

Figure 6.2: Perpendicular and parallel spectra of the Alfvénic fluctuations. The critical balance predictions: $k_\perp^{-5/3}$ for the perpendicular spectra and $k_\parallel^{-2}$ for the parallel spectra are observed in simulations.

regularize fine scale structure.

6.3 Alfvénic turbulent cascade

The Goldreich-Sridhar critical balance theory [1, 19, 20] predicts the Alfvénic turbulence to have $k_\perp^{-5/3}$ perpendicular, and $k_\parallel^{-2}$ parallel spectra. The precise spectral exponent is a highly debated issue in the community—Boldyrev et al. [177–180] argue that scale-dependent dynamic alignment needs to be included in the critical-balance theory for MHD turbulence, which ends up predicting a $k_\perp^{-3/2}$ perpendicular spectrum, whereas Beresnyak et al. [163, 164] observe the Goldreich-Sridhar $k_\perp^{-5/3}$ spectrum in their simulations. The resolution requirements to settle this controversy are beyond the capability of present day GPUs, and hence this issue is not addressed in our work. In our simulations, we observe the perpendicular spectrum to be $k_\perp^{-5/3}$ (see Fig. 6.2), which we consider to be consistent with the theories on either side of this debate. The parallel spectrum is seen to be $k_\parallel^{-2}$ (see Fig. 6.2), which is a

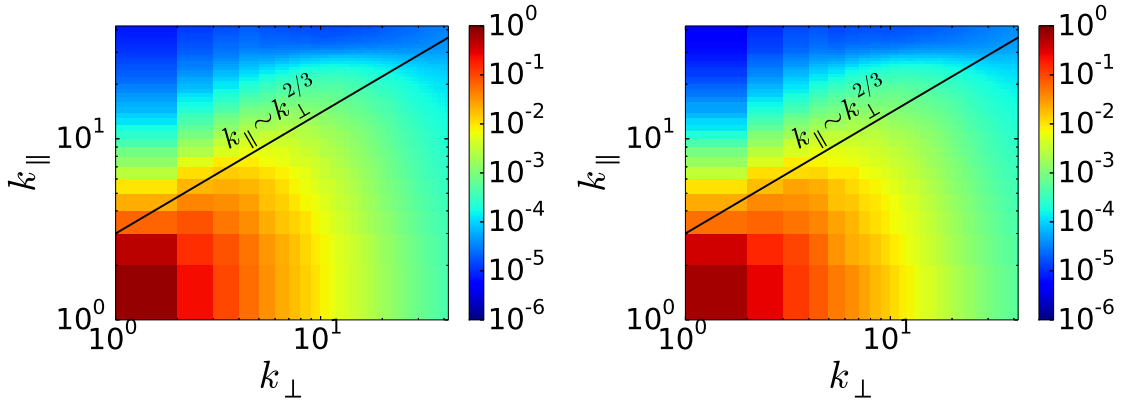

Figure 6.3: Kinetic (left) and magnetic (right) energy vs $k_\perp, k_\parallel$.

prediction of both the theories. Our numerical spectra are broadly consistent with observations in the solar wind [104, 135, 141, 148–151].

In addition to the power law spectra having different spectral exponents in the perpendicular and the parallel directions, the wavenumber anisotropy predicted by critical-balance can also be seen in the 2D spectra plotted in Fig. 6.3. The energy containing region is seen to bounded by the $k_\parallel \sim k_\perp^{2/3}$ line as predicted by critical balance[†].

6.4 Slow mode turbulent cascade

Being passively mixed, the compressive fluctuations are predicted to have the same perpendicular spectrum as the Alfvénic fluctuations, $k_\perp^{-5/3}$. This is observed in our simulations as shown in Fig. 6.4. Interestingly, the compressive fluctuations are also observed to undergo a parallel cascade (see Figs. 6.4 and 6.5), and have the

[†]The anisotropy constant given by the ratio $k_\parallel/k_\perp^{2/3}$ used here is not predicted by critical balance. We use the constant measured in numerical simulations by Beresnyak [163] to plot the analytical predictions in Fig. 6.3.

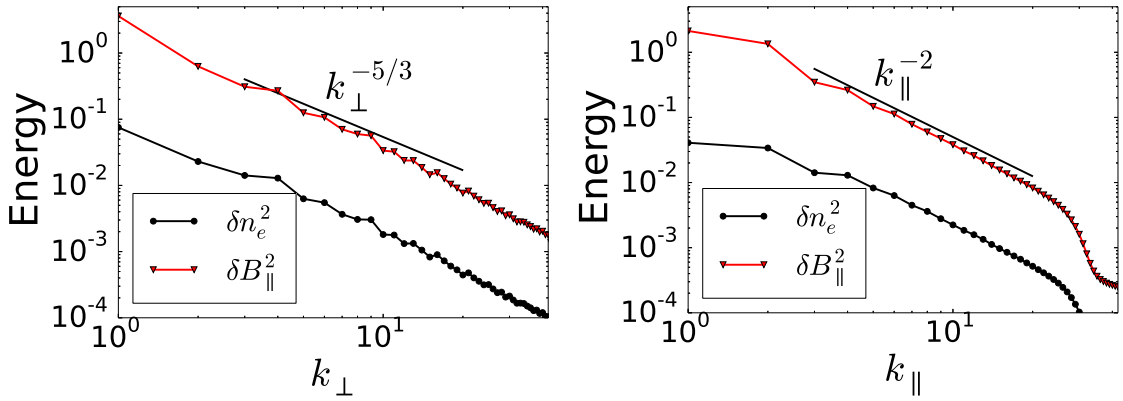

Figure 6.4: Perpendicular and parallel spectra of the density and field strength fluctuations. The compressive fluctuations being passively mixed, inherit the same perpendicular spectrum as the Alfvénic fluctuations, consistent with the theoretical prediction. The parallel spectra for compressive modes are also observed to be the same as that for the Alfvénic perturbations, indicating that the compressive fluctuations undergo a parallel cascade, with the parallel correlation lengths being set by the Alfvénic turbulence.

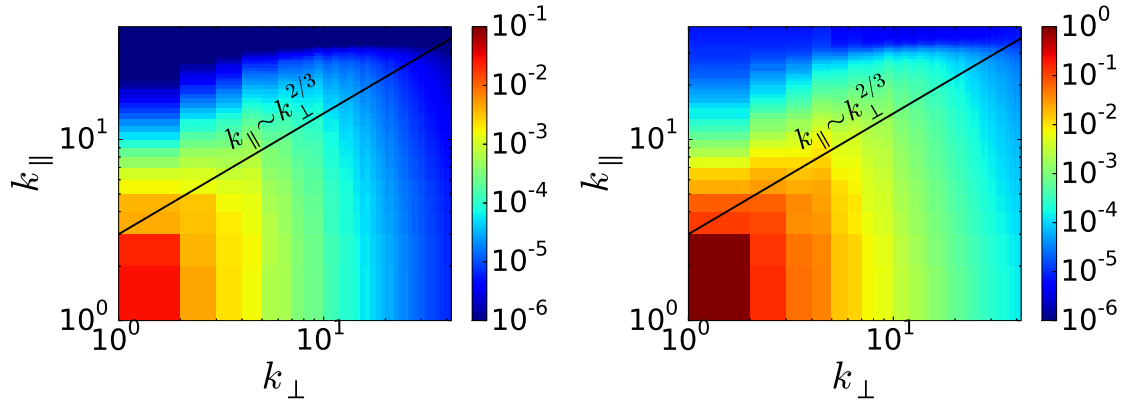

Figure 6.5: Density (left) and field strength fluctuations (right) vs $k_\perp, k_\parallel$.

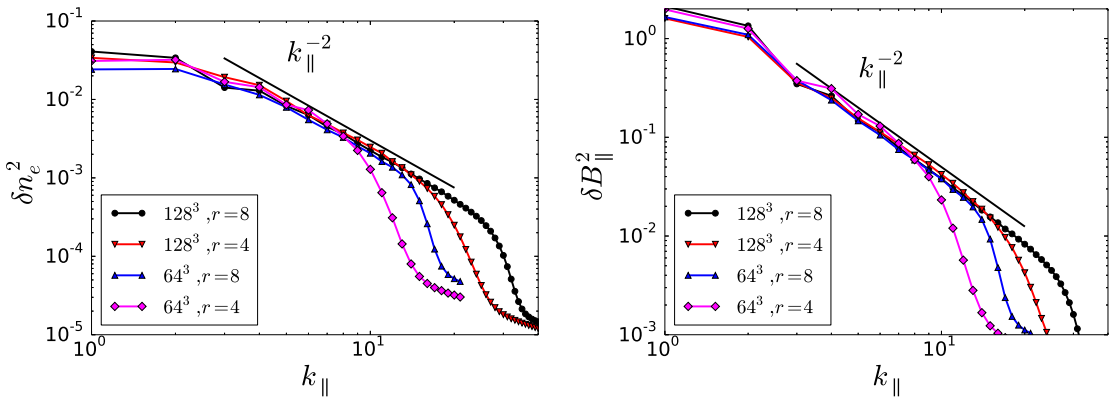

Figure 6.6: Density (left) and field strength spectra (right) vs $k_\parallel$, for different resolutions and hyper-dissipation exponents—similar to Fig. 2.2. The first number corresponds to the resolution used, the second number is the hyper-diffusion exponent.

same parallel spectra as the Alfvénic cascade. These are preliminary results, and we are still in the process of diagnosing the reasons behind such a parallel cascade. However, we carried out a convergence study (see Fig. 6.6), and are fairly confident in our numerical results.

These results show that compressive fluctuations are unable to stay correlated along the perturbed fieldlines as suggested by Schekochihin et al. [1], and do develop small scale structure along the perturbed magnetic field. However, it is not yet clear as to why despite cascading to small parallel scales, the slow modes remain undamped.

6.5 Suppression of phase-mixing

We saw in Chapter 5, that for a kinetic passive scalar being nonlinearly advected by a chaotic velocity field, phase mixing is significantly suppressed due to

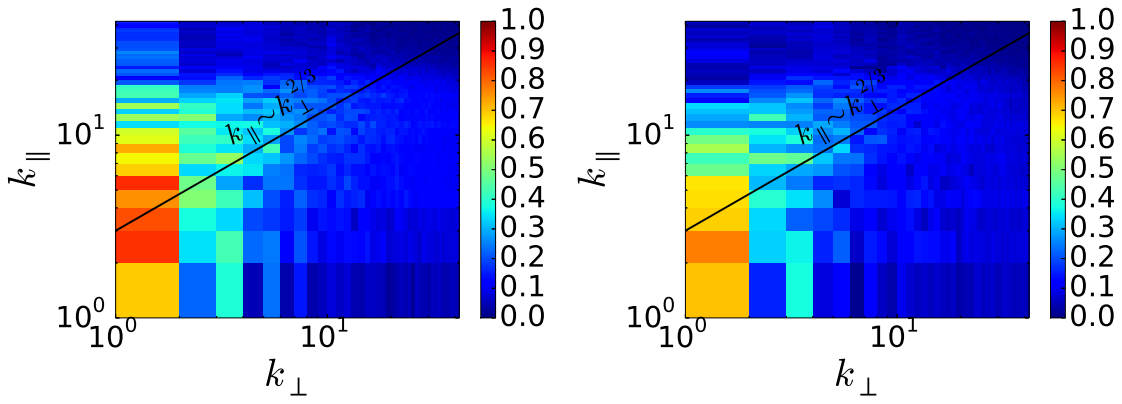

Figure 6.7: Normalized flux vs $k_\perp - k_\parallel$, at $m = 1$ for g^+ on the left, and g^- on the right (see Eq. (A.38)). Phase-mixing is nearly completely suppressed in the critical-balance cone, $k_\parallel \lesssim k_\perp^{2/3}$.

the turbulent plasma echo. In this section we argue that even though compressive fluctuations develop small spatial structure along the fieldline, and should be heavily damped by phase mixing, they remain undamped because of the echo.

We diagnose the plasma echo using the normalized flux diagnostic developed in Chapter 5 (see discussion after Eq. (5.9)), except, we use the exact form for the flux: $\Gamma_{s,\mathbf{k}} = |k_\parallel| v_{\rm th} \sqrt{(m+1)/2}\, {\rm Re}\langle \tilde{g}_{m+1,\mathbf{k}} \tilde{g}^\star_{m,k} \rangle$—we do so because the approximate expression for the flux is valid only at large values of $\sqrt{m}$, and we wish to diagnose the amount of flux out of the first Hermite moment. In steady state, the flux to higher Hermite moments is seen to be nearly zero (see Fig. 6.7)—this is especially true in the critical balance cone $k_\parallel \lesssim k_\perp^{2/3}$, which is the energy containing region for our system. Since, in steady state, the amount of energy transferred to higher Hermite moments out of the first moment is nearly zero, the compressive fluctuations have a fluid-like turbulent cascade that remains unaffected by phase mixing. As a result, we observe power law spectra for density and field strength fluctuations

extending all the way to the ion Larmor radius.

6.6 Conclusions

Preliminary results from direct numerical simulations of the kinetic reduced MHD equations show that compressive fluctuations undergo a parallel cascade in the inertial range, and they do not maintain long correlations along the perturbed field as suggested by Schekochihin et al [1]. This also suggests that the anisotropic eddies observed in the solar wind [104] are probably due to the anisotropy at the outer scale—unfortunately, since our analytical, and numerical framework does not include the outer scale, this can not be tested in our simulations.

Despite the parallel cascade, the compressive fluctuations remain undamped in the inertial range, which contradicts the linear prediction that these fluctuations should be heavily damped due to transit-time damping. This happens because the Alfvénic turbulence drives a substantial return flux for the compressive fluctuations from small to large velocity space scales (similar to the echo in Chapter 5)—as a result, phase mixing is suppressed, and power law spectra for density and field strength fluctuations are observed.

Chapter 7

Summary and discussion

In this thesis, we have presented fundamental results pertaining to passive scalar turbulence in kinetic systems—we analytically derived the fluctuation-dissipation relations for a kinetic scalar (Chapter 3), and we showed numerical results which shed light on how linear phase mixing for a kinetic passive scalar is modified due to nonlinear advection (chapters 4 and 5). In particular, in Chapter 5, we identified the turbulent analog of the plasma echo, and demonstrated, with the aid of a simple model, that phase mixing may be siginificantly suppressed due to the echo in collisionless systems. We developed a new code, *Gandalf* (Chapter 2) to simulate the kinetic reduced MHD equations [1], which describe the Alfvénic and compressive components of the turbulent cascade in the solar wind at scales larger than the ion Larmor radius. In Chapter 6, we addressed two key questions regarding the compressive cascade in the inertial range using numerical simulations — 1. Do the compressive fluctuations have a parallel cascade? 2. Why are the density and field strength fluctuations undamped at kinetic scales? We found that the compressive perturbations do indeed have a parallel cascade, and have the same perpendicular and parallel power law spectra as the Alfvénic fluctuations. We showed, by diagnosing the flux in Hermite space, that despite the parallel cascade compressive fluctuations remain undamped due to the stochastic plasma echo.

Even in the absence of a parallel cascade for the slow modes, the power law spectra can be explained using the results from Chapter 4. In this limit, the slow modes cascade to small perpendicular spatial scales before they can phase mix, resulting in a fluid-like turbulent cascade, hence, exhibit power law spectra.

We would like to investigate the cascade of compressive fluctuations further, in particular, to understand how the parallel cascade comes about. After developing solid understanding of this problem, we hope to study how the compressive cascade, in particular the plasma echo, is dependent on parameters like the plasma beta, the ion charge, and the ion to electron temperature ratio. Another direction forward would be to add more physics to *Gandalf*. This can be done in two possible ways. Firstly, by implementing non-Maxwellian distribution functions—this would enable further numerical investigations into solar wind turbulence near the marginal stability boundaries for firehose and mirror instabilities. Secondly, making *Gandalf* fully gyrokinetic by including finite Larmor radius effects. The work in this thesis was restricted to scales larger than the ion Larmor radius, where linear phase mixing is the only phase mixing process available to the system. With a gyrokinetic code, the ideas developed here could be generalized to include finite Larmor radius effects, specifically, to investigate the role nonlinear phase mixing [8] plays in the turbulent cascade at sub-Larmor scales.

The analytical and numerical framework developed as a part of this thesis fits in a larger program to understand the properties of turbulence in weakly collisional magnetized plasmas like the solar wind, in particular, to study the dissipation mechanisms favored by the system, and to learn how the dissipated energy is partitioned

between different species of the plasma.

Appendix A

Mathematical framework: Kinetic reduced MHD

A.1 Introduction

A kinetic plasma is described by the distribution function $f_s(t, \mathbf{r}, \mathbf{v})$—the probability of finding a particle of species s (ions or electrons) at position $\mathbf{r}$ with velocity $\mathbf{v}$ at time t. The distribution function evolves according to the Boltzmann equation:

$$\frac{\partial f_s}{\partial t} + \mathbf{v} \cdot \nabla f_s + \frac{q_s}{m_s}\left(\mathbf{E} + \frac{\mathbf{v} \times \mathbf{B}}{c}\right) \cdot \frac{\partial f_s}{\partial \mathbf{v}} = \left(\frac{\partial f_s}{\partial t}\right)_{\text{coll}}, \tag{A.1}$$

where q_s and m_s are the species' charge and mass, c is the speed of light; the right hand side is the (quadratic in f) Landau collision operator. The electric and magnetic fields, $\mathbf{E}$ and $\mathbf{B}$, are calculated using Maxwell's equations:

$$\nabla \times \mathbf{B} = \frac{4\pi}{c}\mathbf{j} + \frac{1}{c}\frac{\partial \mathbf{E}}{\partial t}, \tag{A.2}$$

$$\nabla \times \mathbf{E} = -\frac{1}{c}\frac{\partial \mathbf{B}}{\partial t}, \tag{A.3}$$

$$\nabla \cdot \mathbf{E} = 4\pi\rho, \tag{A.4}$$

$$\nabla \cdot \mathbf{B} = 0, \tag{A.5}$$

$$\rho = \sum_s q_s \int d^3\mathbf{v} f_s, \quad \mathbf{j} = \sum_s q_s \int d^3\mathbf{v}\mathbf{v} f_s, \tag{A.6}$$

where ρ and $\mathbf{j}$ are the charge and current densities.

Although a complete description, the Boltzmann-Maxwell set of Eqs. (A.1–A.5) is computationally prohibitively expensive. A more tractable, reduced set of equations can be derived by limiting to a description of plasmas with a strong mean magnetic field. It is assumed that the turbulent fluctuations in such a plasma are (i) spatially anisotropic with respect to the mean field, (ii) have frequencies that are smaller than the ion cyclotron frequency, (iii) and are small in amplitude in comparison with the equilibrium quantities. The dimensionality of the phase space is then reduced from six to five by averaging over the fast cyclotron motion of the particles. This set of equations is known as gyrokinetics, which though simpler, is still a fully kinetic description.

Depending on the research problems in mind, even simpler, hybrid models can be derived by making further approximations. All the results in this thesis pertain to the behavior of weakly collisional plasmas at scales larger than the ion gyro-radius: the so called "inertial range". By expanding the gyrokinetic equation in the smallness of the ion gyro-radius, one can derive kinetic reduced magnetohydrodynamics, an asymptotically valid description of these systems in the inertial range. All the work in this thesis is done in the limit where KRMHD is true. In the next two sections we describe the gyrokinetic and the KRMHD set of equations.

A.2 Gyrokinetics

A.2.1 Introduction

Linear [42–46] and nonlinear gyrokinetics [1, 17, 47–51, 181] has been used in studying magnetized plasmas for over four decades. Historically, gyrokinetics has been a popular choice to study turbulence and transport generated by micro-instabilities in fusion plasmas ([182–190] are a handful of examples). In the past ten years, however, there has been substantial work studying the relevance and utility of gyrokinetics for space and astrophysical plasmas [1, 16, 17, 138, 168, 191–196] . Traditionally, these plasmas have been described using magnetohydrodynamics. However, there are many examples of astrophysical plasmas where small-scale perturbations have wavelengths smaller than the ion mean free path, and therefore require a kinetic description. MHD turbulence has a natural propensity to drive the system towards increasing anisotropy as energy is cascaded to small scales [21, 22]. The intrinsic anisotropic nature of the MHD turbulent cascade also implies that the frequencies of these small-scale fluctuations remain far below the ion cyclotron frequency (this is so because the frequencies of the turbulence are proportional to the parallel wavenumbers). Hence, such plasmas are well described by gyrokinetics.

A.2.2 Equations

First separate the distribution function and the fields into equilibrium and fluctuating parts (the δf approximation):

$$f_s = F_{0s} + \delta f_s,\ \mathbf{B} = \mathbf{B}_0 + \delta\mathbf{B},\ \mathbf{E} = \delta\mathbf{E}, \tag{A.7}$$

where F_{0s} is the equilibrium distribution function, which to zeroth order is a Maxwellian:

$$F_{0s} = \frac{n_{0s}}{\left(\pi v_{ths}^2\right)^{3/2}} \exp\left(-\frac{v^2}{v_{ths}^2}\right), \quad v_{ths} = \sqrt{\frac{2T_{0s}}{m_s}}, \tag{A.8}$$

n_{0s} and T_{0s} are the density and temperature of species s. We further assume that the equilibrium is homogeneous, i.e., there are no gradients of the equilibrium density and temperature. The background magnetic field $\mathbf{B_0}$ is assumed to be a straight, uniform magnetic field:

$$\mathbf{B}_0 = B_0\hat{\mathbf{z}}. \tag{A.9}$$

The two homogeneous Maxwell's Eqs. (A.3) and (A.5) can be solved by expressing the fields in terms of potentials,

$$\delta\mathbf{E} = -\nabla\varphi - \frac{1}{c}\frac{\partial A_\parallel}{\partial t}, \quad \delta\mathbf{B} = \nabla\times\mathbf{A}, \tag{A.10}$$

φ and $\mathbf{A}$ are the electrostatic and magnetic vector potentials respectively; we also choose the Coulomb gauge $\nabla\cdot\mathbf{A} = 0$.

The gyrokinetic approximation is formalized by the following ordering assump-

tions:

$$\frac{\delta f_s}{F_{0s}} \sim \frac{\delta B}{B_0} \sim \frac{\delta E}{(v_{ths}/c)B_0} \sim \frac{k_\parallel}{k_\perp} \sim \frac{\omega}{\Omega_i} \sim \epsilon \ll 1, \tag{A.11}$$

where $k_\parallel$ and $k_\perp$ are the spatial wavenumbers along and across the magnetic field, ω is the typical frequency of the fluctuations and Ω_i is the ion cyclotron frequency.

The perturbed distribution function can be further split into two parts,

$$\delta f_s = -\frac{q_s \varphi(t, \mathbf{r})}{T_{0s}} F_{0s} + h_s(t, \mathbf{R}_s, v_\perp, v_\parallel), \tag{A.12}$$

where the first term is the Boltzmann response. The second term is the distribution function of the centers of the particle gyro-orbits. Note that the gyrocenter distribution function is evaluated at the guiding center position $\mathbf{R}_s$ and not at the particle position $\mathbf{r}$,

$$\mathbf{R}_s = \mathbf{r} + \frac{\mathbf{v}_\perp \times \hat{\mathbf{z}}}{\Omega_s}, \tag{A.13}$$

and is a function of the velocity space variables $v_\perp$ and $v_\parallel$ *. The function h_s satisfies the gyrokinetic equation:

$$\frac{\partial h_s}{\partial t} + v_\parallel \frac{\partial h_s}{\partial z} + \frac{c}{B_0} \{\langle \chi \rangle_{\mathbf{R_s}}, h_s\} = \frac{q_s F_{0s}}{T_{0s}} \frac{\partial \langle \chi \rangle_{\mathbf{R_s}}}{\partial t} + \left(\frac{\partial h_s}{\partial t} \right)_{\text{coll}}, \tag{A.14}$$

where χ is the gyrokinetic potential,

$$\chi = \varphi - \frac{v_\parallel A_\parallel}{c} - \frac{\mathbf{v}_\perp \cdot \mathbf{A}_\perp}{c}. \tag{A.15}$$

*This choice of velocity space co-ordinates is convenient for homogeneous plasmas. For inhomogeneous plasmas, the conserved quantities energy and magnetic moment make better co-ordinates [47].

The Poisson bracket is defined as,

$$\{P, Q\} = \hat{\mathbf{z}} \cdot \left(\frac{\partial P}{\partial \mathbf{R}_s} \times \frac{\partial Q}{\partial \mathbf{R}_s} \right). \tag{A.16}$$

The angle brackets in Eq. (A.14) denote an average over the Larmor motion of the particle at a fixed guiding center position:

$$\langle \chi \left(t, \mathbf{r}, v_\parallel, \mathbf{v}_\perp \right) \rangle_{\mathbf{R}_s} = \frac{1}{2\pi} \int_0^{2\pi} d\theta \, \chi \left(t, \mathbf{R}_s - \frac{\mathbf{v}_\perp \times \hat{\mathbf{z}}}{\Omega_s}, v_\perp, v_\parallel \right), \tag{A.17}$$

where θ is the angular velocity-space co-ordinate in a cyclindrical co-ordinate system:

$$\mathbf{v} = v_\parallel \hat{\mathbf{z}} + v_\perp \left(\cos\theta \hat{\mathbf{x}} + \sin\theta \hat{\mathbf{y}} \right). \tag{A.18}$$

Observe that the ring average in Eq. (A.17) is evaluated at constant guiding center position, but the gyrokinetic potential is a function of the particle position. Another thing to notice is that the ring average, as well as the guiding center position $\mathbf{R}_s$ depends on the particle species index s.

The electromagnetic fields are calculated consistently from h_s using Maxwell's equations. In the non-relativistic limit, Poisson's Eq. (A.4) turns into a quasineutrality condition,

$$0 = \sum_s q_s \delta n_s = \sum_s q_s \left[\frac{-q_s \varphi}{T_{0s}} n_{0s} + \int d^3\mathbf{v} \langle h_s \rangle_{\mathbf{r}} \right]; \tag{A.19}$$

the parallel and perpendicular components of the Ampere's law take the following

forms:

$$\nabla_\perp^2 A_\parallel = -\frac{4\pi}{c} j_\parallel = -\frac{4\pi}{c} \sum_s q_s \int d^3\mathbf{v} v_\parallel \langle h_s \rangle_{\mathbf{r}}, \tag{A.20}$$

$$\nabla_\perp^2 \delta B_\parallel = -\frac{4\pi}{c} \hat{\mathbf{z}} \cdot (\nabla_\perp \times \mathbf{j}_\perp) = -\frac{4\pi}{c} \hat{\mathbf{z}} \cdot \left[\nabla_\perp \times \sum_s q_s \int d^3\mathbf{v} \langle \mathbf{v}_\perp h_s \rangle_{\mathbf{r}} \right], \tag{A.21}$$

where $\delta B_\parallel = \hat{\mathbf{z}} \cdot (\nabla_\perp \times \mathbf{A}_\perp)$ is the field strength fluctuation. Notice that since the electromagnetic field variables φ, $A_\parallel$ and $\delta B_\parallel$ are functions of the particle position and not the guiding center position, the charge and current densities are calculated by gyroaveraging the guiding center distribution at fixed $\mathbf{r}$ (a dual operation to the one in Eq. (A.17)),

$$\langle h_s \left(t, \mathbf{R}_s, v_\parallel, \mathbf{v}_\perp \right) \rangle_{\mathbf{r}} = \frac{1}{2\pi} \int_0^{2\pi} d\theta \, \chi \left(t, \mathbf{r} + \frac{\mathbf{v}_\perp \times \hat{\mathbf{z}}}{\Omega_s}, v_\perp, v_\parallel \right). \tag{A.22}$$

Gyrokinetic Eq. (A.14) for ions and electrons, along with the field Eqs. (A.19–A.21) form a complete, self-consistent set of equations.

A.2.3 Conserved quantity

In absence of collisions, the gyrokinetic system of equations conserves the following quantity, which is the gyrokinetic version of the free energy:

$$W = \int d^3\mathbf{r} \left[\sum_s \left(\int d^3\mathbf{v} \frac{T_{0s} \langle h_s^2 \rangle_{\mathbf{r}}}{2F_{0s}} - \frac{q_s^2 \varphi^2 n_{0s}}{T_{0s}} \right) + \frac{|\delta \mathbf{B}|^2}{8\pi} \right] = \int d^3\mathbf{r} \left(\sum_s \int d^3\mathbf{v} \frac{T_{0s} \delta f_s^2}{2F_{0s}} + \frac{|\delta \mathbf{B}|^2}{8\pi} \right). \tag{A.23}$$

W is the quantity that is cascaded in the phase-space in gyrokinetic turbulence, and is eventually destroyed by collisions, which generates entropy and heats the plasma.

A.3 $k_\perp \rho_i \ll 1$: Kinetic Reduced MHD

A.3.1 Equations

Even though gyrokinetics is a reduced set of computationally tractable equations, solving them numerically can prove to be quite expensive [†]. In this section, we present a simpler hybrid model which is derived by taking the $k_\perp \rho_i \ll 1$ limit of the gyrokinetic set of equations. This range of wavenumbers corresponds to the "inertial range" of the turbulent cascade. In this limit, dynamics of Alfvén waves decouples from that of the slow waves. The Alfvén waves satisfy reduced MHD, a system of equations that can be derived from MHD in the collisional limit, but are true even in the collisionless limit.

Define stream and flux function Φ and Ψ as,

$$\Phi = \frac{c}{B_0}\varphi, \quad \Psi = -\frac{A_\parallel}{\sqrt{4\pi m_i n_{0i}}}. \tag{A.24}$$

The Alfvénic turbulence then evolves according to the following (reduced MHD) equations:

$$\frac{\partial \Psi}{\partial t} = v_A \hat{\mathbf{b}} \cdot \nabla \Phi, \tag{A.25}$$

$$\frac{d \nabla_\perp^2 \Phi}{dt} = v_A \hat{\mathbf{b}} \cdot \nabla \nabla_\perp^2 \Psi, \tag{A.26}$$

where $v_A = B_0/\sqrt{4\pi m_i n_{0i}}$ is the Alfvén velocity. This seemingly strange result of a collisional theory being valid at collisionless scales happens because the Alfvénic part

[†]Though not impossible, there are numerous gyrokinetic codes used widely to study turbulence in magnetized plasmas.

of the distribution function (the part that describes the $\mathbf{E}\times\mathbf{B}$ drift of the plasma and the magnetic fieldlines), is a shifted Maxwellian with a mean perpendicular flow velocity $\mathbf{u}_\perp = \mathbf{u}_E = \hat{\mathbf{z}}\times\Phi$, the $\mathbf{E}\times\mathbf{B}$ velocity:

$$f_i = \underbrace{\frac{n_{0i}}{\left(\pi v_{thi}^2\right)^{3/2}}\exp\left[-\frac{\left(\mathbf{v}_\perp - \mathbf{u}_E\right)^2 + v_\parallel^2}{v_{thi}^2}\right]}_{\text{Alfvénic fluctuations}} + \underbrace{\frac{v_\perp^2}{v_{thi}^2}\frac{\delta B_\parallel}{B_0}F_{0i} + g}_{\text{Compressive fluctuations}} \quad . \tag{A.27}$$

Since the Alfvénic fluctuations do not alter the Maxwellian character of the distribution function, it is unsurprising that the equations satisfied by the Alfvén waves are the same in the collisional and the collisionless limit.

The compressive fluctuations still require a kinetic description in terms of the function g (see Eq. (A.27)), g turns out to be a kinetic passive scalar, which evolves according to a kinetic equation that involves the density (δn_e) and the field strength ($\delta B_\parallel$) fluctuations, and is turbulently mixed by the Alfvénic turbulence. The density and field strength fluctuations in turn depend on g. The complete set of equations describing the compressive fluctuations are:

$$\frac{dg}{dt} + v_\parallel\hat{\mathbf{b}}\cdot\nabla\left[g + \left(\frac{Z}{\tau}\frac{\delta n_e}{n_{0e}} + \frac{v_\perp^2}{v_{thi}^2}\frac{\delta B_\parallel}{B_0}\right)F_{0i}\right] = \left\langle C_{ii}\left[g + \frac{v_\perp^2}{v_{thi}^2}\frac{\delta B_\parallel}{B_0}F_{0i}\right]\right\rangle_{\mathbf{R}_i}, \tag{A.28}$$

$$\frac{\delta n_e}{n_{0e}} = \left[\frac{Z}{\tau} + 2\left(1+\frac{1}{\beta_i}\right)\right]^{-1}\frac{1}{n_{0i}}\int d^3\mathbf{v}\left[\frac{v_\perp^2}{v_{thi}^2} - 2\left(1+\frac{1}{\beta_i}\right)\right]g, \tag{A.29}$$

$$\frac{\delta B_\parallel}{B_0} = \left[\frac{Z}{\tau} + 2\left(1+\frac{1}{\beta_i}\right)\right]^{-1}\frac{1}{n_{0i}}\int d^3\mathbf{v}\left[\frac{v_\perp^2}{v_{thi}^2} + \frac{Z}{\tau}\right]g, \tag{A.30}$$

where

$$\frac{d}{dt} = \frac{\partial}{\partial t} + \{\Phi,\ldots\}, \quad \hat{\mathbf{b}}\cdot\nabla = \frac{\partial}{\partial z} + \frac{1}{v_A}\{\Psi,\ldots\}, \tag{A.31}$$

and

$$Z = \frac{q_i}{q_e}, \quad \tau = \frac{T_{0i}}{T_{0e}}, \quad \beta_i = \frac{v_{thi}^2}{v_A^2} = \frac{8\pi n_{0i} T_{0i}}{B_0^2}. \tag{A.32}$$

C_{ii} is the gyro-averaged, linearized ion-ion collision operator, that acts on the non-Maxwellian part of the distribution function.

Eqs. (A.25) and (A.26) can be rewritten in a more intuitive form in terms of the Elsasser potentials,

$$\xi^{\pm} = \Phi \pm \Psi. \tag{A.33}$$

The Alfvén waves then satisfy (see also Eq. (1.16) and the following discussion),

$$\frac{\partial \nabla_\perp^2 \xi^{\pm}}{\partial t} \mp v_A \frac{\partial \nabla_\perp^2 \xi^{\pm}}{\partial z} = -\frac{1}{2}\left[\{\xi^+, \nabla_\perp^2 \xi^-\} + \{\xi^-, \nabla_\perp^2 \xi^+\} \mp \nabla_\perp^2 \{\xi^+, \xi^-\}\right]. \tag{A.34}$$

In this form, the "+" and "−" potentials have physical interpretations—they are counter-propagating Alfvén waves. In the collisionless limit, Eqs. (A.28–A.30) can be reduced to a simpler form as well. If the collision operator in Eq. (A.28) is ignored, the $v_\perp$ dependence can be integrated over. Define function $g_n(v_\parallel)$ and $g_B(v_\parallel)$ such that,

$$\int dv_\parallel g_n = \frac{\delta n_e}{n_{0e}}, \quad \int dv_\parallel g_B = \frac{\delta B_\parallel}{B_0}. \tag{A.35}$$

Then Eq. (A.28) becomes two coupled equations,

$$\begin{aligned} \frac{dg_n}{dt} + v_\parallel \hat{\mathbf{b}} \cdot \nabla g_n = &- \left[\frac{Z}{\tau} + 2\left(1 + \frac{1}{\beta_i}\right)\right]^{-1} v_\parallel F_0(v_\parallel) \\ &\times \hat{\mathbf{b}} \cdot \nabla \left[\frac{Z}{\tau}\left(1 + \frac{2}{\beta_i}\right)\frac{\delta n_e}{n_{0e}} + \frac{2}{\beta_i}\frac{\delta B_\parallel}{B_0}\right], \end{aligned} \tag{A.36}$$

$$\frac{dg_B}{dt} + v_\parallel \hat{\mathbf{b}} \cdot \nabla g_B = -\left[\frac{Z}{\tau} + 2\left(1 + \frac{1}{\beta_i}\right)\right]^{-1} v_\parallel F_0(v_\parallel) \times \hat{\mathbf{b}} \cdot \nabla \left[\frac{Z}{\tau}\left(1 + \frac{Z}{\tau}\right)\frac{\delta n_e}{n_{0e}} + \left(2 + \frac{Z}{\tau}\right)\frac{\delta B_\parallel}{B_0}\right], \tag{A.37}$$

where $F_0(v_\parallel) = \left(1/\sqrt{\pi v_{thi}}\right) \exp\left(-v_\parallel^2/v_{thi}^2\right)$ is a one dimensional Maxwellian in $v_\parallel$. Further define,

$$g^+ = \frac{1}{\sigma}\left(1 + \frac{Z}{\tau}\right) g_n + g_B, \quad g^- = g_n + \frac{1}{\sigma}\frac{\tau}{Z} g_B, \tag{A.38}$$

where

$$\sigma = 1 + \frac{\tau}{Z} + \frac{1}{\beta_i} + \sqrt{\left(1 + \frac{\tau}{Z}\right)^2 + \frac{1}{\beta_i^2}}. \tag{A.39}$$

Then Eqs. (A.36) and (A.37) can be reduced to the following decoupled equations:

$$\frac{dg^\pm}{dt} + v_\parallel \nabla_\parallel g^\pm = \frac{v_\parallel F_0(v_\parallel)}{\Lambda^\pm} \hat{\mathbf{b}} \cdot \nabla \int dv_\parallel g^\pm, \tag{A.40}$$

where

$$\Lambda^\pm = -\frac{\tau}{Z} + \frac{1}{\beta_i} \pm \sqrt{\left(1 + \frac{\tau}{Z}\right)^2 + \frac{1}{\beta_i^2}}. \tag{A.41}$$

Eqs. (A.34) and (A.40) together constitute the KRMHD model.

g^+ and g^-, as defined in Eq. (A.38) do not have obvious physical meanings like the Elsasser variables for Alfvénic turbulence. However, it is somewhat instructive to consider the large and small beta limits: for $\beta_i \gg 1$, $g^- \approx g_n$, while for $\beta_i \ll 1$, $g^+ \approx g_B$.

A.3.2 Conserved quantity

In the $k_\perp \rho_i \ll 1$ limit, the conserved quantity from Sec. A.2.3 splits into four parts which are all separately conserved:

$$W = W^+_{\rm AW} + W^-_{\rm AW} + W^+_{\rm compr} + W^-_{\rm compr}, \tag{A.42}$$

where

$$W^\pm_{\rm AW} = \int d^3\mathbf{r} \frac{m_i n_{0i}}{2} \left|\nabla_\perp \xi^\pm\right|^2 \tag{A.43}$$

are free-energies of the right and left-going Alfvénic fluctuations, and

$$W^\pm_{\rm compr} = \int d^r\mathbf{r} \frac{n_{0i} T_{0i}}{2} \left[\int dv_\parallel \frac{(g^\pm)^2}{F_0} - \frac{1}{\Lambda^\pm}\left(\int dv_\parallel g^\pm\right)^2\right] \tag{A.44}$$

are free-energies of the $+$ and $-$ components of the compressive fluctuations, as defined in the previous section.

Appendix B

An alternative choice for the source term in Chapter 3

The source term in Eq. (3.4), providing direct forcing of density perturbations, was a choice of convenience: it allowed us to compare directly the FDR for the potential field φ in a kinetic system with the FDR for the Langevin equation (3.1). If, instead, one strives for a form of energy injection with a more transparent physical interpretation, it is natural to imagine it coming from a fluctuating electric field. This changes Eq. (3.4) to the following:

$$\frac{\partial g}{\partial t} + v\,\frac{\partial g}{\partial z} + vF_0\frac{\partial \varphi}{\partial z} = \chi_1(t) v F_0 + C[g], \tag{B.1}$$
$$\langle \chi_1(t)\chi_1(t')\rangle = \varepsilon\delta(t-t'),$$

where $\chi_1(t)$ is the fluctuating parallel electric field, which we model (again, for analytical convenience) as a Gaussian white noise.

The new forcing injects fluctuations of momentum, rather than density. Indeed, in terms of Hermite moments, instead of Eqs. (3.26) and (3.27), we now have

$$\frac{\partial g_0}{\partial t} + \frac{\partial}{\partial z}\frac{g_1}{\sqrt{2}} = 0, \tag{B.2}$$
$$\frac{\partial g_1}{\partial t} + \frac{\partial}{\partial z}\left(g_2 + \frac{1+\alpha}{\sqrt{2}}\,g_0\right) = \frac{\chi_1}{\sqrt{2}}, \tag{B.3}$$

and Eq. (3.28) is unchanged. The field that is directly forced is $g_1 = \sqrt{2}\int \mathrm{d}v\, v g(v)$,

which is proportional to the mean velocity associated with the perturbed distribution g. The new free-energy equation, an analog of Eqs. (3.7) and (3.30), is

$$\frac{\mathrm{d}W}{\mathrm{d}t} = \frac{\varepsilon}{4} + \int \mathrm{d}v \, \frac{\langle gC[g] \rangle}{F_0} = \frac{\varepsilon}{4} - \nu \sum_{m=2}^{\infty} m \langle g_m^2 \rangle. \tag{B.4}$$

This immediately gives us the universal Hermite spectrum and the FDR for the total free energy: we repeat the calculation in Sec. 3.4.4 (which is unchanged because nothing has changed at high m's) using the steady-state version of Eq. (B.4) instead of Eq. (3.46) to get

$$A_k = \frac{\varepsilon_k}{2\sqrt{2}|k|} \tag{B.5}$$

in the expression (3.44) for the Hermite spectrum. Therefore,

$$\frac{1}{2} \sum_{m=1}^{\infty} C_{m,k} = \frac{\Gamma(1/3)}{4 \cdot 3^{2/3}} \frac{1}{\nu^{1/3} |k|^{2/3}} \, \varepsilon_k \tag{B.6}$$

replaces Eq. (3.48) as the FDR for the total free energy. The only differences are in numerical prefactors and the α dependence, which has now disappeared. This is because in our previous forcing model, the source term injected energy into g_0 (density fluctuations), which got scaled by the factor of $1 + \alpha$ when passed on to g_1 (see Eq. (3.27)), whereas in the case we are considering now, the energy is injected directly into g_1, which is then phase mixed to higher m's, without ever encountering any α dependence.

Let us also give here the results one obtains in the collisionless limit by back-

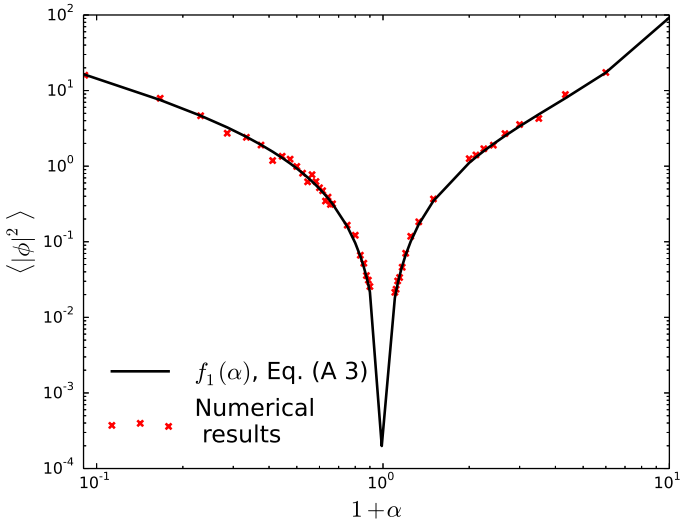

Figure B.1: Normalized steady-state amplitude $2\pi|k|\langle|\varphi_k|^2\rangle/\varepsilon_k = f_1(\alpha)$ vs. $1+\alpha$ for the case of momentum forcing: the solid line is the analytical prediction $f_1(\alpha)$ (Eq. (B.13)), the crosses are computed from the long-time limit of $\langle|\varphi_k|^2\rangle$ obtained via direct numerical solution of Eq. (B.1).

tracking to Eq. (B.1) and solving for g explicitly, as we did in Secs. 3.3 and 3.4.2:

$$g_{k\omega} = -\left(\varphi_{k\omega} + \frac{i\chi_{1,k\omega}}{k}\right)\frac{vF_0}{v-\omega/k}. \tag{B.7}$$

This gives

$$\varphi_{k\omega} = -\frac{i\chi_{1,k\omega}}{k}\frac{1+\zeta Z(\zeta)}{D_\alpha(\zeta)}, \tag{B.8}$$

$$g_{m,k\omega} = -\frac{i\chi_{1,k\omega}}{k}\frac{1}{\alpha}\frac{(-\operatorname{sgn}k)^m}{\sqrt{2^m m!}}\frac{\zeta Z^{(m)}(\zeta)}{D_\alpha(\zeta)}, \quad m \geq 1, \tag{B.9}$$

where $\zeta = \omega/|k|$ as usual. From the last formula, proceeding in the same manner

as we did to get Eq. (3.37), we recover again the Hermite spectrum:

$$C_{m,k} = \frac{\varepsilon_k}{2\pi|k|}\frac{1}{\alpha^2}\frac{1}{2^m m!}\int_{-\infty}^{+\infty} \mathrm{d}\zeta \left|\frac{\zeta Z^{(m)}(\zeta)}{D_\alpha(\zeta)}\right|^2 \tag{B.10}$$

$$\approx \left[\frac{\varepsilon_k}{\sqrt{2\pi}|k|}\frac{1}{\alpha^2}\int_{-\infty}^{+\infty}\frac{\mathrm{d}\zeta\,\zeta^2 e^{-\zeta^2}}{|D_\alpha(\zeta)|^2}\right]\frac{1}{\sqrt{m}} = \frac{\varepsilon_k}{2\sqrt{2}|k|}\frac{1}{\sqrt{m}}. \tag{B.11}$$

The latter expression was obtained in the limit of $m \gg 1$ (see Sec. 3.4.3) and is the same result as Eq. (B.5). The integral is already familiar from Eq. (3.58). For completeness, the "$-$"-mode spectrum (3.58) becomes

$$C^-_{m,k} \approx \left[\frac{\varepsilon_k}{8\sqrt{2\pi}|k|}\frac{1}{\alpha^2}\int_{-\infty}^{+\infty}\frac{\mathrm{d}\zeta\,\zeta^4 e^{-\zeta^2}}{|D_\alpha(\zeta)|^2}\right]\frac{1}{m^{3/2}} = \frac{\varepsilon_k(3+\alpha)}{32\sqrt{2}|k|}\frac{1}{m^{3/2}}. \tag{B.12}$$

The integral was done by Kramers–Kroning relations for the function $h(\zeta) = \zeta^4/D_\alpha(\zeta) - \alpha\zeta^4 - \alpha^2\zeta^2/2 - \alpha^2(3+\alpha)/4$. While again numerical prefactors and α dependence are different, none of the substantive arguments in Sec. 3.4.5 are affected.

Finally, from Eq. (B.8), proceeding in the same manner as in Sec. 3.3, we obtain the FDR relation for the mean square fluctuation amplitude of the potential:

$$\langle|\varphi_k|^2\rangle = \frac{\varepsilon_k}{2\pi|k|}f_1(\alpha), \quad f_1(\alpha) = \int_{-\infty}^{+\infty}\mathrm{d}\zeta\left|\frac{1+\zeta Z(\zeta)}{D_\alpha(\zeta)}\right|^2, \tag{B.13}$$

which is the new version of Eq. (3.13). The function $f_1(\alpha)$ is plotted in Fig. B.1, along with the results of the direct numerical solution of Eq. (B.1). While formally it is a different function than $f(\alpha)$, it exhibits very similar behavior (see Fig. 3.1).

Its asymptotics are (see Secs. 3.3.1 and 3.3.2)

$$\alpha \to -1: \quad f_1(\alpha) \approx \frac{|k|}{\gamma_L} \quad \Rightarrow \quad \langle|\varphi_k|^2\rangle \approx \frac{\varepsilon_k}{2\pi\gamma_L}, \tag{B.14}$$

$$\alpha \to \infty: \quad f_1(\alpha) \approx \frac{\pi\alpha|k|}{4\gamma_L} \quad \Rightarrow \quad \langle|\varphi_k|^2\rangle \approx \frac{\alpha\varepsilon_k}{8\gamma_L}. \tag{B.15}$$

Whereas in both limits there is still an inverse relationship between the mean square fluctuation amplitude and the Landau damping rate γ_L, the numerical coefficients are not easily interpretable in terms of any simple "fluid" Langevin models for φ—not a surprising outcome as, already examining Eqs. (B.2) and (B.3), we might have observed that they do not map on any obvious Langevin-like equation for $\varphi = \alpha g_0$. The elementary Landau-fluid closure that in Sec. 3.4.6 neatly mapped the $\alpha \to -1$ limit onto a "fluid" Langevin equation, when reworked for the case of the momentum forcing, gives

$$\frac{\partial\varphi_k}{\partial t} + \gamma_L\varphi_k = \frac{\operatorname{sgn} k}{\sqrt{\pi}}\chi_{1,k}. \tag{B.16}$$

Thus, a Langevin equation still, but with an order-unity adjusted noise term.

Bibliography

[1] A. A. Schekochihin, S. C. Cowley, W. Dorland, G. W. Hammett, G. G. Howes, E. Quataert, and T. Tatsuno. Astrophysical gyrokinetics: kinetic and fluid turbulent cascades in magnetized weakly collisional plasmas. *ApJS*, 182:310, 2009.

[2] J. W. Armstrong, B. J. Rickett, and S. R. Spangler. Electron density power spectrum in the local interstellar medium. *ApJ*, 443:209–221, 1995.

[3] E. Marsch and C.Y. Tu. Spectral and spatial evolution of compressible turbulence in the inner solar wind. *J. Geophys. Res.*, 95:11945, 1990.

[4] L. Landau. On the vibration of the electronic plasma. *J. Phys. USSR*, 10:25, 1946.

[5] L. Tonks and I. Langmuir. A general theory of the plasma of an arc. *Phys. Rev.*, 34(6):876, 1929.

[6] N. G. Van Kampen. On the theory of stationary waves in plasmas. *Physica*, 21:949, 1955.

[7] K. M. Case. Plasma oscillations. *Ann. Phys.*, 7:349, 1959.

[8] T. Tatsuno, W. Dorland, A. A. Schekochihin, G. G. Plunk, M. Barnes, S. C. Cowley, and G. G. Howes. Nonlinear Phase Mixing and Phase-Space Cascade of Entropy in Gyrokinetic Plasma Turbulence. *Phys. Rev. Lett.*, 103:015003, 2009.

[9] R. W. Gould, T. M. O'Neil, and J. H. Malmberg. Plasma wave echo. *Phys. Rev. Lett.*, 19:219, 1967.

[10] J. H. Malmberg, C. B. Wharton, R. W. Gould, and T. M. O'Neil. Plasma Wave Echo Experiment. *Phys. Rev. Lett.*, 20:95, 1968.

[11] J. H. Malmberg, C. B. Wharton, R. W. Gould, and T. M. O'neil. Observation of plasma wave echoes. *Phys. Fluids*, 11(6):1147, 1968.

[12] C. H. Su and C. Oberman. Collisional Damping of a Plasma Echo. *Phys. Rev. Lett.*, 20:427, 1968.

[13] A. N. Kolmogorov. Dissipation of energy in locally isotropic turbulence. In *Dokl. Akad. Nauk SSSR*, volume 32, pages 16–18, 1941.

[14] A. S. Monin and A. M. Yaglom. Statistical fluid mechanics. vol. 2, 1975.

[15] T. N. Parashar and C. Salem. Turbulent dissipation challenge: A community driven effort, 2013.

[16] A. A. Schekochihin, S. C. Cowley, W. Dorland, G. W. Hammett, G. G. Howes, G. G. Plunk, E. Quataert, and T. Tatsuno. Gyrokinetic turbulence: a nonlinear route to dissipation through phase space. *Plasma Phys. Control. Fusion*, 50:124024, 2008.

[17] G. G. Howes, S. C. Cowley, W. Dorland, G. W. Hammett, E. Quataert, and A. A. Schekochihin. Astrophysical Gyrokinetics: Basic Equations and Linear Theory. *ApJ*, 651:590, 2006.

[18] R. H. Kraichnan. Inertial-range spectrum of hydromagnetic turbulence. *Phys. Fluids*, 8(7):1385–1387, 1965.

[19] P. Goldreich and S. Sridhar. Toward a theory of interstellar turbulence. 2: Strong alfvenic turbulence. *ApJ*, 438:763, 1995.

[20] P. Goldreich and S. Sridhar. Magnetohydrodynamic Turbulence Revisited. *ApJ*, 485:680, 1997.

[21] S. Galtier, S. V. Nazarenko, A. C. Newell, and A. Pouquet. A weak turbulence theory for incompressible magnetohydrodynamics. *Journal of Plasma Physics*, 63(05):447–488, 2000.

[22] A. A. Schekochihin, S. V. Nazarenko, and T. A. Yousef. Weak alfvén-wave turbulence revisited. *Phys. Rev. E*, 85:036406, 2012.

[23] E. Quataert. Particle Heating by Alfvenic Turbulence in Hot Accretion Flows. *ApJ*, 500:978, 1998.

[24] E. Quataert and A. Gruzinov. Turbulence and Particle Heating in Advection-dominated Accretion Flows. *ApJ*, 520:248, 1999.

[25] G. G. Howes, S. C. Cowley, W. Dorland, G. W. Hammett, E. Quataert, and A. A. Schekochihin. A model of turbulence in magnetized plasmas: Implications for the dissipation range in the solar wind. *J. Geophys. Res.*, 113:A05103, 2008.

[26] J. W. Armstrong, J. M. Cordes, and B. J. Rickett. Density power spectrum in the local interstellar medium. *Nature*, 291(5816):561–564, 1981.

[27] T. J. W. Lazio, J. M. Cordes, A. G. De Bruyn, and J. P. Macquart. The microarcsecond sky and cosmic turbulence. *New Astronomy Reviews*, 48(11):1439–1457, 2004.

[28] R. V. E. Lovelace, E. E. Salpeter, L. E. Sharp, and D. E. Harris. Analysis of observations of interplanetary scintillations. *The Astrophysical Journal*, 159:1047, 1970.

[29] R. Woo and J. W. Armstrong. Spacecraft radio scattering observations of the power spectrum of electron density fluctuations in the solar wind. *J. Geophys. Res.*, 84(A12):7288–7296, 1979.

[30] L. M. Celnikier, C. C. Harvey, R. Jegou, P. Moricet, and M. Kemp. A determination of the electron density fluctuation spectrum in the solar wind, using the ISEE propagation experiment. *Astron. Astrophys.*, 126:293, 1983.

[31] L. M. Celnikier, L. Muschietti, and M. V. Goldman. Aspects of interplanetary plasma turbulence. *Astron. Astrophys.*, 181:138, 1987.

[32] W. A. Coles and J. K. Harmon. Propagation observations of the solar wind near the sun. *ApJ*, 337:1023–1034, 1989.

[33] W. A. Coles, W. Liu, J. K. Harmon, and C. L. Martin. The solar wind density spectrum near the sun: Results from voyager radio measurements. *J. Geophys. Res.*, 96(A2):1745–1755, 1991.

[34] A. Bershadskii and K. R. Sreenivasan. Intermittency and the passive nature of the magnitude of the magnetic field. *Phys. Rev. Lett.*, 93:064501, 2004.

[35] B. Hnat, S. C. Chapman, and G. Rowlands. Compressibility in solar wind plasma turbulence. *Phys. Rev. Lett.*, 94:204502, 2005.

[36] P. J. Kellogg and T. S. Horbury. Rapid density fluctuations in the solar wind. *Ann. Geophys.*, 23:3765, 2005.

[37] O. Alexandrova, V. Carbone, P. Veltri, and L. Sorriso-Valvo. Small-Scale Energy Cascade of the Solar Wind Turbulence. *ApJ*, 674:1153, 2008.

[38] A. Barnes. Collisionless damping of hydromagnetic waves. *Phys. Fluids*, 9:1483, 1966.

[39] G. G. Plunk. Landau damping in a turbulent setting. *Phys. Plasmas*, 20:032304, 2013.

[40] G. G. Plunk and J. T. Parker. Irreversible energy flow in forced Vlasov dynamics. *arXiv:1402.7230*, 2014.

[41] C. Mouhot and C. Villani. On landau damping. *Acta mathematica*, 207(1):29–201, 2011.

[42] E. A. Rutherford, P. H.and Frieman. Drift instabilities in general magnetic field configurations. *Phys. Fluids*, 11(3):569–585, 1968.

[43] J. B. Taylor and R. J. Hastie. Stability of general plasma equilibria-I formal theory. *Plasma Physics*, 10(5):479, 1968.

[44] P. J. Catto. Linearized gyro-kinetics. *Plasma Physics*, 20(7):719, 1978.

[45] T. M. Antonsen Jr. and B. Lane. Kinetic equations for low frequency instabilities in inhomogeneous plasmas. *Phys. Fluids (1958-1988)*, 23(6):1205–1214, 1980.

[46] P. J. Catto, W. M. Tang, and D. E. Baldwin. Generalized gyrokinetics. *Plasma Physics*, 23(7):639, 1981.

[47] E. A. Frieman and L. Chen. Nonlinear gyrokinetic equations for low-frequency electromagnetic waves in general plasma equilibria. *Phys. Fluids*, 25:502, 1982.

[48] D. H. E. Dubin, J. A. Krommes, C. Oberman, and W. W. Lee. Nonlinear gyrokinetic equations. *Phys. Fluids*, 26(12):3524–3535, 1983.

[49] W. W. Lee. Gyrokinetic approach in particle simulation. *Phys. Fluids*, 26(2):556–562, 1983.

[50] W. W. Lee. Gyrokinetic particle simulation model. *J. Comput. Phys.*, 72(1):243–269, 1987.

[51] T. S. Hahm, W. W. Lee, and A. Brizard. Nonlinear gyrokinetic theory for finite β plasmas. *Phys. Fluids*, 31(7):1940–1948, 1988.

[52] B. B. Kadomtsev and O. P. Pogutse. Nonlinear helical perturbations of a plasma in the tokamak. *Soviet Phys. JETP*, 38:283, 1974.

[53] H. R. Strauss. Nonlinear, three-dimensional magnetohydrodynamics of noncircular tokamaks. *Phys. Fluids*, 19:134, 1976.

[54] A. M. Obukhov. On the problem of geostrophic wind. *Izv. Akad. Nauk SSSR Ser. Geogr. Geofiz.*, 13:58, 1949.

[55] S. Corrsin. On the Spectrum of Isotropic Temperature Fluctuations in an Isotropic Turbulence. *J. Applied Phys.*, 22:469, 1951.

[56] G. K. Batchelor. Small-scale variation of convected quantities like temperature in turbulent fluid. Part 1. General discussion and the case of small conductivity. *J. Fluid Mech.*, 5:113, 1959.

[57] R. H. Kraichnan. Small-Scale Structure of a Scalar Field Convected by Turbulence. *Phys. Fluids*, 11:945, 1968.

[58] R. H. Kraichnan. Convection of a passive scalar by a quasi-uniform random straining field. *J. Fluid Mech.*, 64:737, 1974.

[59] R. H. Kraichnan. Anomalous scaling of a randomly advected passive scalar. *Phys. Rev. Lett.*, 72(7):1016, 1994.

[60] H. Aref. Stirring by chaotic advection. *J. Fluid Mech.*, 143:1–21, 1984.

[61] J Chaiken, CK Chu, M Tabor, and QM Tan. Lagrangian turbulence and spatial complexity in a stokes flow. *Phys. Fluids*, 30(3):687–694, 1987.

[62] J. M. Ottino. *The kinematics of mixing: stretching, chaos, and transport*, volume 3. Cambridge University Press, 1989.

[63] Y. B. Zeldovich, S. A. Molchanov, Ruzmaikin, A. A., and D. D. Sokoloff. Intermittency, diffusion and generation in a nonstationary random medium. *Sov. Sci. Rev. Sect. C, Math. Phys. Rev*, 7:1–110, 1988.

[64] E. Ott and T. M. Antonsen Jr. Chaotic fluid convection and the fractal nature of passive scalar gradients. *Phys. Rev. Lett.*, 61(25):2839, 1988.

[65] E. Ott and T. M. Antonsen Jr. Fractal measures of passively convected vector fields and scalar gradients in chaotic fluid flows. *Phys. Rev. A*, 39(7):3660, 1989.

[66] T. M. Antonsen Jr. and E. Ott. Multifractal power spectra of passive scalars convected by chaotic fluid flows. *Phys. Rev. A*, 44(2):851, 1991.

[67] R. Ramshankar and J. P. Gollub. Transport by capillary waves. Part II: Scalar dispersion and structure of the concentration field. *Phys. Fluids A*, 3(5):1344–1350, 1991.

[68] T. H. Solomon, E. R. Weeks, and H. L. Swinney. Observation of anomalous diffusion and Lévy flights in a two-dimensional rotating flow. *Phys. Rev. Lett.*, 71(24):3975, 1993.

[69] K. R. Sreenivasan. On local isotropy of passive scalars in turbulent shear flows. *Proc. Royal Soc. London. Ser. A*, 434(1890):165–182, 1991.

[70] C. Van Atta. Local isotropy of the smallest scales of turbulent scalar and velocity fields. *Proc. Royal Soc. London. Ser. A*, 434(1890):139–147, 1991.

[71] R. T. Pierrehumbert. Tracer microstructure in the large-eddy dominated regime. *Chaos, Solitons & Fractals*, 4(6):1091–1110, 1994.

[72] T. M. Antonsen Jr., Z. F. Fan, and E. Ott. k spectrum of passive scalars in lagrangian chaotic fluid flows. *Phys. Rev. Lett.*, 75(9):1751, 1995.

[73] U. Frisch. *Turbulence: the legacy of AN Kolmogorov*. Cambridge university press, 1995.

[74] K. R. Sreenivasan. The passive scalar spectrum and the Obukhov–Corrsin constant. *Phys. Fluids*, 8(1):189–196, 1996.

[75] O. Boratav, A. Eden, and A. Erzan. Turbulence modeling and vortex dynamics. In *Lecture Notes in Physics, Berlin Springer Verlag*, volume 491, 1997.

[76] M Lesieur. Turbulence in fluids, 1997, 1977.

[77] B. I. Shraiman and E. D. Siggia. Scalar turbulence. *Nature*, 405(6787):639–646, 2000.

[78] Z. Warhaft. Passive scalars in turbulent flows. *Ann. Rev. Fluid Mech.*, 32(1):203–240, 2000.

[79] W. M. Elsasser. The hydromagnetic equations. *Phys. Rev.*, 79(1):183, 1950.

[80] A. Lenard and I. B. Bernstein. Plasma oscillations with diffusion in velocity space. *Phys. Rev.*, 112:1456, 1958.

[81] S. A. Orszag. Accurate solution of the Orr–Sommerfeld stability equation. *J. Fluid Mech.*, 50(04):689–703, 1971.

[82] C. Basdevant, B. Legras, R. Sadourny, and M. Beland. A study of barotropic model flows: intermittency, waves and predictability. *J. Atmos. Sci.*, 38(11):2305–2326, 1981.

[83] M. Meneguzzi, U. Frisch, and A. Pouquet. Helical and nonhelical turbulent dynamos. *Phys. Rev. Lett.*, 47(15):1060, 1981.

[84] J. C. McWilliams. The emergence of isolated coherent vortices in turbulent flow. *J. Fluid Mech.*, 146:21–43, 1984.

[85] T. Passot and A. Pouquet. Hyperviscosity for compressible flows using spectral methods. *J. Comp. Phys.*, 75(2):300–313, 1988.

[86] V. Borue and S. A. Orszag. Forced three-dimensional homogeneous turbulence with hyperviscosity. *Europhys. Lett.*, 29(9):687, 1995.

[87] S. A. Orszag and C. M. Tang. Small-scale structure of two-dimensional magnetohydrodynamic turbulence. *J. Fluid Mech.*, 90(01):129–143, 1979.

[88] P. Langevin. *On the theory of Brownian motion.* 1908.

[89] R. Kubo. The fluctuation-dissipation theorem. *Rep. Prog. Phys.*, 29:255, 1966.

[90] G. W. Hammett and F. W. Perkins. Fluid moment models for Landau damping with application to the ion-temperature-gradient instability. *Phys. Rev. Lett.*, 64:3019, 1990.

[91] G. W. Hammett, W. Dorland, and F. W. Perkins. Fluid models of phase mixing, Landau damping, and nonlinear gyrokinetic dynamics. *Phys. Fluids B*, 4:2052, 1992.

[92] C. L. Hedrick and J.-N. Leboeuf. Landau fluid equations for electromagnetic and electrostatic fluctuations. *Phys. Fluids B*, 4:3915, 1992.

[93] W. Dorland and G. W. Hammett. Gyrofluid turbulence models with kinetic effects. *Phys. Fluids B*, 5:812, 1993.

[94] M. A. Beer and G. W. Hammett. Toroidal gyrofluid equations for simulations of tokamak turbulence. *Phys. Plasmas*, 3:4046, 1996.

[95] P. B. Snyder, G. W. Hammett, and W. Dorland. Landau fluid models of collisionless magnetohydrodynamics. *Phys. Plasmas*, 4:3974, 1997.

[96] P. B. Snyder and G. W. Hammett. A Landau fluid model for electromagnetic plasma microturbulence. *Phys. Plasmas*, 8:3199, 2001.

[97] P. B. Snyder and G. W. Hammett. Electromagnetic effects on plasma microturbulence and transport. *Phys. Plasmas*, 8:744, 2001.

[98] T. Passot and P. L. Sulem. A Landau fluid model for dispersive magnetohydrodynamics. *Phys. Plasmas*, 11:5173, 2004.

[99] P. Goswami, T. Passot, and P. L. Sulem. A Landau fluid model for warm collisionless plasmas. *Phys. Plasmas*, 12:102109, 2005.

[100] J. J. Ramos. Fluid formalism for collisionless magnetized plasmas. *Phys. Plasmas*, 12:052102, 2005.

[101] T. Passot and P. L. Sulem. A fluid model with finite Larmor radius effects for mirror mode dynamics. *J. Geophys. Res.*, 111:A04203, 2006.

[102] T. Passot and P. L. Sulem. Collisionless magnetohydrodynamics with gyrokinetic effects. *Phys. Plasmas*, 14:082502, 2007.

[103] T. Passot, P. L. Sulem, and P. Hunana. Extending magnetohydrodynamics to the slow dynamics of collisionless plasmas. *Phys. Plasmas*, 19:082113, 2012.

[104] C. H. K. Chen, A. Mallet, A. A. Schekochihin, T. S. Horbury, R. T. Wicks, and S. D. Bale. Three-dimensional structure of solar wind turbulence. *ApJ*, 758(2):120, 2012.

[105] B. D. Fried and S. D. Conte. *The Plasma Dispersion Function*. Academic Press, New York, 1961.

[106] T. P. Armstrong. Numerical studies of the nonlinear Vlasov equation. *Phys. Fluids*, 10:1269, 1967.

[107] F. C. Grant and M. R. Feix. Fourier-Hermite solutions of the Vlasov equations in the linearized limit. *Phys. Fluids*, 10:696, 1967.

[108] G. W. Hammett, M. A. Beer, W. Dorland, S. C. Cowley, and S. A. Smith. Developments in the gyrofluid approach to tokamak turbulence simulations. *Plasma Phys. Control. Fusion*, 35:973, 1993.

[109] S. E. Parker and D. Carati. Renormalized dissipation in plasmas with finite collisionality. *Phys. Rev. Lett.*, 75:441, 1995.

[110] C. S. Ng, A. Bhattacharjee, and F. Skiff. Kinetic eigenmodes and discrete spectrum of plasma oscillations in a weakly collisional plasma. *Phys. Rev. Lett.*, 83:1974, 1999.

[111] T.-H. Watanabe and H. Sugama. Kinetic simulation of steady states of ion temperature gradient driven turbulence with weak collisionality. *Phys. Plasmas*, 11:1476, 2004.

[112] A. Zocco and A. A. Schekochihin. Reduced fluid-kinetic equations for low-frequency dynamics, magnetic reconnection, and electron heating in low-beta plasmas. *Phys. Plasmas*, 18:102309, 2011.

[113] N. F. Loureiro, A. A. Schekochihin, and A. Zocco. Fast collisionless reconnection and electron heating in strongly magnetized plasmas. *Phys. Rev. Lett.*, 111:025002, 2013.

[114] D. R. Hatch, F. Jenko, A. Bañón Navarro, and V. Bratanov. Transition between saturation regimes of gyrokinetic turbulence. *Phys. Rev. Lett.*, 111:175001, 2013.

[115] M. Abramowitz and I. A. Stegun. *Handbook of mathematical functions: with formulas, graphs, and mathematical tables*. Number 55. Courier Dover Publications, 1972.

[116] H. A Kramers. *La diffusion de la lumiere par les atomes.* Atti Cong. Intern. Fisici (Transactions of Volta Centenary Congress), Como, vol. 2, 1927.

[117] R. Kronig. On the theory of dispersion of X-rays. *J. Opt. Soc. America*, 12:547, 1926.

[118] A. A. Schekochihin, A. Kanekar, G. W. Hammett, W. Dorland, and N. F. Loureiro. Stochastic advection and phase mixing in a collisionless plasma. *in preparation*, 2014.

[119] E. A. Foote and R. M. Kulsrud. Hydromagnetic waves in high beta plasmas. *ApJ*, 233:302, 1979.

[120] Y. Lithwick and P. Goldreich. Compressible magnetohydrodynamic turbulence in interstellar plasmas. *ApJ*, 562:279, 2001.

[121] A. Kanekar, A. A. Schekochihin, G. W. Hammett, W. Dorland, and N. F. Loureiro. Passive advection of a kinetic field in a collisionless plasma. *in preparation*, 2014.

[122] J. Maron and P. Goldreich. Simulations of incompressible magnetohydrodynamic turbulence. *ApJ*, 554(2):1175, 2001.

[123] A. Busse and W.-C. Müller. Diffusion and dispersion in magnetohydrodynamic turbulence: The influence of mean magnetic fields. *Astron. Nachr.*, 329(7):714–716, 2008.

[124] J. Mason, S. Boldyrev, F. Cattaneo, and J. C. Perez. The statistics of a passive scalar in field-guided magnetohydrodynamic turbulence. *Geophysical & Astrophysical Fluid Dynamics*, pages 1–10, 2014.

[125] S. Sur, L. Pan, and E. Scannapieco. Mixing in magnetized turbulent media. *ApJ*, 784(2):94, 2014.

[126] G. E. Uhlenbeck and L. S. Ornstein. On the theory of the Brownian motion. *Phys. Rev.*, 36(5):823, 1930.

[127] S. Chandrasekhar. Stochastic problems in physics and astronomy. *Rev. Mod. Phys.*, 15(1):1, 1943.

[128] M. C. Wang and G. E. Uhlenbeck. On the theory of the Brownian motion II. *Rev. of Mod. Phys.*, 17(2-3):323–342, 1945.

[129] N. G. Van Kampen. *Stochastic processes in physics and chemistry*, volume 1. Elsevier, 1992.

[130] C. W. Gardiner. Handbook of stochastic methods for physics, chemistry and the natural sciences. *Appl. Optics*, 25:3145, 1986.

[131] D. T. Gillespie. *Markov processes: an introduction for physical scientists*. Elsevier, 1991.

[132] D. T. Gillespie. The multivariate Langevin and Fokker–Planck equations. *Amer. J. Phys.*, 64(10):1246–1257, 1996.

[133] F. Reif. *Fundamentals of statistical and thermal physics.* Waveland Press, 2009.

[134] S. P. Gary, H. Karimabadi, and V. S. Roytershteyn. Dissipation Wavenumbers for Turbulence in Electron-Positron Plasmas. *ApJ*, 701:1695, 2009.

[135] J. J. Podesta, J. E. Borovsky, and S. P. Gary. A Kinetic Alfvén Wave Cascade Subject to Collisionless Damping Cannot Reach Electron Scales in the Solar Wind at 1 AU. *ApJ*, 712:685, 2010.

[136] G. G. Howes, W. Dorland, S. C. Cowley, G. W. Hammett, E. Quataert, A. A. Schekochihin, and T. Tatsuno. Kinetic Simulations of Magnetized Turbulence in Astrophysical Plasmas. *Phys. Rev. Lett.*, 100:065004, 2008.

[137] M. Barnes, F. I. Parra, and A. A. Schekochihin. Critically Balanced Ion Temperature Gradient Turbulence in Fusion Plasmas. *Phys. Rev. Lett.*, 107:115003, 2011.

[138] J. M. TenBarge and G. G. Howes. Evidence of critical balance in kinetic Alfvén wave turbulence simulations. *Phys. Plasmas*, 19(5):055901, 2012.

[139] F. Sahraoui, M. L. Goldstein, P. Robert, and Y. V. Khotyaintsev. Evidence of a Cascade and Dissipation of Solar-Wind Turbulence at the Electron Gyroscale. *Phys. Rev. Lett.*, 102:231102, 2009.

[140] O. Alexandrova, J. Saur, C. Lacombe, A. Mangeney, J. Mitchell, S. J. Schwartz, and P. Robert. Universality of Solar-Wind Turbulent Spectrum from MHD to Electron Scales. *Phys. Rev. Lett.*, 103:165003, 2009.

[141] C. H. K. Chen, T. S. Horbury, A. A. Schekochihin, R. T. Wicks, O. Alexandrova, and J. Mitchell. Anisotropy of Solar Wind Turbulence between Ion and Electron Scales. *Phys. Rev. Lett.*, 104:255002, 2010.

[142] F. Sahraoui, M. L. Goldstein, G. Belmont, P. Canu, and L. Rezeau. Three Dimensional Anisotropic k Spectra of Turbulence at Subproton Scales in the Solar Wind. *Phys. Rev. Lett.*, 105:131101, 2010.

[143] O. Alexandrova, C. Lacombe, A. Mangeney, R. Grappin, and M. Maksimovic. Solar Wind Turbulent Spectrum at Plasma Kinetic Scales. *ApJ*, 760:121, 2012.

[144] F. Sahraoui, S. Y. Huang, G. Belmont, M. L. Goldstein, A. Rétino, P. Robert, and J. De Patoul. Scaling of the Electron Dissipation Range of Solar Wind Turbulence. *ApJ*, 777:15, 2013.

[145] C. H. K. Chen, S. Boldyrev, Q. Xia, and J. C. Perez. Nature of Subproton Scale Turbulence in the Solar Wind. *Phys. Rev. Lett.*, 110:225002, 2013.

[146] A. Kanekar, A. A. Schekochihin, W. Dorland, and N. F. Loureiro. Fluctuation-dissipation relations for a plasma-kinetic Langevin equation. *J. Plasma Phys.*, FirstView:1–21, 9 2014. doi: 10.1017/S0022377814000622.

[147] P. J. Coleman. Turbulence, viscosity, and dissipation in the solar-wind plasma. *ApJ*, 153:371–388, 1968.

[148] W. H. Matthaeus and M. L. Goldstein. Measurement of the rugged invariants of magnetohydrodynamic turbulence in the solar wind. *J. Geophys. Res.*, 87(A8):6011–6028, 1982.

[149] S. D. Bale, P. J. Kellogg, F. S. Mozer, T. S. Horbury, and H. Reme. Measurement of the electric fluctuation spectrum of magnetohydrodynamic turbulence. *Phys. Rev. Lett.*, 94(21):215002, 2005.

[150] J. J. Podesta, D. A. Roberts, and M. L. Goldstein. Spectral exponents of kinetic and magnetic energy spectra in solar wind turbulence. *The Astrophysical Journal*, 664(1):543, 2007.

[151] J. A. Tessein, C. W. Smith, B. T. MacBride, W. H. Matthaeus, M. A. Forman, and J. E. Borovsky. Spectral indices for multi-dimensional interplanetary turbulence at 1 AU. *ApJ*, 692(1):684, 2009.

[152] J. W. Belcher and L. Davis. Large-amplitude Alfvén waves in the interplanetary medium, 2. *J. Geophys. Res.*, 76(16):3534–3563, 1971.

[153] R. M. Kinney and J. C. McWilliams. Turbulent cascades in anisotropic magnetohydrodynamics. *Phys. Rev. E*, 57(6):7111, 1998.

[154] J. Cho and E. T. Vishniac. The anisotropy of magnetohydrodynamic Alfvénic turbulence. *The Astrophysical Journal*, 539(1):273, 2000.

[155] J. Cho, A. Lazarian, and E. T. Vishniac. New regime of magnetohydrodynamic turbulence: cascade below the viscous cutoff. *ApJ*, 566(1):L49, 2002.

[156] P. Dmitruk and W. H. Matthaeus. Low-frequency waves and turbulence in an open magnetic region: Timescales and heating efficiency. *ApJ*, 597(2):1097, 2003.

[157] D. Müller, W. C.and Biskamp and R. Grappin. Statistical anisotropy of magnetohydrodynamic turbulence. *Phys. Rev. E*, 67(6):066302, 2003.

[158] Nils Erland L Haugen, Axel Brandenburg, and Wolfgang Dobler. Simulations of nonhelical hydromagnetic turbulence. *Phys. Rev. E*, 70(1):016308, 2004.

[159] S. Oughton, P. Dmitruk, and W. H. Matthaeus. Reduced magnetohydrodynamics and parallel spectral transfer. *Phys. Plasmas*, 11(5):2214–2225, 2004.

[160] W. C. Müller and R. Grappin. Spectral energy dynamics in magnetohydrodynamic turbulence. *Phys. Rev. Lett.*, 95(11):114502, 2005.

[161] J. Mason, F. Cattaneo, and S. Boldyrev. Numerical measurements of the spectrum in magnetohydrodynamic turbulence. *Phys. Rev. E*, 77(3):036403, 2008.

[162] J. C. Perez and S. Boldyrev. On weak and strong magnetohydrodynamic turbulence. *ApJ*, 672:L61, 2008.

[163] A. Beresnyak. Basic properties of magnetohydrodynamic turbulence in the inertial range. *MNRAS*, 422(4):3495–3502, 2012.

[164] A. Beresnyak. Spectral Slope and Kolmogorov Constant of MHD Turbulence. *Phys. Rev. Lett.*, 106(7):075001, Feb 2011.

[165] J. Mason, F. Perez, J. C.and Cattaneo, and S. Boldyrev. Extended scaling laws in numerical simulations of magnetohydrodynamic turbulence. *ApJ*, 735(2):L26, 2011.

[166] J. Mason, J. C. Perez, S. Boldyrev, and F. Cattaneo. Numerical simulations of strong incompressible magnetohydrodynamic turbulence. *Phys. Plasmas*, 19(5):055902, 2012.

[167] J. C. Perez, J. Mason, S. Boldyrev, and F. Cattaneo. On the energy spectrum of strong magnetohydrodynamic turbulence. *Phys. Rev. X*, 2(4):041005, 2012.

[168] G. G. Howes. Inertial range turbulence in kinetic plasmas. *Phys. Plasmas*, 15:055904, 2008.

[169] K. D. Nielson, G. G. Howes, and W. Dorland. Alfvén wave collisions, the fundamental building block of plasma turbulence. II. Numerical solution. *Phys. Plasmas*, 20(7):072303, 2013.

[170] J. Cho and A. Lazarian. Compressible Sub-Alfvénic MHD Turbulence in Low-β Plasmas. *Phys. Rev. Lett.*, 88:245001, May 2002.

[171] J. Cho and A. Lazarian. Compressible magnetohydrodynamic turbulence: mode coupling, scaling relations, anisotropy, viscosity-damped regime and astrophysical implications. *MNRAS*, 345(1):325–339, 2003.

[172] A. Beresnyak, A. Lazarian, and J. Cho. Density scaling and anisotropy in supersonic magnetohydrodynamic turbulence. *ApJ*, 624(2):L93, 2005.

[173] J. Cho and A. Lazarian. Generation of compressible modes in mhd turbulence. *Theor. Comput. Fluid Dyn.*, 19(2):127–157, 2005.

[174] G. Kowal, A. Lazarian, and A. Beresnyak. Density fluctuations in MHD turbulence: spectra, intermittency, and topology. *ApJ*, 658(1):423, 2007.

[175] K. G. Klein, G. G. Howes, J. M. TenBarge, S. D. Bale, C. H. K. Chen, and C. S. Salem. Using Synthetic Spacecraft Data to Interpret Compressible Fluctuations in Solar Wind Turbulence. *ApJ*, 755:159, 2012.

[176] C. H. K. Chen. Private communication, 2014.

[177] S. Boldyrev. On the spectrum of magnetohydrodynamic turbulence. *ApJ*, 626(1):L37, 2005.

[178] S. Boldyrev. Spectrum of magnetohydrodynamic turbulence. *Phys. Rev. Lett.*, 96(11):115002, 2006.

[179] S. Boldyrev, J. Mason, and F. Cattaneo. Dynamic alignment and exact scaling laws in magnetohydrodynamic turbulence. *ApJ*, 699:L39, 2009.

[180] S. Boldyrev, J. C. Perez, J. E. Borovsky, and J. J. Podesta. Spectral scaling laws in magnetohydrodynamic turbulence simulations and in the solar wind. *ApJ*, 741(1):L19, 2011.

[181] I. G. Abel, G. G. Plunk, E. Wang, M. Barnes, S. C. Cowley, W. Dorland, and A. A. Schekochihin. Multiscale Gyrokinetics for Rotating Tokamak Plasmas: Fluctuations, Transport and Energy Flows. *Rep. Prog. Phys.*, 76:116201, 2013.

[182] A. M. Dimits, T. J. Williams, J. A. Byers, and B. I. Cohen. Scalings of Ion-Temperature-Gradient-Driven Anomalous Transport in Tokamaks. *Phys. Rev. Lett.*, 77:71, 1996.

[183] W. Dorland, F. Jenko, M. Kotschenreuther, and B. N. Rogers. Electron Temperature Gradient Turbulence. *Phys. Rev. Lett.*, 85:5579, 2000.

[184] F. Jenko, W. Dorland, M. Kotschenreuther, and B. N. Rogers. Electron temperature gradient driven turbulence. *Phys. Plasmas*, 7(5):1904–1910, 2000.

[185] B. N. Rogers, W. Dorland, and M. Kotschenreuther. Generation and stability of zonal flows in ion-temperature-gradient mode turbulence. *Phys. Rev. Lett.*, 85(25):5336, 2000.

[186] F. Jenko, W. Dorland, and G. W. Hammett. Critical gradient formula for toroidal electron temperature gradient modes. *Phys. Plasmas*, 8(9):4096–4104, 2001.

[187] F. Jenko and W. Dorland. Nonlinear electromagnetic gyrokinetic simulations of tokamak plasmas. *Plasma Phys. Control. Fusion*, 43(12A):A141, 2001.

[188] F. Jenko and W. Dorland. Prediction of significant tokamak turbulence at electron gyroradius scales. *Phys. Rev. Lett.*, 89(22):225001, 2002.

[189] J. Candy, R. E. Waltz, and W. Dorland. The local limit of global gyrokinetic simulations. *Phys. Plasmas*, 11(5):L25, 2004.

[190] S. E. Parker, Y. Chen, W. Wan, B. I. Cohen, and W. M. Nevins. Electromagnetic gyrokinetic simulations. *Phys. Plasmas*, 11(5):2594–2599, 2004.

[191] G. G. Howes, S. C. Cowley, W. Dorland, G. W. Hammett, E. Quataert, and A. A. Schekochihin. Dissipation-scale turbulence in the solar wind. *arXiv preprint arXiv:0707.3149*, 2007.

[192] R. Numata, G. G. Howes, T. Tatsuno, M. Barnes, and W. Dorland. AstroGK: Astrophysical gyrokinetics code. *J. Comput. Phys.*, 229(24):9347–9372, 2010.

[193] G. G. Howes, J. M. Tenbarge, W. Dorland, E. Quataert, A. A. Schekochihin, R. Numata, and T. Tatsuno. Gyrokinetic Simulations of Solar Wind Turbulence from Ion to Electron Scales. *Phys. Rev. Lett.*, 107:035004, 2011.

[194] J. M. Tenbarge and G. G. Howes. Collisionless damping at electron scales in solar wind turbulence. *ApJ*, Jan 2013.

[195] J. M. TenBarge and G. G. Howes. Current sheets and collisionless damping in kinetic plasma turbulence. *ApJ*, 771(2):L27, 2013.

[196] J. M. TenBarge, G. G. Howes, W. Dorland, and G. W. Hammett. An oscillating langevin antenna for driving plasma turbulence simulations. *Comp. Phys. Comm.*, 185(2):578–589, 2014.